Standardizing Rigid Inclusions for Transportation Projects—Phase I

Jie Han, Ph.D., P.E.
Sameep Lamsal
Haohua Chen
Robert Parsons, Ph.D., P.E.
Yuqiu Ye, Ph.D.
The University of Kansas

A Transportation Pooled Fund Study - TPF-5(503)

Kansas
Department of Transportation

1 Report No. FHWA-KS-25-02	2 Government Accession No.	3 Recipient Catalog No.	
4 **Title and Subtitle** Standardizing Rigid Inclusions for Transportation Projects — Phase I		5 **Report Date** December 2025	
		6 **Performing Organization Code**	
7 **Author(s)** Jie Han, Ph.D., P.E.; Sameep Lamsal; Haohua Chen; Robert L. Parsons, Ph.D., P.E.; Yuqiu Ye, Ph.D.		8 **Performing Organization Report No.**	
9 **Performing Organization Name and Address** The University of Kansas Department of Civil, Environmental & Architectural Engineering 1530 West 15th St. Lawrence, Kansas 66045-7609		10 **Work Unit No. (TRAIS)**	
		11 **Contract or Grant No.** C2218	
12 **Sponsoring Agency Name and Address** Kansas Department of Transportation Bureau of Research 2300 SW Van Buren Topeka, Kansas 66611-1195		13 **Type of Report and Period Covered** Final Report June 2023 – November 2025	
		14 **Sponsoring Agency Code** RE-0872-01 TPF-5(503)	
15 **Supplementary Notes** For more information write to address in block 9.			

16 **Abstract**

Rigid inclusions (RIs) have increasingly been used in ground improvement technology in the United States because they effectively reduce settlement, increase bearing capacity, and enhance stability. Several design methods have been developed to analyze RI-supported embankments based on various assumptions for transportation applications. This study assessed the state of the practice of RIs for embankment and structure support in transportation projects, including construction specifications, installation effects, slope stability, and design methods for vertical load transfer. An internet survey was conducted to gather opinions from owners, engineers, and researchers in the United States.

Evaluation of the design methods involved a comparison of results calculated from the popular design methods BS 8006-1, EBGEO, CUR226, and the Federal Highway Administration (FHWA) for three key design parameters (load efficacy, differential settlement and reinforcement strain). The measured data were available in the literature, including 24 full-scale experiments and four model tests. The comparison results revealed variations and inconsistencies of the calculated results among the design methods. Numerical analyses were also performed for two case studies, and their results were compared with the results from the design methods. Methods CUR226 and FHWA comparatively more accurately predicted all three design parameters, while BS 8006-1 overestimated all these parameters.

This study also utilized the Column-Wall Method (CWM), Equivalent Strength Method (ESM), Stress Reduction Method (SRM), and Pile Support Method (PSM) to evaluate the stability of RIS embankments. The results showed that the ESM led to a high strength of the equivalent area that prevented deep-seated failure. The SRM overestimated the factors of safety (FS) by more than 10% compared to those from the CWM while the PSM significantly overestimated the FS as compared to the CWM. This study reviewed the effects of RI installation on existing adjacent structures based on a limited number of documented case studies. This study also summarized the special provisions for RI projects of four state departments of transportation, identified the knowledge gaps in the current practice, and developed a plan for second-phase field evaluation of RIs for embankment/wall supports.

17 **Key Words** Columns; Design; Soil stabilization; Standardization; State of the practice; Structural supports	18 **Distribution Statement** No restrictions. This document is available to the public through the National Technical Information Service www.ntis.gov.		
19 **Security Classification (of this report)** Unclassified	20 **Security Classification (of this page)** Unclassified	21 **No. of pages** 151	22 **Price**

Form DOT F 1700.7 (8-72)

This page intentionally left blank.

Standardizing Rigid Inclusions for Transportation Projects — Phase I

Final Report

Prepared by

Jie Han, Ph.D., P.E.
Sameep Lamsal
Haohua Chen
Robert L. Parsons, Ph.D., P.E.
Yuqiu Ye, Ph.D.

The University of Kansas

PREFACE

The Kansas Department of Transportation (KDOT) is the lead agency for this pooled fund project for the Federal Highway Administration (FHWA). This ongoing, cooperative, and comprehensive research program addresses state transportation needs using academic and research resources from the Kansas Department of Transportation (KDOT), Texas Department of Transportation (TxDOT), Pennsylvania Department of Transportation (PennDOT), Idaho Transportation Department (ITD), Minnesota Department of Transportation (MnDOT), Maryland Department of Transportation (MDOT), Louisiana Department of Transportation and Development (LaDOTD), Federal Highway Administration, and the University of Kansas.

NOTICE

The authors and the state of Kansas do not endorse products or manufacturers. Trade and manufacturers names appear herein solely because they are considered essential to the object of this report.

This information is available in alternative accessible formats. To obtain an alternative format, contact the Office of Public Affairs, Kansas Department of Transportation, 700 SW Harrison, 2nd Floor – West Wing, Topeka, Kansas 66603-3745 or phone (785) 296-3585 (Voice) (TDD).

DISCLAIMER

The contents of this report reflect the views of the authors who are responsible for the facts and accuracy of the data presented herein. The contents do not necessarily reflect the views or the policies of the state of Kansas. This report does not constitute a standard, specification or regulation.

Abstract

Rigid inclusions (RIs) have increasingly been used in ground improvement technology in the United States because they effectively reduce settlement, increase bearing capacity, and enhance stability. Several design methods have been developed to analyze RI-supported embankments based on various assumptions for transportation applications. This study assessed the state of the practice of RIs for embankment and structure support in transportation projects, including construction specifications, installation effects, slope stability, and design methods for vertical load transfer. An internet survey was conducted to gather opinions from owners, engineers, and researchers in the United States.

Evaluation of the design methods involved a comparison of results calculated from the popular design methods BS 8006-1, EBGEO, CUR226, and the Federal Highway Administration (FHWA) for three key design parameters (load efficacy, differential settlement and reinforcement strain). The measured data were available in the literature, including 24 full-scale experiments and four model tests. The comparison results revealed variations and inconsistencies of the calculated results among the design methods. Numerical analyses were also performed for two case studies, and their results were compared with the results from the design methods. Methods CUR226 and FHWA comparatively more accurately predicted all three design parameters, while BS 8006-1 overestimated all these parameters.

This study also utilized the Column-Wall Method (CWM), Equivalent Strength Method (ESM), Stress Reduction Method (SRM), and Pile Support Method (PSM) to evaluate the stability of RI-supported (RIS) embankments. The results showed that the ESM led to a high strength of the equivalent area that prevented deep-seated failure. The SRM overestimated the factors of safety (FS) by more than 10% compared to those from the CWM while the PSM significantly overestimated the FS as compared to the CWM. This study reviewed the effects of RI installation on existing adjacent structures based on a limited number of documented case studies. This study also summarized the special provisions for RI projects of four state departments of transportation, identified the knowledge gaps in the current practice, and developed a plan for second-phase field evaluation of RIs for embankment/wall supports.

Acknowledgments

Table of Contents

List of Tables

List of Figures

Chapter 1: Introduction

1.1 Background and Problem Statement

The low strength and high compressibility of soft soils create significant challenges in geotechnical engineering practices. Conventional ground improvement methods such as preloading with vertical drains, soil stabilization with lime or cement, and deep replacement by stone columns are commonly employed to improve soil properties. Although these methods are effective under normal conditions, they can be time-consuming and may not be suitable for projects that require rapid construction or stringent settlement control. In such scenarios, rigid inclusions (RIs) can be an effective and efficient solution because these vertically installed, stiff elements transfer loads from the surface to deeper, more stable soil layers — enhancing load-bearing capacity and minimizing settlement. RI applications, which offer the dual benefits of rapid construction and reduced deformations, span a wide range of infrastructure projects in the United States, including embankments, retaining walls, and box culverts for highways and railways.

A variety of equipment and installation methods, often marketed under different trade names, are currently used for RI installation. Depending on the chosen equipment, installation technique, and soil conditions, the installation process can result in partial or full displacement of the surrounding soil, potentially disturbing adjacent soils, neighboring inclusions, and nearby structures. Typically, these inclusions are installed beneath a load transfer platform (LTP) to help support embankments or structures. However, many of these installation methods are proprietary and closely guarded for commercial advantage, leaving Departments of Transportation (DOTs) highly dependent on contractors for design and implementation. At present, no universally accepted design methodologies or construction specifications exist to evaluate the load transfer mechanism and installation-induced effects on surrounding soils, adjacent inclusions, or existing structures.

The failures of RI-supported (RIS) earth structures recently have highlighted the lack of stability analysis of such systems. A two-phase approach, starting with a comprehensive review of current practices (Phase I) followed by full-scale field testing (Phase II), is needed to evaluate installation effects and improve or develop design methodologies that account for installation effects and slope stability. These methodologies should include the analysis of load transfer

behavior and vertical and lateral deformations under loading. The research should also verify or improve the guidelines for the load transfer technology with RI systems as one of the ground modification methods for highway structures developed through the NCHRP 10-121 project.

1.2 Objectives

The main objectives of this research included assessing the state of the practice of RIs used to support embankments and structures in transportation applications and assessing and evaluating available data and design methodologies or guidelines in the literature. This study also sought to identify knowledge gaps, missing data, and procedures for future studies and to develop a plan for full-scale field tests to be carried out in the Phase II study.

1.3 Scope of Work

1.3.1 Literature Review and Assessment of Current Practices

This task included a comprehensive review of the global and U.S. practices and research of RIs used for vertical load support and embankment stability. The review included the effect of RI installation, load transfer mechanisms, design methodologies, construction specifications, and slope stability to identify gaps in these areas. To supplement the literature review, an online survey was offered state DOT engineers, design/consulting professionals, and contractors to obtain their insights into current practices. Relevant test data from different case studies were also collected.

1.3.2 Evaluation of Design Methodologies

Based on findings from the literature and survey responses, four commonly-used design methodologies were reviewed and evaluated using available test results supplemented with numerical analyses. Knowledge gaps and missing data were identified that may be addressed through a future full-scale field test program.

1.3.3 Development of a Full-Scale Field Test Program

The research team developed a full-scale field test program to address the identified knowledge gaps and collect additional test data to validate and improve existing design methods or develop new ones.

1.4 Research Methodologies

This study adopted the following research methodologies:

1. A literature review was used to gather the information about terminologies, equipment and installation methods, installation effects, load transfer mechanisms, available design methods for LTPs, global stability analysis, construction specifications, and case studies of RI usage for transportation applications and a future survey questionnaire.

2. An online survey was used to assess the current state of the practice for RIs in transportation projects through the U.S.

3. Design methodologies and guidelines were evaluated based on the available data from collected case histories and supplemented with numerical results obtained in this study to identify gaps and missing data.

4. A field test plan was developed for the Phase II study to address the identified gaps and missing data.

1.5 Organization of the Report

This report is organized into seven chapters. Chapter 1 presents the background and problem statement for the study, research objectives, scope of the work, methodologies, and overall organization of the report. Chapter 2 contains a comprehensive literature review of the definition, historical development, applications, advantages/limitations, installation methods, existing design methods for load transfer platforms, installation effects, slope stability, construction specifications, and case histories of transportation projects involving RIs. Chapter 3 contains survey responses from the state of the practice internet survey. Chapter 4 summarizes four commonly used design methodologies for LTPs and compares their accuracy with data from the collected case studies and numerical analysis conducted in this study. Chapter 5 evaluates the available analysis methods for global slope stability of RI-supported embankments. Chapter 6 identifies knowledge gaps in RI practice for transportation applications and outlines a plan for a field test program for the Phase II project. Chapter 7 provides conclusions and recommendations for future studies.

Chapter 2: Literature Review

2.1 Definition and Background

Rigid inclusions (RIs) are vertically installed columns or elements (e.g., cementitious, timber, or steel) with significantly higher stiffness than their surrounding soil. Their stability is achieved without any lateral confinement of the surrounding soil. RIs are installed in the soft ground to enhance the overall ground performance by increasing bearing capacity, reducing settlement, and improving ground stability. To facilitate effective load sharing with the surrounding soil, a load transfer platform (LTP) or cushion is typically installed between the top of the RIs and the bottom of the embankments or footings. The LTP may be unreinforced or reinforced by geosynthetics (primarily geogrids and woven geotextiles).

RIs have recently been a subject of significant interest in geotechnical engineering due to their rapid installation and effective enhancement of the overall performance of embankments and structures over weak and highly compressible soils, especially for accelerated construction as compared with traditional ground improvement methods (e.g., preloading and stone columns).

Van Eekelen and Han (2020) found that researchers and engineers worldwide use various terminologies to describe RI technology, including geosynthetic-reinforced pile-supported embankments; geosynthetic-reinforced column-supported embankments; basal reinforced piled embankments; RI ground improvement; and flexible, semi-rigid, and rigid columns or inclusions.

The current study focused on rigid columns or inclusions. For clarity and consistency, the term "RIs" refers to rigid inclusions or rigid inclusion elements in this report while the term "RIS system" designates a rigid inclusion-supported system to describe an entire ground improvement system. If columns and piles were rigid in the literature, they are referred to as rigid inclusions or RIs in this report. Table 2.1 provides various RI definitions.

Table 2.1: RI Definitions from the Literature

Reference	Definition
Briançon et al. (2004)	The system consists of two main components: (1) vertically installed RIs that serve in transmitting loads to deeper soil layers and (2) a load transfer platform, typically made of compacted granular materials, that transfers surface loads efficiently onto the head of the inclusions.
Jenck et al. (2005)	The structural load is transferred to the underlying stiffer substratum through a granular mat built on the soft soil layer reinforced by a vertical grid of rigid piles.
Le Hello (2007)	RIS system incorporates a reinforced geosynthetic sheet on top of the pile network.
Rangel-Núñez et al. (2008)	In contrast to traditional piles, RIs do not establish a direct connection with the raft foundation.
Chu et al. (2009)	RIs are semi-rigid to rigid integrated columns or bodies installed in soft soils to improve bearing capacity, control settlement, and enhance overall ground performance.
Chevalier et al. (2011)	This technique involves installing a granular layer at the top of the pile network to reduce the vertical load on the soft soil and the vertical settlement of the supported structure.
EBGEO (2011)	Geosynthetic-reinforced earth structures on point or linear bearing elements are suitable as systems for transmitting static and variable loads on soft soils to adequately load-bearing, deeper strata. The ratio of the subgrade reaction moduli of the bearing element to the ground in the contact plane of the reinforced earth structure should be greater than 75 if full arching is considered.
IREX (2012)	RIs, in the strict sense of the term, contain vertical, slender, and mechanically continuous elements (often cylindrical), and are installed in a regular mesh pattern based on the nature and geometry of applied load and soil conditions. These inclusions have constant cross-section and stiffness significantly greater than that of the surrounding soil.
Simon (2012)	RIs are generically referred to as columns, pile-like inclusions, or non-contact settlement-reducing piles. Depending on the installation technique, they may be deep mixed columns, lime columns, or jet grouting columns. In proprietary contexts, terms like controlled modulus columns (CMCs) or vibro concrete columns (VCCs) are commonly used.
Cirión et al. (2013)	RIs are a set of inclusions installed in highly compressible and weak soil to form a composite soil-inclusion system with enhanced mechanical properties.
Neagoe (2013)	The RI system is composed of rigid or semi-rigid vertical inclusions and a granular platform through which the loads are transferred from the structure to the inclusions.
Han (2015)	The modulus of columns should be 100 times or more than that of the surrounding soil to fully mobilize soil arching.

2.1.1 Historical Development of the RIS System

An early application of RIS embankments in Holland was recorded in the 1930s (Van Eekelen & Han, 2020). Rathmayer (1975) reported that RIs were utilized in the late 1970s for road embankments in Scandinavian countries, and Holtz and Massarsch (1976) reported the early use of geosynthetic reinforcement in RIS embankments in Sweden in 1975. Another early documented

geosynthetic-reinforced RIS embankment was constructed in Scotland in 1983 as part of a bridge approach project (Reid & Buchanan, 1984). In France, this RI technology was developed during the 1990s (IREX, 2012) with the introduction of Controlled Modulus Columns (CMCs). The widespread application of RIs began in the mid-2000s in North America (Masse et al., 2020) although a large diameter storage tank was constructed over a geosynthetic-reinforced column-supported platform in Philadelphia, Pennsylvania, prior to that time (Schaefer et al., 1997).

2.1.2 Applications

In transportation projects, RIs are primarily used to support embankments (Figure 2.1) and retaining walls (Figure 2.2) to reduce excessive settlement, improving bearing capacity, and enhancing slope stability. Figures 2.1 and 2.2 show the various components of a RIS system including embankments/structures, LTP with or without Geosynthetic Reinforcement (GR), RIs, and soft soil or in-situ soil. Figure 2.2 also shows the temporary sheet piles and MSE walls for construction purposes.
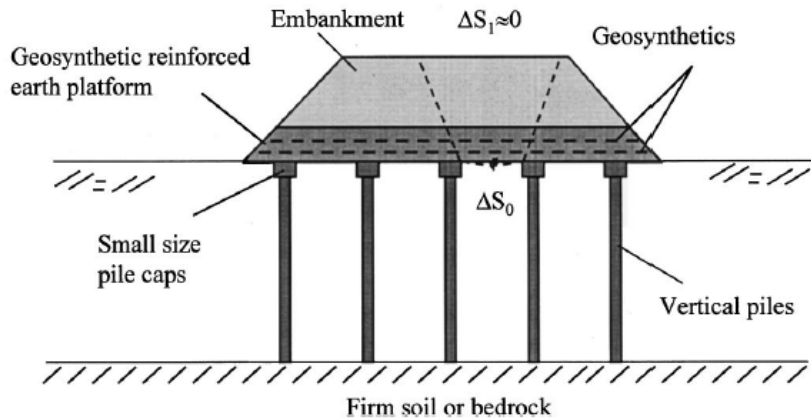
Figure 2.1: Embankment Supported by RIs in Soft Soils
Source: Han and Gabr (2002)
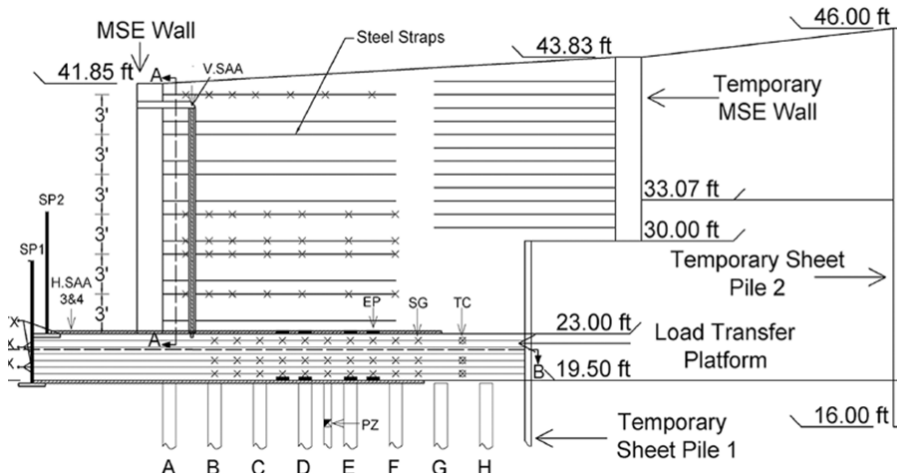
Figure 2.2: Mechanically Stabilized Earth (MSE) Wall Supported by RIs
Source: Izadifar et al. (2024)

2.1.3 Advantages/Limitations of Rigid Inclusions

RIS systems are advantageous because RIs provide high load capacity; thus, reducing loads on the surrounding soil and excessive settlement. Because the surrounding soil shares a portion of the applied load, RIs can also be installed in configurations with relatively wide spacing, resulting in a low area replacement ratio. The use of RIs facilitates faster construction compared to traditional ground improvement methods, and RIs can be installed using various techniques, making them suitable for a variety of soil conditions. The use of RIs may result in lower costs compared to deep foundation methods.

Despite their advantages, however, RIs also have several limitations. Although there are recommended FHWA design methods for load transfer platforms, no well accepted design or analysis methods for RIs and global stability are currently available in the U.S. RI design requires expertise in RIs and composite ground, which demands a thorough understanding of load transfer mechanisms, design, and implementation. The use of RIs may not result in faster construction (due to the need for shallow footing systems) compared to traditional deep foundation methods. In addition, RIs may be subjected to lateral and shear forces from earth structures and seismic events, creating bending moments in the inclusions and posing challenges to their structural capacity. Finally, RI installation may induce lateral displacements in soils that affect previously installed RIs and adjacent existing structures.

7

2.2 Installation Methods

Depending on the type of RIs, they may have different materials and be installed with different equipment. In general, they can be classified into two methods: (1) displacement method and (2) partial/no-displacement method. Basu et al. (2010) summarized common RI installation methods.

2.2.1 Displacement Method

In the displacement method, the installation process causes lateral displacements in the soil and minimizes the generation of spoil because the inclusions are drilled, driven or jacked into the ground. In this process, the stress state of the in-situ soil may undergo significant changes, resulting in a generally stiff load-displacement response and improved bonding between the soil and the inclusion. Densification caused by lateral displacements in granular soils enhances the density, strength, and modulus of the surrounding soil. For saturated soft clays, RI installation causes ground heave and lateral movement of the in-situ soil (as well as a spike in pore water pressures, even at considerable distances from the pile being constructed). Common RI types constructed using this method include: drilled displacement columns (DDCs) or drilled displacement piles (DDPs), vibro-concrete columns (VCCs), driven columns (DCs), and grouted stone columns (GSCs). VCCs were often used in the past but drilled RIs have recently been most commonly used in practice.

2.2.2 Partial/Non-Displacement Method

In the partial/non-displacement method, inclusions are constructed by excavating a cylinder of soil from the ground and filling the resulting void with concrete and reinforcement if needed. Because partial or no lateral displacement of soil occurs, this process results in decreased side bond resistance between the soil and inclusions and the generation of a large amount of spoils. Common RI types constructed using this method include auger cast-in-place (ACIP) piles and continuous flight auger (CFA) piles.

Notably, deep-mixed columns or other soil-mix columns are not classified as RIs in this study, so the mixing method is not discussed further unless needed for comparison purposes.

2.3 Drilling Tools

According to Basu et al. (2010), the drilling tool installing a drilled displacement (DD) RI typically contains a soil displacement body (an enlarged-diameter section designed to facilitate lateral soil movement), a helical, partial-flight auger segment that directs the soil toward the displacement body (except for Schnecken-Verdrängungsbohrpfahl [SVB] piles, which use a large-stem auger), and a specially engineered sacrificial tip fixed to the bottom of the tool. The configuration of the displacement body varies depending on the inclusion type, but it is generally cylindrical and may incorporate one or more helices. Figure 2.3 shows several common drilling tools used in practice.
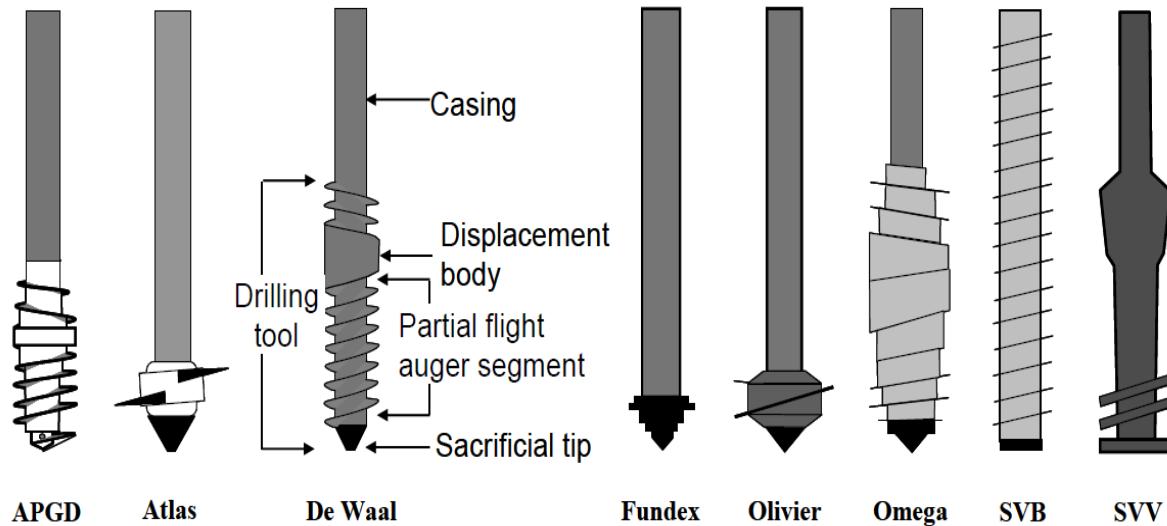
Figure 2.3: Drilling Tools to Install DDCs
Source: Basu et al. (2010)

2.4 Installation Effects

Despite its significant advantages, RI technology also introduces challenges that require careful consideration. The installation process can induce lateral soil movement, ground heave, surrounding soil disturbance, and changes in in-situ stresses, and potentially impacting pre-installed RIs and adjacent structures. Suleiman et al. (2016) conducted a full-scale field unit test to assess the short-term effects of CMC installation on the surrounding soil. They used advanced

instrumentation to monitor changes in lateral soil stresses, pore water pressures, and lateral displacements. Results showed that RI installation caused increased lateral stresses and significant radial soil movement extending 2 to 3 times the inclusion diameter.

King et al. (2018) conducted a field case study with a group RIs under high embankments with significant lateral stresses and found results similar to Suleiman et al. (2016). They also found that the lateral displacement of the soil imposed bending moments and shear forces on pre-installed inclusions. Unreinforced RIs are prone to cracking from installation-induced movement and force, resulting in decreased lateral resistance — a critical factor often neglected in design. King et al. (2018) recommended adopting a more realistic approach in numerical modeling that accounts for the potential cracking of unreinforced inclusions and the reduction in lateral resistance due to installation effects. In another study, Samy et al. (2023) used a cylindrical cavity expansion approach in the finite element numerical analysis to determine the lateral displacement contours showing the installation effect extending up to four times the inclusion diameter, as shown in Figure 2.4.
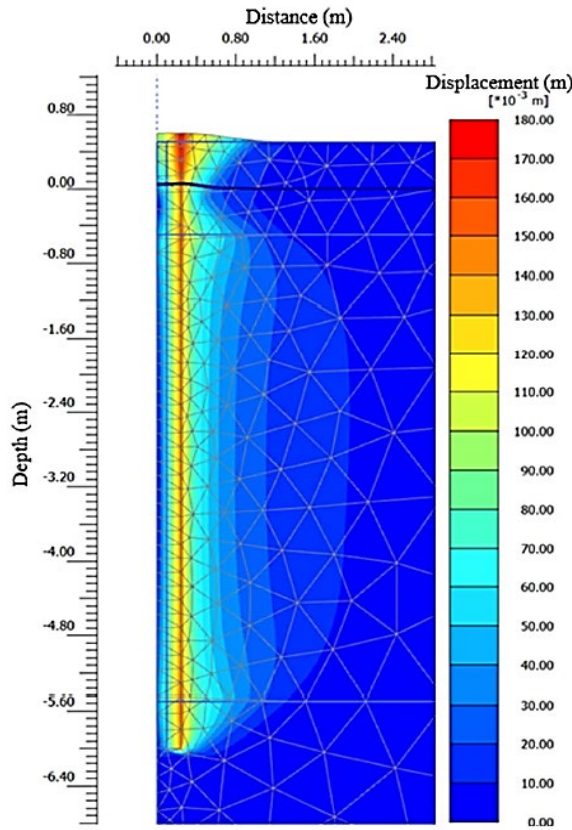
Figure 2.4: Radial Displacement Contours Due to RI Installation
Source: Samy et al. (2023)

Lamb et al. (2022) measured the lateral soil displacements caused by the installation of DDCs in a test RIS embankment and found that lateral soil movements up to 5.5 in. occurred at approximately 3 ft (double the inclusion diameter) and up to 3 in. at 10 ft (6.75 times the inclusion diameter) away from the array of inclusions. They also observed a harmless permanent deformation of approximately 0.4 to 0.6 in. at the adjacent foundation structure (bridge pier cap) during installation. Larisch et al. (2015) observed the vertical uplifts and lateral shifts of pre-installed inclusions caused by the installation of subsequent inclusions. They recommended conducting pre-construction trials to optimize the installation sequence, considering site-specific geological conditions and project requirements. Gallant et al. (2020) tested single and group inclusions to observe installation effects on RIs. They found that group installation led to increased interface friction due to the resulting soil confinement and densification, which enhanced load transfer via downdrag in the subsoil. Nguyen et al. (2019) conducted a three-dimensional

numerical analysis to investigate the effects of RI installation on pre-installed RIs at different curing days by considering different installation sequency and demonstrated that the installation sequence, as shown in Figures 2.5 and 2.6, influences the uplift, lateral deformation, and bending moment of existing RIs. They also found that less tensile yielding occurred on the existing RIs cured for 28 days compared to inclusions cured for 1 day. For both installation sequences (away from or approaching to the target RI), the installation of the closest RI had the most effect. Their finding highlighted the importance of numerical modeling to increase understanding of the complex interactions between RI installation, soil behavior, and existing inclusions.

Due to the high cost and difficulty of conducting such studies, only a limited number of documented full-scale field case studies have investigated the installation effects of RIs. Consequently, numerical simulations based on the cavity expansion approach have primarily been utilized to investigate these effects. When previous studies such as Hill (1998), Bishop et al. (1945), and Yu (2000) adopted the cavity expansion theory to simulate installation, they simplified the penetrating object geometry as a half-sphere since the stress distribution around a spherical body is reasonably well understood. This approach overlooked the complex strain path near the tip of inclusions and the non-spherical geometry, so advanced numerical techniques such as the arbitrary Lagrangian-Eulerian (ALE) method (Liyanapathirana, 2009) and the coupled Eulerian-Lagrangian (CEL) method (Pucker & Grabe, 2012; Hamann et al., 2015) have demonstrated superior capability for capturing penetration patterns, maintaining mesh quality, and effectively overcoming the limitations of traditional methods. However, further validation through additional case studies is necessary to better understand the installation effects of RIs.
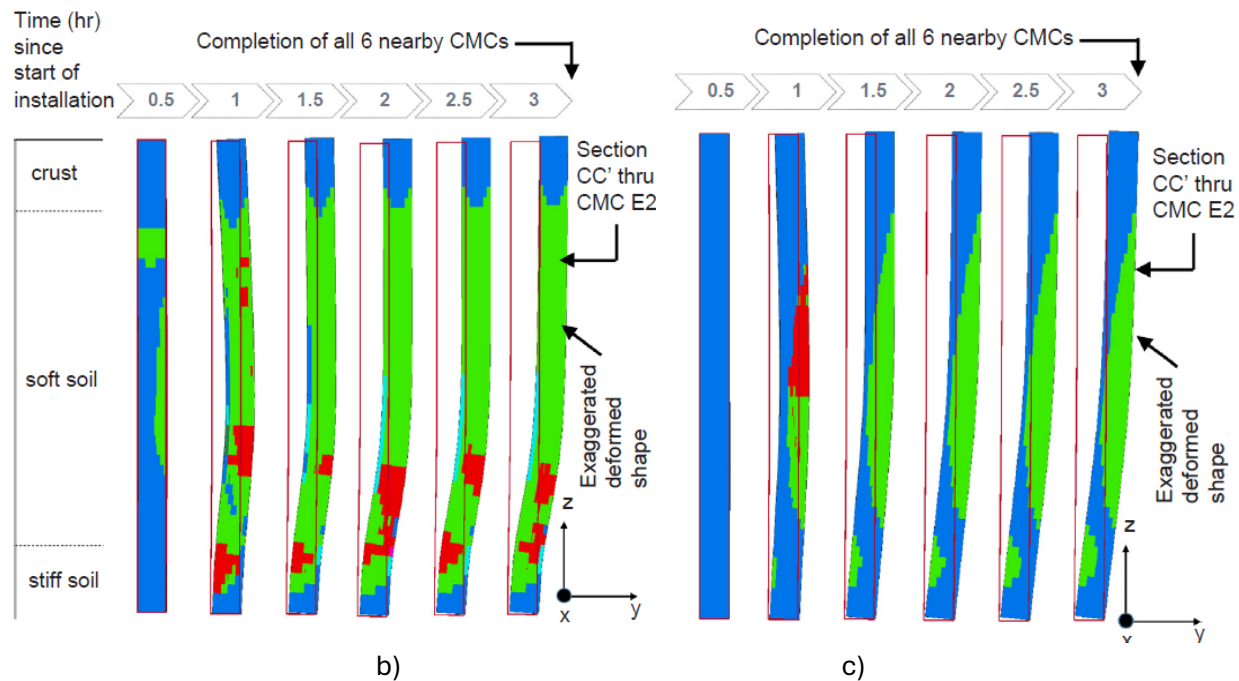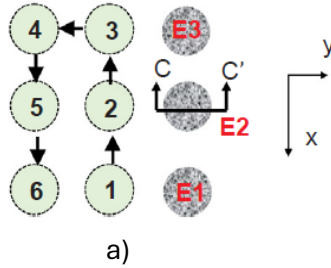
Figure 2.5: Evolution of Tension Plasticity on RI (E2): (a) Installation Sequence 1; (b) Day 1 Curing; and (c) Day 28 Curing before RI (1-6) Installation
Source: Nguyen et al. (2019)
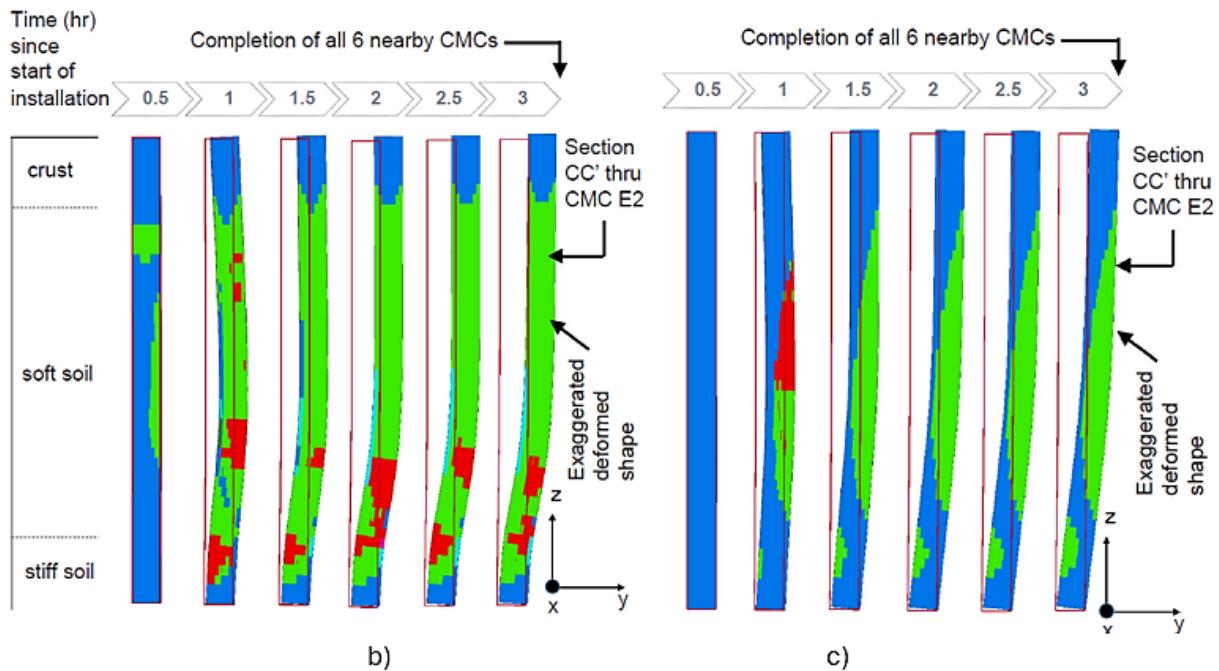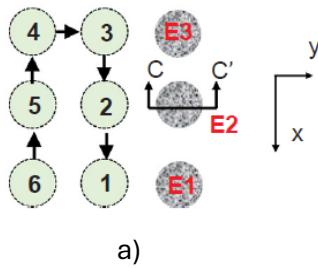
Figure 2.6: Evolution of Tension Plasticity on RI (E2): (a) Installation Sequence 2; (b) Day 1 Curing; and (c) Day 28 Curing before RI (1-6) Installation
Source: Nguyen et al. (2019)

14

2.5 Load Transfer Mechanisms

LTPs may be unreinforced or reinforced by geosynthetic reinforcement. Load transfer mechanisms in the geosynthetic-reinforced RIS embankment system are primarily associated with the LTP via soil arching and tensioned membrane. The unreinforced LTP does not have the tensioned membrane mechanism. Below the LTP, negative skin friction or downdrag occurring below the neutral plane of the RIs causes additional load transfer on RIs.

2.5.1 Soil Arching

Terzaghi (1943) defined soil arching as a mechanical phenomenon where stress is redistributed when part of a soil mass yields while neighboring areas remain stationary. As the yielding soil moves, shear resistance develops along the interface with its adjacent stationary mass. This resistance reduces the stress within the yielding zone while increasing the stress within the adjacent stable region, effectively transferring the load due to the shear forces. This load transfer is called positive soil arching, as shown in Figure 2.7(a). Comparatively, if the load transfer occurs due to upward movement of the yielding mass and generation of shear stress in the downward direction along the interface, it is regarded as negative soil arching, as illustrated in Figure 2.7(b). The soil arching effect in the geosynthetic-reinforced RIS embankment is also represented by Part 'A' in Figure 2.8.
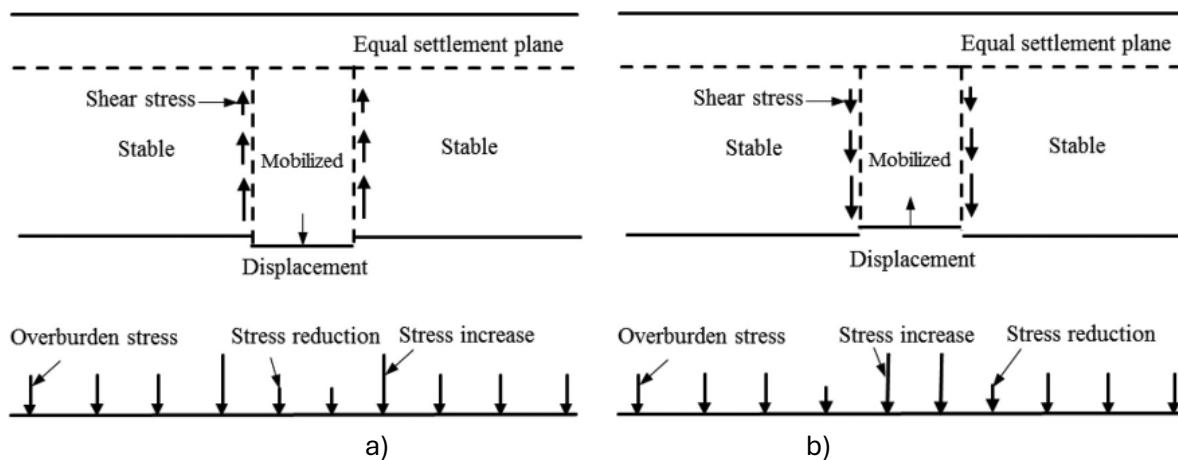
Figure 2.7: Schematics of Soil-Arching Effect: (a) Positive Soil Arching; (b) Negative Soil Arching
Source: Han et al. (2017)
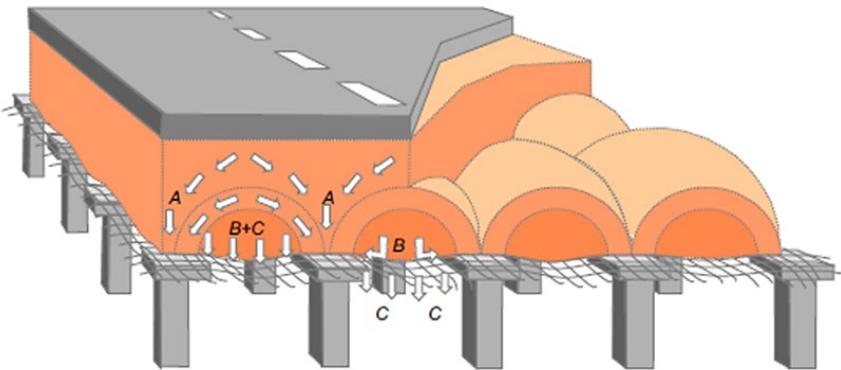
Figure 2.8: Load Transfer in RIS Embankment
Source: Van Eekelen and Han (2020)

2.5.2 Tensioned Membrane

In geosynthetic-reinforced RIS embankments, when the soil between the inclusions deforms or yields, the geosynthetic layer undergoes deformation. This deformation generates tensile forces along the geosynthetic layer. The vertical component of this tension helps resist the downward movement of the soil mass while simultaneously transferring additional load to the inclusions, creating the tensioned membrane effect, as known as Part 'B' in Figure 2.8. The combined action of soil arching and the tensioned membrane effect facilitates efficient load transfer (A+B), as shown in Figure 2.8, from the subsoil to the RIs, enhancing the contributions of RIs and minimizing the load on the subsoil.

2.5.3 Negative Skin Friction

When RIs are subjected to embankment loads or surcharges, the subsoil under the LTP and the RIs settle under the distributed loads resulting from the soil arching and tensioned membrane effect if geosynthetic reinforcement is used. The types and properties of soils immediately below the LTP play an important role in load transfer due to the load sharing inherent in RI systems unless voids develop below the LTP. In RI system applications, the subsoil often has high compressibility so that it settles more than the RIs above a neutral plane. This downward movement of the subsoil exerts a shear force acting along the surface area of the RIs, gradually relieving the load from the soil and increasing the load on the inclusions down to the neutral plane.

16

This effect is known as the downdrag effect and the shear stress along the RIs is negative skin friction, as shown in Figure 2.9.
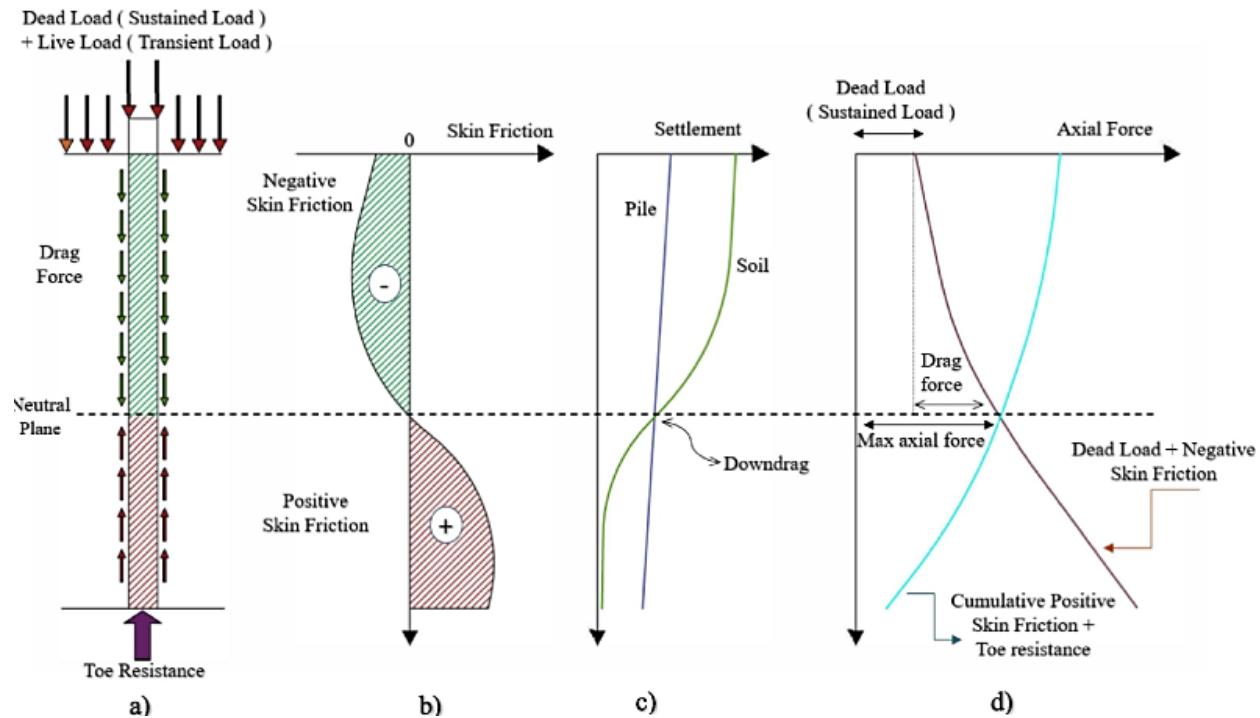
Figure 2.9: Schematics of Force Distribution and Deformation: (a) Drag Force and Neutral Plane; (b) Skin Friction along RI Shaft; (c) Settlement of RI and Soil; and (d) Axial Force along the RI
Source: Chalajour and Blatz (2024)

2.6 Design Methods for Load Transfer Platform

The design and analysis of RIS embankments, particularly geosynthetic-reinforced RIS systems, have evolved over time. Terzaghi (1943) initially laid the early theoretical foundation for understanding load transfer mechanisms in the RIS embankment by proposing an arching theory for a two-dimensional (2D) trapdoor arrangement. This theory explains how stress is redistributed from the soil to stiffer elements such as RIs due to differential settlement. However, Terzaghi's model did not account for the role of geosynthetic reinforcement, which later became a critical component in the RIS systems. Hewlett and Randolph (1988) advanced the theoretical basis for this application by introducing a semi-spherical arching model based on three-dimensional (3D)

17

model tests. Their work provided a more comprehensive understanding of soil arching in RIS systems but still did not consider the effect of geosynthetic reinforcement. This limitation was addressed by Low et al. (1994), who incorporated a body force into the plane-strain differential equation of equilibrium to consider geosynthetic reinforcement. Chen et al. (2008) applied Terzaghi's soil arching concept to develop a theoretical solution for RIS embankments on soft soils considering one-dimensional compression and downdrag effect in an axi-symmetrical unit cell. Abusharar et al. (2009) refined Low's method by adding a uniform surcharge on top of the embankment fill, making the model more applicable to real-world conditions.

The BS 8006-1 (2010) design code adopted a modified version of the Marston and Anderson method and the method from Hewlett and Randolph (1988) to calculate vertical load distribution (the latter method has been more commonly used since the publication of the standard in 2010), while the EBGEO (2011) guidelines were developed based on Zaeske (2001) and Kempfert et al. (2004) which estimated the load on subsoil without reinforcement and then calculated the required geosynthetic tension. Van Eekelen et al. (2013) introduced the Concentric Arches model, which combined and extended the elements of the method in Hewlett and Randolph and the EBGEO (2011) guidelines. This model was incorporated into the Dutch Design Guideline also named CUR226 (2016). Validated by Lee et al. (2021) that the vertical stress distribution on the geosynthetic reinforcement (GR) changed from an inversely triangular shape for low subsoil stiffness to a uniform shape for high subsoil stiffness described in Van Eekelen et al. (2013).

Using the adapted method from Terzaghi (1943), Filz and Smith (2006) developed a design procedure that was adopted in the FHWA ground modification reference manual, as documented by Schaefer et al. (2017). Filz et al. (2019) refined their method by limiting vertical shearing to the portion below the critical height and considering different RI arrangements and two embankment layers (a bridging layer and a general fill). McGuire et al. (2022) updated the calculation spreadsheet GeogridBridge 3.0, by incorporating the incremental form of the adapted Terzaghi method to overcome the limitations of the closed-form solutions presented in Filz et al. (2019). This method is referred to as the FHWA method (Schaefer et al., 2017) in later discussions. Other notable contributions include Carlsson (1987), who proposed a triangular soil wedge model for RIS embankments, and Collin (2004), who improved the method by Guido et al. (1987) using

multiple layers of reinforcement to create a stiff platform. The approach by Collin (2004) was also included in the FHWA ground modification reference manual (Schaefer et al. 2017).

Based on experimental and numerical studies, researchers have proposed different soil arching models and corresponding calculation methods for reduced stress due to soil arching. These models can be categorized according to their deformation patterns: (a) curved, (b) triangular and (c) vertical. However, McGuire and Filz (2008) found that these models resulted in significant differences in the calculated vertical stresses on the geosynthetic. As a result, the tensile forces in the geosynthetic reinforcement calculated by these models differed by 10 times, which is not acceptable for practice. According to Han (2021a, b), the primary reasons for these differences was different stages of soil arching were assumed in the model development of these models. Han (2021a, b) proposed a simplified method considering progressive development of soil arching with subsoil movement. Pham and Dias (2021), Izadifar et al. (2023), and Nobahar et al. (2024) also assessed several design methods and found discrepancies between the predicted results and the measured data from various field case studies documented in the literature. Among these methods, BS 8006-1 (2010), EBGEO (2011), CUR226 (2016), and Schaefer et al. (2017) are most common in the literature and practice, so they are described in the following sections. Due to the complexities of RIS embankments, numerical methods have been increasingly used to design these systems.

2.6.1 BS 8006-1 Method

The British Standard BS 8006-1:2010+A1:2016 or BSI (2016) is a newer version of the BS 8006-1 (2010) and commonly used for designing RIS embankments due to its simplicity. In this report, BS 8006-1 (2010) is referred because this designation is commonly used in the literature. This method consists of two theoretical solutions: a modified version of Marston and Anderson (1913)'s formula and Hewlett and Randolph (1988). Although the Marston formula is included in BS 8006-1 (2010), it is used less often because it is a 3D version of a model that was originally developed for culverts under plane strain conditions. The method in Hewlett and Randolph (1988) is more commonly used because it was developed based on a 3D layout of RIs. This approach, which relies on mechanisms observed in model tests, assuming that soil arching

between adjacent RIs creates a series of hemispherical domes, identifies critical failure locations at the crown of the arch and at the inclusion head/cap (Figure 2.10). The arching efficacy or load efficacy (E_a) is the proportion of embankment weight supported by RIs, with the remaining load distributed to the geosynthetic reinforcement ($1 - E_a$). Notably, this method does not account for subsoil support, and the minimum arching efficacy between the crown, E_{crown}, and inclusion head/cap, E_{cap}, governs the design.
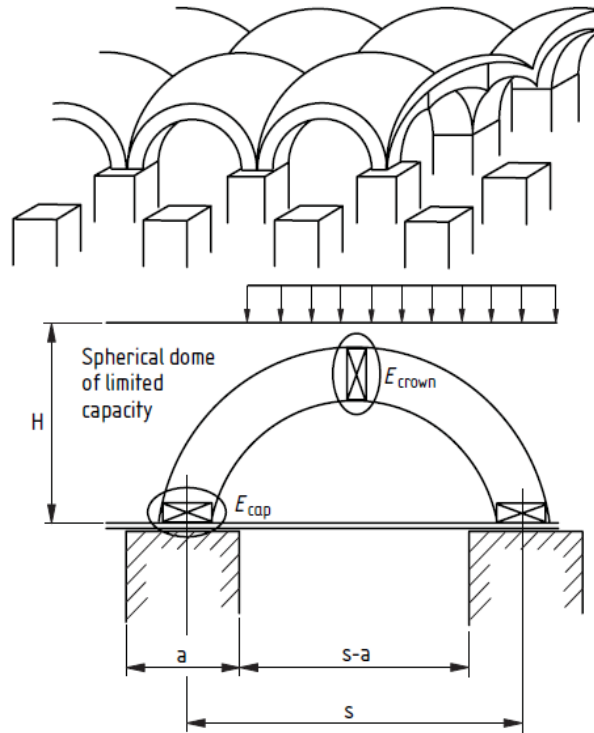
Figure 2.10: Dome-Shape Arching Theory
Source: Hewlett and Randolph (1988)

The arching efficacy on the crown of the arch between the RIs may be determined as:

$$E_{crown} = 1 - \left[1 - \left(\frac{a}{s}\right)^2\right](M - MN + O)$$

Equation 2.1

Where:

a = width or equivalent width of the inclusion head or cap,

s = center-to-center spacing between adjacent inclusions, and

M, N, and O = calculation coefficients given by:

20

$$M = \left[1 - \left(\frac{a}{s}\right)\right]^{2(k_p - 1)}$$

$$N = \frac{s}{\sqrt{2}H}\left(\frac{2k_p - 2}{2k_p - 3}\right)$$

$$O = \frac{s - a}{\sqrt{2}H}\left(\frac{2k_p - 2}{2k_p - 3}\right)$$

Equation 2.2

Where:

K_p = the coefficient of passive earth pressure, and

H = height of the embankment

$$K_p = \frac{1 + \sin(\phi')}{1 - \sin(\phi')}$$

Equation 2.3

Where:

ϕ' = effective friction angle of the embankment fill in degrees

The arching efficiency at the inclusion head or cap can be determined by the following expression:

$$E_{cap} = \frac{\beta}{1 + \beta}$$

Equation 2.4

$$\beta = \frac{2K_p}{\left(K_p + 1\right)\left(1 + \frac{a}{s}\right)}\left[\left(1 - \frac{a}{s}\right)^{-K_p} - \left(1 + K_P\frac{a}{s}\right)\right]$$

Equation 2.5

BS 8006-1 (2010) recommends that the minimum load arching efficacy, E_{min}, should be used in the subsequent formulation to determine the maximum distributed load W_T per unit width carried by the reinforcement between adjacent inclusion caps or heads:

$$W_T = \frac{s(\gamma H + q)(1 - E_{min})s^2}{(s^2 - a^2)}$$

<div align="right">**Equation 2.6**</div>

Where:

γ = unit weight of the fill,

q = the surcharge on the embankment crest, and

E_{min} = the minimum of E_{crown} and E_{cap}

The maximum tension in the geosynthetic reinforcement T is then calculated at certain tensile strain ε using the following equation:

$$T = \frac{W_T}{2a}(s - a)\sqrt{1 + \frac{1}{6\varepsilon}}$$

<div align="right">**Equation 2.7**</div>

Although BS 8006-1 (2010) recommends a design strain of 5% in geosynthetic reinforcement, this value may not be practical for all cases. Therefore, Pham (2020) and Pham and Dias (2021) modified Equation 2.7 using the reinforcement tension-strain relationship ($T = J e$):

$$6T^3 - 6\omega^2 T - \omega^2 J = 0$$

<div align="right">**Equation 2.8**</div>

Where:

J = the geosynthetic tensile stiffness

$$\omega = \frac{W_T(s - a)}{2a}$$

<div align="right">**Equation 2.9**</div>

Furthermore, the deformed shape of the reinforcement spanning the void is approximated by a parabolic curve, meaning the maximum differential settlement between the inclusion head or cap and the subsoil, according to BS 8006-1 (2010) can be calculated as:

$$y = (s - a)\sqrt{\frac{3\varepsilon}{8}} = (s - a)\sqrt{\frac{3T}{8J}}$$

<div align="right">**Equation 2.10**</div>

According to the BS 8006-1 method, the total load from the embankment is either directly supported by the RIs or indirectly transferred to them through the reinforcement spanning the inclusions. In other words, a void is assumed under the geosynthetic reinforcement. However, the subsoil between the inclusions may carry a portion of the overlying load in most real situations.

2.6.2 EBGEO Method

The method in EBGEO (2011) or German design guidelines uses the ground arching equilibrium model, based on the multi-arching theory as shown in Figure 2.11, to describe the vertical stress distribution on RI heads or caps and subsoils. This model, which was initially proposed by Kempfert et al. (1999) and Zaeske (2001) and further improved by Kempfert et al. (2004), is based on a lower-bound plasticity theory, pilot-scale tests, and numerical analyses. The method assumes a triangular pressure distribution on the geosynthetic strips between adjacent piles for calculations and introduces elastic subsoil support to consider the bearing mechanism. The guideline provides the following formulas to calculate the vertical stresses on the geosynthetic reinforcement ($\sigma_s{}^a$) and on the top of RIs ($\sigma_c{}^a$):

$$\sigma_s{}^a = l_1{}^x \left(\gamma + \frac{q}{H}\right) \left[H\left(l_1 + h^2{}_g l_2\right)^{-x} + h_g\left((l_1 + \frac{h^2{}_g l_2}{4})^{-x} - \left(l_1 + h^2{}_g l_2\right)^{-x}\right)\right]$$

Equation 2.11

$$\sigma_c{}^a = \left[\left((\gamma H + q) - \sigma_s{}^a\right)\frac{A}{A_c} + \sigma_s{}^a\right]$$

Equation 2.12

Where

$$l_1 = \frac{(S_d - d)^2}{8}; \; l_2 = \frac{S^2 + 2dS_d - d^2}{2S_d{}^2}; \; X = \frac{d(Kp - 1)}{l_2 S_d}; \; S_d = \sqrt{S^2{}_x + S^2{}_y}$$

Equation 2.13

and

$$h_g = \frac{S_d}{2} \; for \; H \geq \frac{S_d}{2} \qquad or \qquad h_g = H \; for \; H < \frac{S_d}{2}$$

Equation 2.14

Where:

q = the surcharge applied on the top of the embankment,

h_g = the arching height,

S_d = the distance along the diagonal between two adjacent RIs,

S_x and S_y = the center-to-center inclusion spacing in the x and y directions, respectively,

A = an influence area of one inclusion head or cap, and

A_c = the area of an inclusion cap.
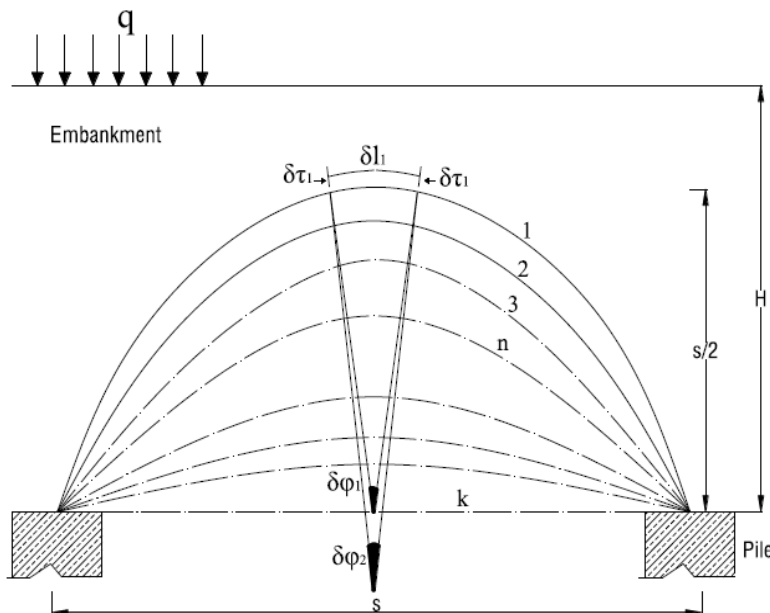
Figure 2.11: Multi-Arching Theory
Source: Kempfert et al. (2004)

Furthermore, a membrane theory is applied to calculate the tensile force, T in the geosynthetic reinforcement. The maximum strain, ε_{max} developed in the geosynthetic can be estimated according to the design charts provided by the EBGEO design guidelines. The maximum tensile force T_{max} due to the membrane action is:

24

$$T_{max} = J\varepsilon_{max}$$

Where *J* is the geosynthetic tensile stiffness.

here:

$$k_s = \frac{E_{s,1,k} \cdot E_{s,2,k} \cdot E_{s,3,k}}{t_{W,1} \cdot E_{s,2,k} \cdot E_{s,3,k} + t_{W,2} \cdot E_{s,1,k} \cdot E_{s,3,k} + t_{W,3} \cdot E_{s,1,k} \cdot E_s}$$
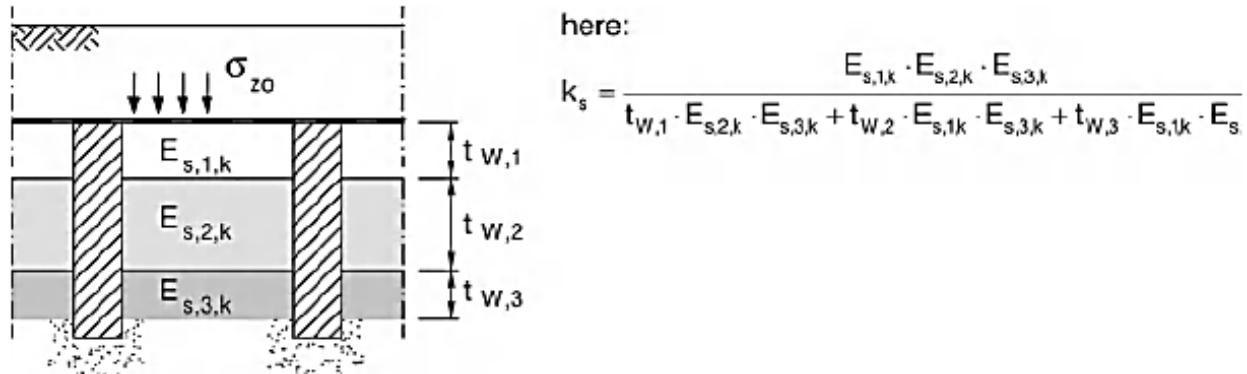
Figure 2.12: Estimation of Modulus of Subgrade Reaction for Stratified Ground below Reinforcement Plane
Source: EBGEO (2011)

EBGEO (2011) estimates the maximum sag or differential settlement of the GR between the RI head or cap and the midspan of the subsoil from the design charts provided by the EBGEO design guidelines. However, researchers, such as Izadifar et al. (2024) and Pham and Dias (2021) used Equation 2.10 from BS 8006-1 (2010) based on the strain obtained from the design charts of EBGEO (2011) to estimate the differential settlement of the GR. The EBGEO design charts use a subgrade reaction modulus, k_s to estimate the tensile strain of the GR. The reaction modulus of the subgrade, k_s, for a homogeneous soft soil stratum with a constrained modulus, E_s, and a thickness, t_w is calculated as:

$$k_s = \frac{E_s}{t_w}$$

Similarly, multiple soil strata with n layers below the reinforcement can be approximately modeled using an average modulus of subgrade reaction, k_s, proportionally weighted to the thicknesses of the individual layer, $t_{w,i}$ and its constrained modulus, $E_{s,i}$:

$$k_s = \frac{\prod_{i=1}^{n} t_{w,i}}{\sum_{i=1}^{n} \frac{t_{w,i}}{E_{s,i}}}$$

Equation 2.17

The subgrade reaction modulus was further modified by Lodder et al. (2012) as follows:

$$k_{s,modified} = \frac{A_{lx} k_s L_w}{J b_{ers}}$$

Equation 2.18

$$b_{ers} = \frac{1}{2} d \sqrt{\pi}$$

Equation 2.19

$$A_{lx} = \frac{1}{2} S_x S_y - d^2 \arctan\left(\frac{S_y}{S_x}\right) \frac{\pi}{180}$$

Equation 2.20

$$A_{ly} = \frac{1}{2} S_x S_y - d^2 \arctan\left(\frac{S_x}{S_y}\right) \frac{\pi}{180}$$

Equation 2.21

Where:

b_{ers} = equivalent width of the RIs,

d = the diameter of RIs,

L_w = the clear spacing between RIs, and

J = geosynthetic tensile stiffness.

2.6.3 CUR226 Method

CUR226 (2016) or the Dutch Design Guidelines incorporates the concentric arches model shown in Figure 2.13, which was developed for the design of geosynthetic-reinforced RIS embankments using a limit equilibrium approach. The concept of concentric arches was derived

from the observations of stress formation during a series of laboratory tests conducted by Van Eekelen et al. (2012). According to this model, the vertical load is divided into three components: load on the inclusion head or cap, which is transferred directly through the arching effect; load on the geosynthetic square area ($F_{GRsquare}$) inside four inclusion heads, resulting from 3D hemispherical arches; and load on the geosynthetic strips ($F_{GRstrips}$) between inclusion heads, resulting from 2D arches between the RIs. A smaller arch applies less load on the GR, while a larger arch exerts more load. Consequently, a significant portion of the embankment load is transferred directly to the inclusion head or cap (load A), while the remaining load is distributed across the GR strips between adjacent RIs.

According to CUR226 (2016), the remaining load acting on the GR and subsoil (P_s^a) is:

$$P_s^a = F_{GRsquare} + F_{GRstrips}$$

Equation 2.22

The proportion of the load transferred directly onto the RI head or cap by arching effect (P_c^a) is:

$$P_c^a = (\gamma H + q)S_x S_y - \left(F_{GRsquare} + F_{GRstrips}\right)$$

Equation 2.23

After calculating the vertical stress, geosynthetic tension is determined by assuming the vertical load distribution along the GR is either uniform or inversely triangular, calculated as:

$$T(x) = T_H\sqrt{1 + \left(y'(x)\right)^2}$$

Equation 2.24

Where:

$y(x)$ = geosynthetic-reinforcement deflection, and

$y'(x)$ = the derivative of the deflection.

The horizontal component of tensile force, T_H, can be obtained using:

$$T_H = \int_0^{\frac{L}{2}} \sqrt{1 + \left(y'(x)\right)^2}\, dx - \frac{L}{2} = (\frac{1}{J_{GR}})\int_0^{\frac{L}{2}} T(x)\, dx$$

Equation 2.25

Where J_{GR} is the tensile stiffness of the geosynthetic reinforcement.

Geosynthetic deflection $y(x)$ is considered the differential settlement in this method.
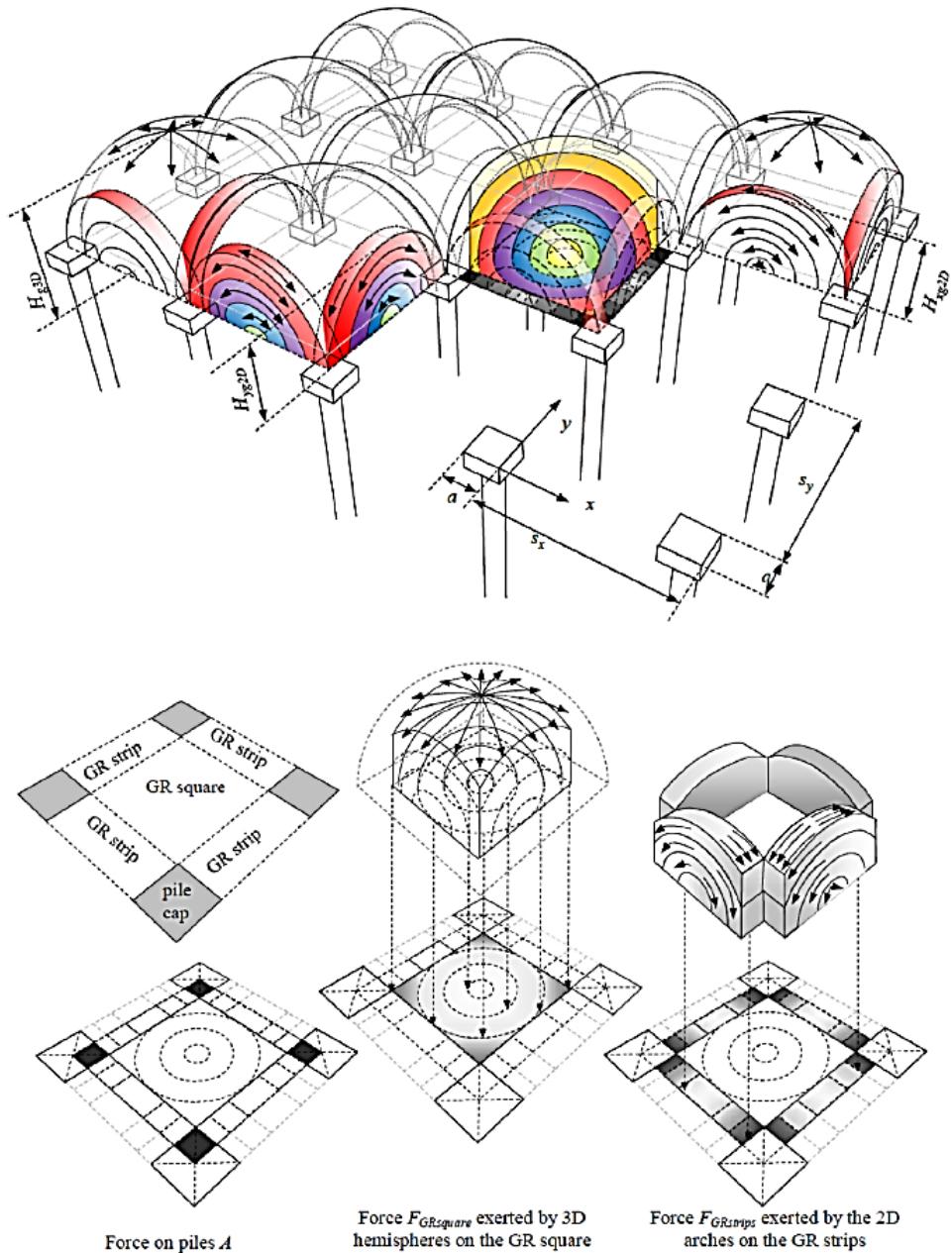
Figure 2.13: Concentric Arches Model
Source: Van Eekelen et al. (2013)

2.6.4 FHWA Method

The FHWA reference manual recommends the use of the load-displacement compatibility (LDC) method to evaluate anticipated settlement and geosynthetic tension for vertical load transfer in RIS embankments (Schaefer et al. 2017). The LDC method, initially developed by Filz and Smith (2006) then modified by McGuire (2011), Sloan (2011), and Filz et al. (2019), simultaneously accounts for three distinct load transfer mechanisms (Figure 2.14): soil arching within the embankment, vertical load transfer due to GR tension, and negative skin friction between the RIs and subsoil, which induces a downdrag force. The LDC method ensures the vertical equilibrium by satisfying Equation 2.26.

$$\sigma_{avg} = \gamma_1 H_1 + \gamma_2 H_2 + q = a_s \sigma_{col,geotop} + (1 - a_s)\sigma_{soil,geotop}$$

Equation 2.26

Where:

σ_{avg} = the average stress imposed at the base of the embankment;

$\gamma_{1,2}$ = unit weight of the embankment soil layers;

$H_{1,2}$ = height of respective embankment layers;

q = surcharge;

a_s = area replacement ratio of A_c/A;

$\sigma_{col,geotop}$ = stress acting on the RIs due to the embankment load, exclusively considering load transfer through soil arching;

$\sigma_{soil,geotop}$ = stress acting on the subsoil due to the embankment load, exclusively considering load transfer through soil arching;

$\sigma_{col,geobot}$ = stress acting on the RIs due to the embankment load, considering both soil arching and the tensioned geosynthetic (if present);

$\sigma_{soil,geobot}$ = stress acting on the subsoil due to the embankment load, considering soil arching and the tensioned geosynthetic (if present), as shown in Figure 2.15.

Terzaghi (1943) developed a 2D analytical model to describe soil arching, assuming no change in soil volume and stationary soil above fixed supports. Russell and Pierpoint (1997) and Russell et al. (2003), extended this model to 3D RIS embankments, by introducing the adapted Terzaghi method, which used the LDC to calculate load transfer through soil arching. Although

this method was initially limited to square inclusion arrays, Sloan (2011) enhanced the method by providing closed-form equations applicable to rectangular and triangular arrays. The details of the development of this method are available in Filz et al. (2019).
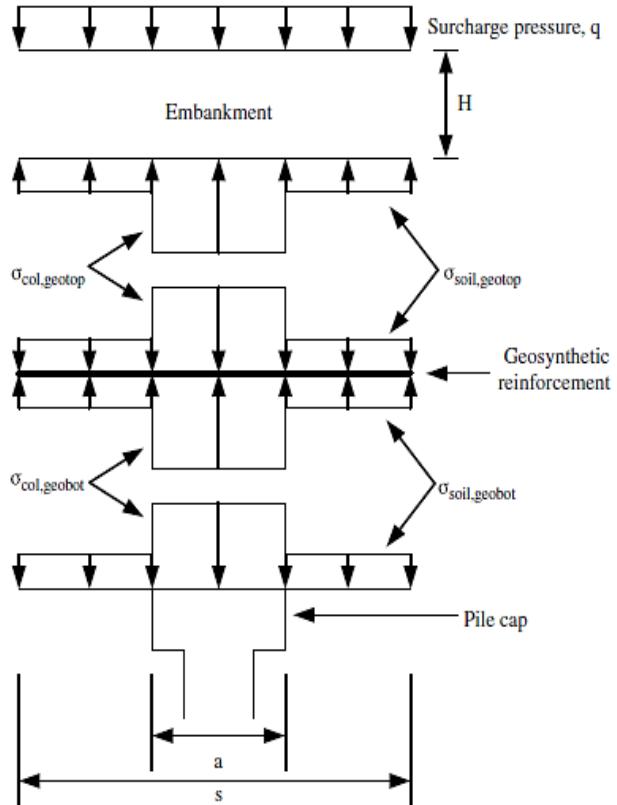
Figure 2.14: Load Transfer Mechanism
Source: McGuire et al. (2022)
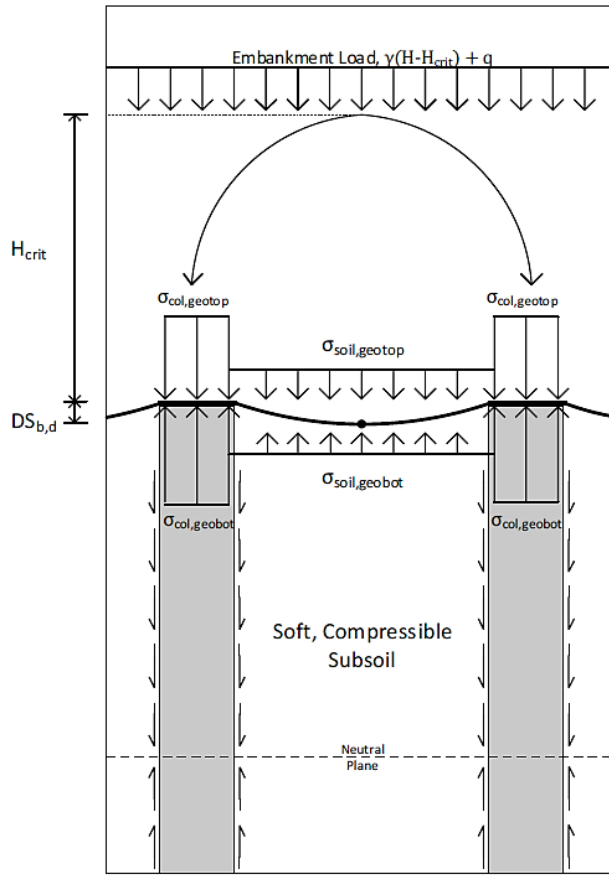
Figure 2.15: Vertical Stress in Profile View
Source: Filz and Smith (2006)

The stress reduction ratio (SRR) quantifies the reduction in the vertical stress on the subsoil or GR due to the weight of the embankment and surface loads, soil arching, and a tensioned membrane effect. According to Filz and Smith (2006), SRR can be expressed as SRR_{emb} for the embankment, SRR_{net} for the GR, and SRR_{fndn} for the foundation soil as follows.

$$SRR_{emb} = \frac{\sigma_{soil,geotop}}{\sigma_{avg}}$$

Equation 2.27

$$SRR_{net} = \frac{\sigma_{net}}{\sigma_{avg}} = \frac{\sigma_{soil,geotop} - \sigma_{soil,geobot}}{\sigma_{avg}}$$

Equation 2.28

$$SRR_{fndn} = \frac{\sigma_{soil,geobot}}{\sigma_{avg}}$$

<div align="right">**Equation 2.29**</div>

The Excel spreadsheet GeogridBridge 3.0 or GGB3 that includes all the calculation procedures reviewed above is available at https://doi.org/10.17605/OSF.IO/HQRBU, which was developed to solve the nonlinear equations for vertical stresses on subsoil and GR (Filz et al., 2019) and compute the value of SRR_{net}. The GeogridBridge 3.0 subsequently introduced incremental soil thickness, addressing the limitations of closed-form solutions and enabling the analysis of embankments with multiple fill materials and achieving high accuracy with sufficient increments. In other words, this spreadsheet allows a user to select a smaller layer thickness for calculations. GeogridBridge 3.0 maintains displacement compatibility by ensuring the maximum differential settlement at the base of the embankment, $DS_{b,d}$, is consistent across all mechanisms (soil arching, tensioned membrane, and subsoil settlement). For the subsoil settlement, $DS_{b,d}$, is calculated as the difference between the elastic compression of the RIs above the neutral plane and the maximum settlement of the subsoil, which is assumed to be twice the average soil settlement according to Russell et al. (2003). The theory manual for GeogridBridge 3.0 provides detailed calculations for the vertical stresses on the subsoil and GR, the differential settlement between RIs and subsoil, and the tension and strain developed in the GR.

2.7 Global Stability

The BS 8006-1 (2010), EBGEO (2011), CUR226 (2016), and Schaefer et al. (2017) methods are primarily used to design LTPs and embankments on RIs under vertical loads within the central portion of the embankment, but the stability of an RIS embankment close to slopes must also be addressed in the design. Without RIs, an embankment on soft ground may develop large deformations and global or deep-seated failures (Abusharar & Han, 2011; Zhang et al., 2014). Traditionally, global stability is analyzed using limit equilibrium methods (LEM), such as Bishop's Method (Bishop, 1955) and Spencer's Method (Spencer, 1967). However, the shape for slip surfaces must be assumed in these methods, and the location of the critical slip surface must be identified via trial and error (Fredlund, 2021). LEM-based software has been widely used to

analyze global stability of embankments over soft ground. Numerical methods, such as the finite element method (FEM) and the finite different method (FDM), have been increasingly used after incorporating the strength reduction method for stability analysis (Duncan, 1996; Dawson et al., 1999; Griffiths & Lane, 1999). Recent research on stability analysis of RIS embankments mainly focuses on failure mechanisms of the inclusion group and simplified methods for analysis.

2.7.1 Failure Mechanisms

Even though deep mixed columns are not considered as RIs in this study, strong and stiff deep mixed columns may have similar behavior as RIs in terms of their stability under embankment loading. Han et al. (2005) concluded that deep mixed columns failed under embankment loading due to their shearing, bending, or rotation with increased column strength and the strong column tended to fail under bending or rotation. Yu et al. (2021) found that RIs beneath the embankment experienced progressive failure, starting from those located at the embankment toe and extending toward the center as embankment loading increased. The presence of geosynthetic reinforcement increased the embankment load at failure. Gallant and Botero-Lopez (2021) concluded that RI fracturing resulted from lateral ground deformations; however, its occurrence alone did not trigger basal instability or contribute to lateral spreading.

2.7.2 Simplified Methods

The literature highlights several simplified methods to evaluate the stability of RIS embankments. The equivalent strength method (ESM), the stress reduction method (SRM), and the pile support method (PSM) are described in the following section and evaluated in Chapter 5 by comparing their results with numerical analysis results.

2.7.2.1 Equivalent Strength Method

The ESM is commonly used for stability analysis of embankments on a composite ground (Abusharar & Han, 2011; Zhang et al., 2014; Han et al., 2004). This method considers the improved ground to be a uniform composite area by using equivalent shear strength to account for the contribution of inclusions, as shown in Figure 2.16. The embankment on the improved ground

represented by an equivalent area can be easily analyzed by a LEM or numerical method. The following equations are used to calculate the properties of the improved area:

$$E_{eq} = E_{ri}a_{ri} + E_s(1 - a_{ri})$$

Equation 2.30

$$c_{eq} = c_{ri}a_{ri} + c_s(1 - a_{ri})$$

Equation 2.31

$$\phi_{eq} = arc\tan(a_{ri}\tan\phi_{ri} + (1 - a_{ri})\tan\phi_s)$$

Equation 2.32

Where:

E_{eq}, c_{eq}, and ϕ_{eq} = the equivalent modulus, cohesion, and friction angle, respectively, of the improved area;

a_{ri} = the area replacement ratio of the RIs;

E_{ri}, c_{ri}, and ϕ_{ri} = the modulus, cohesion, and friction angle, respectively, of the RIs;

E_s, c_s, and ϕ_s = the modulus, cohesion, and friction angle, respectively, of the subsoil.
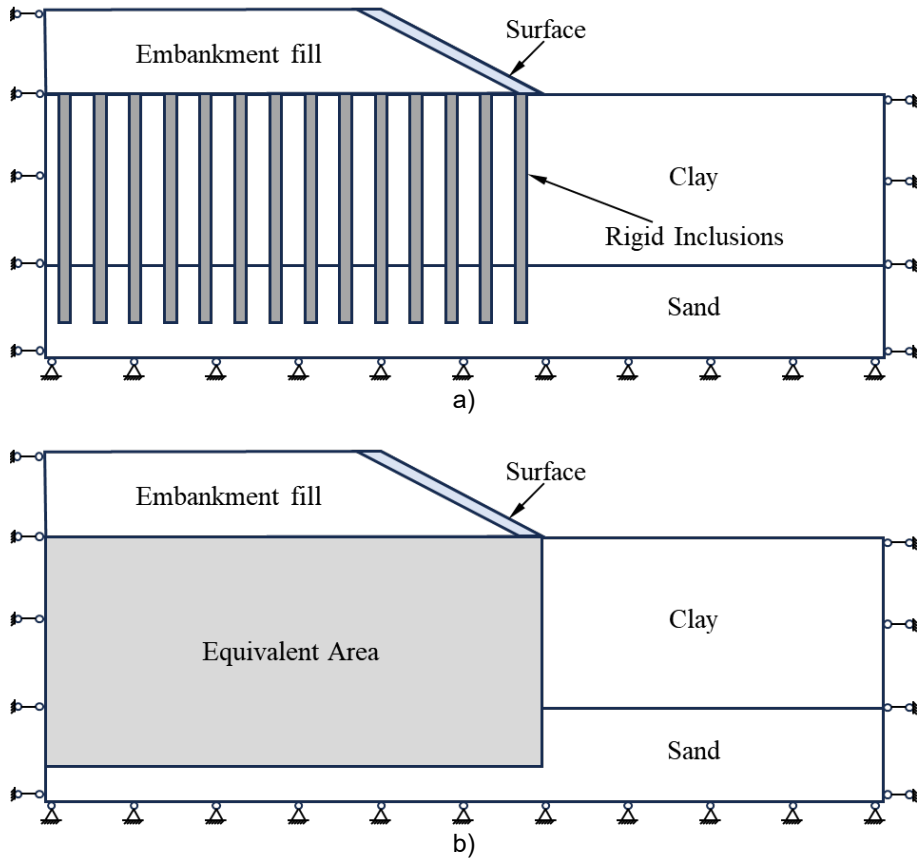
Figure 2.16: Equivalent Strength Method: (a) Cross Section of the RIS Embankment Model; (b) Cross Section of the Embankment Model with the Equivalent Area

2.7.2.2 Stress Reduction Method

When an embankment load is applied to improved ground, the load is distributed on the subsoil and the RIs, and the stress applied on the subsoil significantly decreases due to the stiffness difference between the RIs and the subsoil. Due to the stiffness difference between the RIs and the subsoil, the stress applied onto the subsoil is much reduced. In this study, the reduced stress was determined based on a numerical analysis of a column-wall model. This reduced stress may also be estimated using a soil arching model, which was not investigated in the current study. The SRM analyzes the stability of the RIS embankment as the application of the reduced stress on the soil with no RIs. The contribution of the RIs can be determined by directly applying the reduced stress or by placing the embankment fill with a reduced unit weight on the soil, as shown in Figure 2.17.

The reduced stresses may be estimated by numerical methods (adopted in this study) or soil arching models (not assessed in this study).
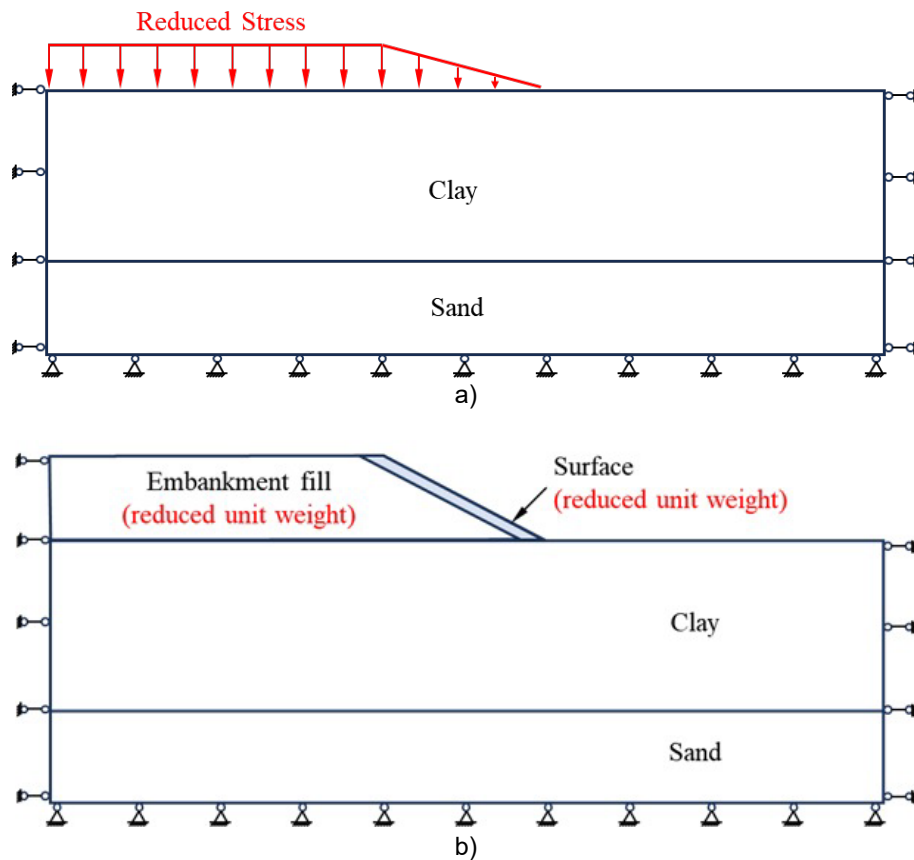
Figure 2.17: Reduced Stress Method: (a)Reducing the Embankment Load; (b) Reducing the Unit Weight of the Embankment

2.7.2.3 Pile Support Method

BS 8006-1 (2010) recommends a PSM to analyze the global stability of a RIS embankment on soft ground, as shown in Figure 2.18. The PSM considers the benefits of the RIs and the GR. The factor of safety (FS) of the global stability of the RIS embankment on the soft ground can be calculated by:

$$FS = \frac{M_{RS} + M_{RP} + M_{RR}}{M_D}$$

Equation 2.33

36

$$M_D = \left[\sum (f_{fs} W_i + f_q b_j W_{si}) \sin \alpha_i \right] R_d$$

Equation 2.34

$$M_{RS} = \sum_{i=1}^{n} \frac{\left[\frac{c' b_i}{f_{ms}} + (f_{fs} W_i + f_q b_j W_{si})(1 - r_u) \frac{\tan \phi'_{cvi}}{f_{ms}} \right] \sec \alpha_i \, R_d}{1 + \frac{\tan \phi'_{cvi} \tan \alpha_i}{f_{ms}}}$$

Equation 2.35

$$M_{RP} = F_{p1} X_{p1} + F_{p2} X_{p2}$$

Equation 2.36

$$M_{RR} = T_r Y$$

Equation 2.37

Where:

FS = the factor of safety;

M_D = the driving moment due to the embankment fill and the surcharge;

M_{RS} = the resisting moment due to the subsoil;

M_{RP} = the resisting moment due to RIs;

M_{RR} = the resisting moment due to the geosynthetic reinforcement;

f_{fs}, f_q, f_{ms} = the load factor for soil mass, load factor for live loads, and soil material factor, respectively;

W_i = the weight of a soil slice;

W_{si} = the surcharge load of a slice;

b_j = the width of the slice;

α_i = the angle of the base of the slice with the horizontal line;

R_d = the radius of the critical slip surface;

c' = effective cohesion of the subsoil;

ϕ'_{cvi} = effective friction angle of the embankment fill;

r_u = the pore pressure ratio;

F_p = resistance of the RI;

X_p = the lever arm of RI resistance to the slip surface center;

T_r = resistance of the geosynthetic reinforcement; and

Y = the lever arm of the geosynthetic resistance to the slip surface center.

For a serviceability limit state, $f_{fs} = f_q = f_{ms} = 1$. When there are no surcharge load and GR, Equations 2.33 to 2.35 become:

$$FS = \frac{M_{RS} + M_{RP}}{M_D}$$

Equation 2.38

$$M_D = \sum W_i \sin \alpha_i R_d$$

Equation 2.39

$$M_{RS} = \sum_{i=1}^{n} \frac{[c'b_i + W_i(1 - r_u) \tan \phi'_{cvi}] \sec \alpha_i R_d}{1 + \tan \phi'_{cvi} \tan \alpha_i}$$

Equation 2.40

$$M_{RP} = F_{p1}X_{p1} + F_{p2}X_{p2}$$

Equation 2.41
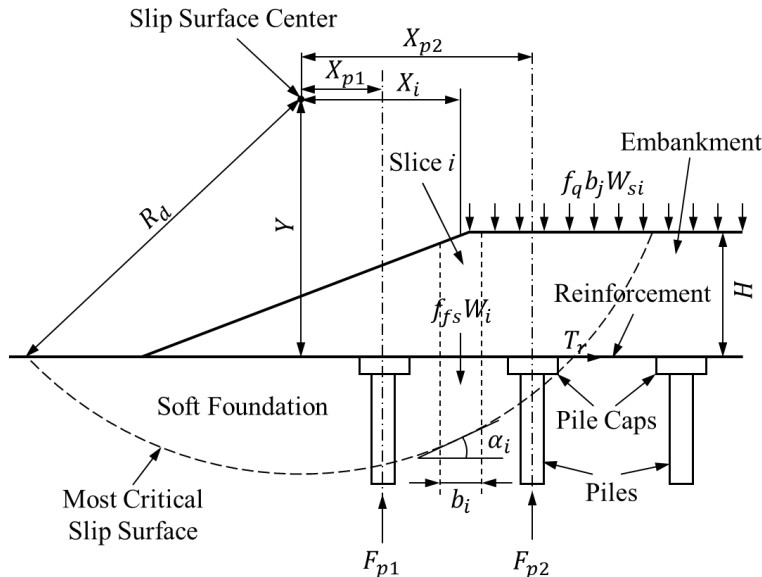
Figure 2.18: Global Stability of RIS Embankments Analyzed by the PSM
Source: BS 8006-1 (2010)

Despite its specifications, BS 8006-1 (2010) does not provide guidelines on how to calculate the resistance of RIs. Therefore, to estimate this resistance, the end bearing capacity and

side friction of the RIs may be considered as the resistance for RIs. The side friction under an undrained condition can be estimated by the α method:

$$f_s = \alpha c_u$$

Equation 2.42

Where α is the interface reduction factor, mostly ranging from 0.5 to 1.0.

A smaller value may be used for a replacement method, but a larger value may be used for a displacement method.

The side friction under a drained condition can be estimated by the β method, that is:

$$f_s = \beta_i \sigma'_{z0}$$

Equation 2.43

Where:

$\beta_i = K \tan \delta_i$;

σ'_{z0} = effective overburden stress;

K = the coefficient of lateral earth pressure, typically 0.5–1.0 K_0;

K_0 = the coefficient of lateral earth pressure at rest;

δ_i = the interface friction angle (mostly 0.8–1.0 times the soil effective friction angle, ϕ') (Han, 2015).

The end bearing capacity of the RIs under an undrained condition is:

$$q_t = N_c^* c_u \approx 9 c_u$$

Equation 2.44

That under a drained condition is:

$$q_t = 0.5 d_{ri} N_\gamma^* + \sigma'_D N_q^*$$

Equation 2.45

Where:

d_{ri} = the diameter of RIs;

σ'_D = effective overburden stress at the depth of the RI toe; and

N_γ^*, N_q^* are provided in Table 2.2.

Table 2.2: N_γ^* and N_q^*

$\phi'(°)$	20	22	24	26	28	30	32	34	36	38	40	42	44	46
N_γ^*	3.3	4.3	5.8	7.4	10	14	19	24	32	48	66	90	120	180
N_q^*	13	16	21	26	33	42	54	69	90	130	170	220	290	400

Source: Vesic (1975, 1977)

2.8 Construction Specifications

The construction specifications for RIs as a ground improvement technology throughout the U.S. are still limited and have not been standardized. However, a few state transportation agencies (DOTs) have developed special provisions and guidelines to implement this technology in specific projects. This study collected some specifications or special provisions from DOTs from Kansas, Minnesota, Iowa, and Pennsylvania including material selection, RI type and configuration, construction methodology, quality control, and performance requirements, that serve as technical guidelines for RI implementation in state transportation projects. The ongoing NCHRP 10-121 project titled Guidelines for the Application of Ground Modification Methods for Highway Structures is expected to provide performance-based guidelines for the selection, design, construction, and acceptance of appropriate ground modification methods for transportation applications including the load transfer technology using RI systems. The guidelines cover agency's responsibility, contractor responsibility, and applicable delivery methods including both risk and construction liability.

2.8.1 Kansas Department of Transportation

Table 2.3 provides the construction specifications as special provisions for KDOT.

Table 2.3: KDOT Construction Specifications

No.	Category	Detail
	Provision	15-PSXXXX
	Purpose	Column-Supported Embankments (CSEs)
1	RI types allowed	Auger cast pile, steel pile, prestressed pile, cast in place concrete pile, grout columns (compaction grouting)
2	RI diameter	Not explicitly defined but as per FHWA-NHI-16-028
3	RI spacing	Not explicitly defined but as per FHWA-NHI-16-028
4	RI length	Must penetrate the required bearing layer
5	Caps	Concrete caps constructed with rounded edges allowed
6	Equipment	Equipment for column installation must meet the FHWA criteria for the type of columns selected; equipment for fill and geosynthetic placement shall not cause excessive loads or settlement
7	Working platform	No provision
8	Load transfer platform	SB-2 aggregate
9	Geosynthetics	Class 1 separation geotextile and base course reinforcement geosynthetic - minimum overlap of 12 to 36 in. for adjacent rolls
10	Load testing requirement	No explicit provision, but column performance criteria must be met (payment tied to performance)
11	Integrity testing	No explicit provision/mention for pile integrity testing
12	Instrumentation	Monitor the settlement every week (minimum) until 60 days after embankment completion; install piezometers, inclinometers, and vibration monitoring of additional structures as per design and contract documents (if required)
13	Performance criteria	Maximum allowable differential settlement = 0.25 in. (unit cell), maximum allowable total settlement = 0.75 in. (unit cell), maximum allowable differential settlement = 0.5 in. (within 100 ft between two points), maximum allowable total settlement = 1.5 in. (within 100 ft between two points), and local stability of embankment side slopes and the global stability of the whole system ≥1.5
14	QC requirements	Quality control plan
15	Obstruction handling	No provision

2.8.2 Minnesota Department of Transportation

The Minnesota DOT (MnDOT) uses construction specifications in the form of special provisions, as summarized in Table 2.4.

Table 2.4: MnDOT Construction Specifications

No.	Category	Detail
No.	Provisions	SP 2105, 2411, 2452
	Project	TH 10 WB
	Purpose	Widening roadway (CSE)
1	RI types allowed	CMC, CFA, VCC, or DDC
2	RI diameter	Min. 12 in.
3	RI spacing	Max 10 ft
4	RI length	Extends to > 2 times the column diameter into the dense stratum
5	Caps	Steel caps for H-pile (diameter 36 in., thickness 1 in.)
6	Equipment	Drilling equipment capable of installing RIs to a depth of 100 ft and adhere to SP 2452
7	Working platform	No provision
8	Load transfer platform	LTP Type-A crushed aggregate base, Class 6 (MnDOT 3138) LTP Type-B concrete Mix (MnDOT 2401)
9	Geosynthetics	For LTP Type A, biaxial geogrid, ultimate tensile strength (MARV)-1850 lb/ft, tensile strength at 5% strain (MARV)-1200 lb/ft (ASTM D6637), coefficient of interaction (Ci)-0.8 (ASTM D6706) For LTP Type B, welded wire steel fabric, 2"x 2" Square, 0.250" thick (2-3/4 gauge) wire diameter, cold rolled carbon steel, woven-lock crimp weave fabric (ASTM A1064)
10	Load testing requirement	Minimum 2 static tests (200% design load) (ASTM D1143)
11	Lateral reinforcement	Steel bars, plates, coupler (MnDOT 3306)
12	Integrity testing	Pile integrity testing – Minimum 2% of production not sooner than 10 days (ASTM D-5882)
13	Instrumentation	Settlement plates - one at the top of the working pad, centered over a column, one at the top of the LTP, centered between adjacent columns, and one in the embankment fill centered between adjacent columns - monitor the settlement ≤ 100 ft intervals along the CSE until the end of construction contract; horizontal shape acceleration array (SAA) - at least one; vibrating wire piezometers at ≤300 ft interval
14	Performance criteria	Total settlement ≤ 1.5 in.; differential settlement ≤ 1 in./100 ft in 50 years (roadway pavement); differential settlement ≤ 0.5 in./100 ft (drainage, utility structures or sewer, subgrade surface), and global factor of safety ≥ 1.5
15	QC requirements	Quality control plan and program; concrete and grout strength test (MnDOT schedule of materials control)
16	Obstruction handling	Offset/pre-drill or additional columns

2.8.3 Iowa Department of Transportation

The Iowa DOT (IaDOT) has construction specifications in the form of special provisions, as summarized in Table 2.5.

Table 2.5: IaDOT Construction Specifications

No.	Category	Detail	
	Provision	SP-120107	SP-150320
	Project	NHSX-100-1(77)-3H-57-Linn County	IM-NHS-029-3(115)48-03-78-Pottawattamie County
	Purpose	Highway embankment fill	MSE wall with Light-weight Foam concrete fill (LFCF)
1	RI types allowed	Grout: CMC, APGD, or concrete: VCC	Grout: CMC, APGD, ORTD; concrete: GCC
2	RI diameter	Contractor's design	Contractor design
3	RI spacing	Contractor's design	Optimized based on static load test
4	RI length	Deeper to suitable bearing stratum	Deeper to suitable bearing stratum
5	Caps	No provision	No provision
6	Equipment	Combination of machines or equipment in good working condition, safe to operate, no vibration, and producing specified results (SP 150320.03)	Combination of machines or equipment in good working condition, safe to operate, no vibration, and producing specified results (SP 150320.03), and RI installing equipment must be equipped with installation monitoring capabilities such as (i) applied torque, (ii) applied static down pressure, (iii) advance rate, (iv) grout pressure, and (v) grout volume
7	Working platform	5 ft of embankment fill	Working pad (macadam stone, ≥2 ft)
8	Load transfer platform	Granular fill with high-strength geotextile (SP 120107.02)	No provision
9	Geosynthetic reinforcement	Geotextiles (GRI GT7-92)	Geotextiles (GRI GT7-92)
10	Load testing requirement	2 verification load tests (300% of design load), ASTM D1143; axial load test on production RIs (150% of design load)	3 verification load tests (300% of design load), ASTM D1143; axial load test on production RIs (150% of design load)
11	Integrity testing	Pile integrity testing – 50 production RIs (VCC, APGD, and CMC) (ASTM D5882-07)	Pile integrity testing – approximately 5% of production RIs (ASTM D5882)
12	Instrumentation	Inclinometer, real-time monitoring and strain gauges-5 levels on test RIs, daily real-time monitoring up to 52 weeks from the first reading	Strain gauges (Geokon model 4911, 4911A or approved equivalent)-5 levels on test RIs, daily real-time monitoring
13	Performance criteria	No specific provision	No specific provision
14	QC requirements	Contractor's quality control plan (CQC); materials test (SP 120107.02)	Contractor's Quality Control Plan (CQC); Materials test (SP 150320.02)
15	Obstruction handling	Offset ≤ 1.5 ft, predrill, additional inclusions	Offset ≤ 1.5 ft, predrill, additional inclusions

Note: CMC – controlled modulus column by Menard; VCC – vibro-concrete column; APGD – auger pressure grouted displacement piling by Berkel & Company Contractors, Inc.; ORTD – omega rotary torque displacement pile by Malcolm Drilling Company; RI – rigid inclusions by Hayward Baker; GCC – geo-concrete columns by Tensar - GEOPIER FOUNDATIONS; CFA – continuous flight auger

2.8.4 Pennsylvania Department of Transportation

The Pennsylvania DOT (PennDOT) uses construction specifications in the form of special provisions, as summarized in Table 2.6. PennDOT had a special provision for monitoring the settlement of the embankment for project 75978 (ITEM 9000-0071) that consists of guidelines for installing and monitoring instruments for settlement and groundwater pressure during the construction of embankments for embankment settlement remediation (Table 2.6).

Table 2.6: PennDOT Construction Specifications

No.	Category	Detail		
	Provision	Item 9000-050X XX" Drilled displacement column	CSE and LTP: alternative	Item 9000-0051 Embankment settlement remediation
	Project	I-95: Betsy RossMainln NB-Philadelphia County	I-95: Betsy RossMainln NB-Philadelphia County	I-70 @ P51 Interchange-Westmoreland
	Purpose	Drilled displacement piles	CSE and LTP: alternative	CSE and LTP
1	RI types allowed	Drilled displacement piles (DDPs)	CMC, DDP, or VCC	Steel-driven piles, continuous flight auger (CFA) piles, CMC, or VCC
2	RI diameter	Contractor's design: 12, 16, 18 in.	Contractors' design, FHWA NHI-16-028 GEC 013, Vol. II	Contractors' design, FHWA NHI-16-028, GEC 013, Vol. II
3	RI spacing	Contractor's design	Max. 10 ft., FHWA NHI-16-028 GEC 013, Vol. II, only square pattern allowed	Maximum 14 feet, FHWA NHI-16-028 GEC 013, Vol. II
4	RI length	Must penetrate the required bearing stratum	Must extend to a suitable bearing layer	Steel piles foundations must extend to bedrock
5	Caps	No provision	No provision	For steel piles, a square reinforced concrete cap with a length 1.5 times the column diameter and a width 0.4 times the column spacing
6	Equipment	Suitable equipment proposed by the contractor for the installation of DDPs	Equipment must meet PennDOT and FHWA criteria for the type of column selected	Equipment must meet PennDOT and FHWA criteria for type of column selected
7	Working Platform	No provision	No provision	No provision
8	Load transfer platform	No provision	LTP fill: Pub 408, Section 703.2, PENNDOT NO. 2A, Type C; Minimum thickness: maximum of 3 ft or $0.5(s-a)$, s = c/c column spacing, a = column width; must have a minimum of three layers of biaxial polyester geogrid reinforcement with spacing of 8-12 in.; and overlap PET geogrid with a minimum of 6 ft in MD and a minimum of 6 in. in XD	LTP fill: Pub 408, Section 703.2, PENNDOT NO. 2A, Type C; Minimum thickness: maximum of 3 ft or $0.5(s-a)$, s = c/c column spacing, a = column width; must have a min. of four layers of uniaxial polyester geogrid reinforcement with a max. spacing of 18 in.; overlap PET geogrid with a min. of 6 ft. in MD; and overlap all adjacent edges of geotextile at a min. of 1 ft

#	Category			
9	Geosynthetic reinforcement	No provision	Polymeric coated PET biaxial geogrid: Pub 408, Section 738.3, Class 2, Type C; Geotextile: Pub 408, Section 735, Class 4, Type C	Polymeric coated PET uniaxial geogrid: Pub 408, Section 738.3, Class 1, Type A; Geotextile: Pub 408, Section 735, Class 4, Type A, also used for separation of wick drains
10	Load testing requirement	Axial load capacity must be 2 times the design load (special provision Item 9000-0509)	Static load test on 20 piles (at least 5 tests at each embankment design segment) as per ASTM D1143 by applying load 2 times the design load	Minimum preload - 500 psf (wick drain); static load test on a minimum of 1/250 piles and at least one test on the surficial element at each treatment area as per ASTM D1143 by applying load 2 times the design load
11	Integrity testing	Integrity testing per Special Provision Item 9000-0510	Pile integrity testing on a minimum of 100 production piles	-
12	Instrumentation	No provision	Vibration monitoring control as per Special Provision Item 9005-6002; 3 strain gauges shall be installed with one at the pile top, one at the pile tip, and the last one equally spaced between the two gauges	Acceptable monitoring methods for embankment fill are directed in special provision 9000-0071 embankment settlement monitoring
13	Performance criteria	Max. settlement of the pavement structure ≤ 1 in. after the final construction	Max. long-term settlement ≤ 1 in.; global factor of safety ≥ 1.5, and Factor of Safety for design strength of geogrid ≥ 1.5	Max. remaining settlement after installing wick drains < 1 in.; max. long-term settlement ≤ 0.5 in., and max. diff. settlement ≤ 0.25 in.
14	QC requirements	Notification to allow appropriate PennDOT personnel to be on-site during pile installation and grout test (ASTM C109)	Geogrid test as per ASTM D 4534 and ASTM 6637; High strain dynamic testing (PDA) in conformance with ASTM D4945 is acceptable	-
15	Obstruction handling	Pre-drilling of piles (Pre-drill auger should have the same diameter as finished pile diameter)	Pre-drilling, install additional columns to bridge the obstruction	Pre-drilling, install additional columns to bridge the obstruction, re-driving in case of driven piles

2.8.5 Case Studies

Numerous case studies, including full-scale field tests and model tests, have been documented in the literature to demonstrate the load transfer mechanisms, settlement, stability, and installation effects of geosynthetic-reinforced RIS embankments. The case studies provide a foundation for predicting or interpreting RIS behavior. However, numerical analysis has also become an essential tool for understanding the complex mechanisms and mechanics of RIS, such

as the RI-soil-geosynthetic interaction (Han & Gabr, 2002), the consolidation of soft soil (Huang & Han, 2009), and the interaction between widened and existing embankments (Han et al., 2007). Pham and Dias (2021) summarized case studies of pile-supported embankments, including semi-rigid and rigid inclusions. Because this current research focused on RIs, only case studies of full-scale field and model tests involving RIS embankment/structures are listed in Table 2.7.

2.8.6 Cases with Distresses

RIs have been successfully used to support many embankments and walls for transportation applications. However, there have been a few documented failed or distressed case studies involving RIs around the world. Camp and Siegel (2007) reported a failure of column-supported embankment over soft ground in the U.S. The embankment had a maximum height of 3.6 ft and was supported by vibro-concrete columns (one type of RIs) spaced at 8.2 ft center-to-center. Shortly after construction, the roadway surface began to deform with humps at the column locations with differential settlements between columns. After the evaluation, Camp and Siegel (2007) concluded that "the primary cause of the deformation-related failure was that the embankment load exceeded the tensile resistance available in the geosynthetic layers at the elongation corresponding to the design settlement." Swift et al. (2024) reported another distressed case of the Rodemis site in Germany, in which the dimpling developed after the service of the roadway, causing severe disturbances to drivers. As a result, the entire roadway was taken out of service for reconstruction in 2016. Swift et al. (2024) indicated such distresses may happen when RIs are spaced too far apart or with a too-thin LTP.

Table 2.7: Case Studies of RIS Embankments

No	Application	Soil Condition	RI Type	GR Type	Design Parameters	Performance	Reference
1.	Toll plaza	Compressible peat and estuarine clay	VCC	Geogrid	$H = 7.2 - 18.7$ ft, $S = 7.2 - 8.9$ ft, $d = 1.8$ ft, $N = 2$	Very small differential settlement observed	Maddison and Jones (1996)
2.	MSE wall	Plastic organic material + sandy silt	PC	Geogrid	$H = 15.8$ ft, $S_x = 14.8$ ft, $S_y = 12.5$ ft, $a = 2.3$ ft, $N = 4$	No significant vertical deformation was seen	Vega-Meyer and Shao (2005)

No	Application	Soil Condition	RI Type	GR Type	Design Parameters	Performance	Reference
3.	Embankment	Silty sand + marine deposits of organic clay	PC	Woven geotextile	H = 5.9 ft, S_x = 6.9 ft, S_y = 6.9 ft, a = 3 ft, N = 4	Good performance of the RIS system was observed	Hoppe and Hite (2006)
4.	Model test	Soft marine clay	PC	Geogrid	H = 8.9 ft, S_x = 2 ft, S_y = 2 ft, a = 0.4 ft, N = 1	Embankment supported by the combination of GR and RIs gave better performance for arching efficacy and differential settlement	Oh and Shin (2007)
5.	Embankment	Silty clay	Concrete	Geogrid	H =18.4 ft, S_x = 9.8 ft, S_y = 9.8 ft, a = 3.3 ft, N = 1	Significant load transfer onto the RIs and reduction of excess pore pressure on soft soil were observed	Liu et al. (2007)
6.	Embankment	Soft organic compressible clay	PC	Geogrid	H = 4.1 ft, S_x = 8.2 ft, S_y = 8.2 ft, a = 2.6 ft, N = 1	Settlements measured between adjacent RIs about half the value at the center of four RIs	Almeida et al. (2007)
7.	Embankment	Soft soil	Timber	Geogrid	H = 3.8 ft, S_x = 4.2 ft, S_y = 4.2ft, a = 0.9 ft, N = 1	Considerable support from the soft soil was observed	Van Eekelen et al. (2010)
8.	Embankment	Silt + clayey soil	PTC	Polypropylene grid	H = 19.7 ft, S_x = 6.6 ft, S_y = 6.6 ft, a = 3.3 ft, N = 1	No significant differential settlement	Chen et al. (2010)
9.	Embankment	Sand + soft clay	HSP	Geogrid	H = 8.5 ft, S_x = 6.4 ft, S_y = 4.8 ft, a = 1.1 ft, N = 2	Load distribution angle to the RIs not significantly affected by RI configuration	Duijnen et al. (2010)
10.	Embankment (test)	Soft material	PC	Geogrid	H = 7.5 ft, S_x = 6 ft, S_y = 6 ft, a = 1.8 ft, N = 3	Geosynthetics performed better when positioned low within the embankment	Sloan (2011)

No	Application	Soil Condition	RI Type	GR Type	Design Parameters	Performance	Reference
11.	Embankment (full-scale test)	Clay + sandy clay	PC	Geotextile/ Geogrid	H = 16.4 ft, S_x = 6.6 ft, S_y = 6.6 ft, a = 1.1 ft, N = 1/2	The RI efficiency and settlement reduction significantly improved with LTP compared to without it.	Briançon and Simon (2012)
12.	Model test	Soft soil	PC	Geogrid	H = 1.4 ft, S_x = 1.8 ft, S_y = 1.8 ft, a = 0.3 ft, N = 1	Measured arching not influenced by the stiffness of GR	Van Eekelen et al. (2012)
13.	Fossil plant over geosynthetic reinforced LTP	Silty clay	PHC	Geogrid	H = 13.1 ft, S_x = 9.8 ft, S_y = 9.8 ft, a = 3.3 ft, N = 2	The increase in efficiency of the GR RIS system with the geogrid compared to without geogrid in LTP observed	Xing et al. (2014)
14.	Model test	Fine sand	PC	Geogrid	H = 1.3 ft, S_x = 1.6 ft, S_y = 1.6 ft, a = 1 ft, N = 1	Floating RIs led to greater settlement in embankment and lesser arching	Xu et al. (2016)
15.	Embankment	Silty clay + silty soil	BC	Geogrid	H = 16.4 ft, S_x = 11.5 ft, S_y = 11.5 ft, a = 3.3 ft, N = 1	Embankment, reinforced with fixed GR and higher strength, minimized larger lateral deformation and settlement but a fixed GR approach may not be required in every case	Zhang et al. (2016)
16.	Embankment	Water bag as soft soil model	Steel Beam	Geogrid	H = 10.5 ft, S_x = 5.9 ft, S_y = 5.9 ft, a = 3.3 ft, N = 1	The increase in arching efficacy due to soil consolidation observed	Chen et al. (2016)
17.	Model test	Soft soil	PC	Geogrid	H = 10.5 ft, S_x = 6.6 ft, S_y = 6.36 ft, a = 1.6 ft, N = 1	The application of GR had greater importance than its stiffness on measured arching	Fagundes et al. (2017)

No	Application	Soil Condition	RI Type	GR Type	Design Parameters	Performance	Reference
18.	Embankment	Peat + clay	PC	Geogrid	H = 13.1 ft, S_x = 5.2 ft, S_y = 5.2 ft, a = 0.9 ft, N = 2	Geogrid on LTP could replace the large caps on the head of RIs	Briançon and Simon (2017)
19.	Embankment (test)	Foam	Steel	Woven geotextile	H = 8.4 ft, S_x = 3.9 ft, S_y = 3.9 ft, a = 1.3 ft, N = 1	GR enhanced the arching efficiency compared to systems without GR	Lee et. al. (2020)
20.	Embankment	Clay + silty clay + silty sand	PTC	Geogrid	H = 7.9 ft, S_x = 14.8 ft, S_y = 6.6 ft, a = 3.3 ft, N = 2	The use of PTCs demonstrated good performance in load transfer, settlement reduction, and minimal lateral displacement	Zhao et al. (2019)
21.	Embankment	Lean clay	PHC	Geogrid	H = 9.8 ft, S_x = 9.8 ft, S_y = 9.8 ft, a = 5.9 ft, N = 2	Soil arching fully mobilized once a sufficient differential settlement was achieved	Chen et al. (2020)
22.	Embankment	Soft clay + peat	PC	Geogrid	H = 5.9 ft, S_x = 7.4 ft, S_y = 7.4 ft, a = 2.5 ft, N = 2	Seasonal moisture variations influenced the arching and load distribution, with wet conditions temporarily restored sub-soil support	Van Eekelen et al. (2020)
23.	Embankment	Sandy fill + organic silty-clay soils	GC	Geogrid	H = 15 ft, S_x = 7.9 ft, S_y = 7.9 ft, a = 1.3 ft, N = 2	Permanent deformation of 0.4 to 0.6 in. observed on the adjacent bridge at 15 ft distance	Lamb et al. (2022)
24.	Embankment	Peat + sulphide silt	Timber	Geogrid	H = 5.6 ft, S_x = 3.3 ft, S_y = 3.3 ft (equivalent square), a = 0.7 ft, N = 2	Seasonal frost. Long-term settlement expected due to gradual deformation in the soil over time	Gunnvard et al. (2022)

No	Application	Soil Condition	RI Type	GR Type	Design Parameters	Performance	Reference
25.	Embankment	Compressible organic peat	PC	Woven geotextile	H = 5 ft, S_x = 7.4 ft, S_y = 7.5 ft, a = 2.5 ft, N = 2	High groundwater level led to no change in strain in the geotextile. Seasonal effects observed.	Van Eekelen et al. (2023)
26.	MSE Wall	Stiff lean clay + clayey silt+ Sandy silt	Timber	Geogrid/ Geotextile	H = 23 ft, S_x = 3.5 ft, S_y = 3.5 ft, a = 0.9 ft, N = 6/2	Very small differential settlement observed	Izadifar et al. (2024)
27.	Installation test	Low plastic sandy silt	Concrete	N/A	a = 0.9 ft	Installation effect extending up to 2d – 3d zone from the RI noted	Suleiman et al. (2016)
28.	Embankment/ MSE wall	Clay	Concrete	Geotextile	H = 15.1–36.1 ft, S_x = 6,8 ft, S_y = 6,8 ft, a = 1.3 ft, N = 4	The combination of interface friction and low compressibility was subsurface LTP, further reducing load on soft soil	Gallant et al. (2020)

Note: RI = Rigid Inclusions, LTP = Load Transfer Platform, GR= Geosynthetic Reinforcement, H = embankment height, S_x = spacing in *x*-direction, S_y = spacing in *y*-direction, d = inclusion diameter, a = equivalent square size of RI's head/cap, N = number of geosynthetic layers, VCC = Vibro-Compaction Concrete, PC = Pre-cast Concrete, GC = Grout columns, HSP = High Speed Piles, PTC = Pre-stressed Tubular Concrete, PHC = Pre-stressed High-strength Concrete

Chapter 3: State of the Practice Survey

3.1 Introduction

An online survey was conducted by the research group at the University of Kansas to assess the current practices involving RIs in transportation applications. The survey gathered insights from government agencies, contractors, academics, and consultants. The questionnaire of this survey had a note to respondents that the survey was focused on the use of RIs for transportation applications. The questionnaire was distributed to 67 individuals, and 36 responses were received.

3.2 Methodology

The online survey was comprised of 25 multiple-choice questions administered via the Zoho Survey platform, in which participants received a unique survey link via email invitation. The survey remained open for one month, allowing ample time for completion, and responses were automatically collected and securely stored on the same platform. Although efforts were made to ensure survey validity and reliability, the self-reported data may have been influenced by response bias or inaccuracies due to participants' recall abilities. Furthermore, the sample was drawn from the investigator's professional network, which may not provide a full representative view of the broader population.

3.3 Survey Results

Figure 3.1 presents the affiliations of the 36 survey respondents. Of the respondents, approximately 28% were from government agencies, 25% were from construction companies, 19% were from consulting firms, 19% were from academia, and 8% was classified as "Other" (e.g., high technology companies).
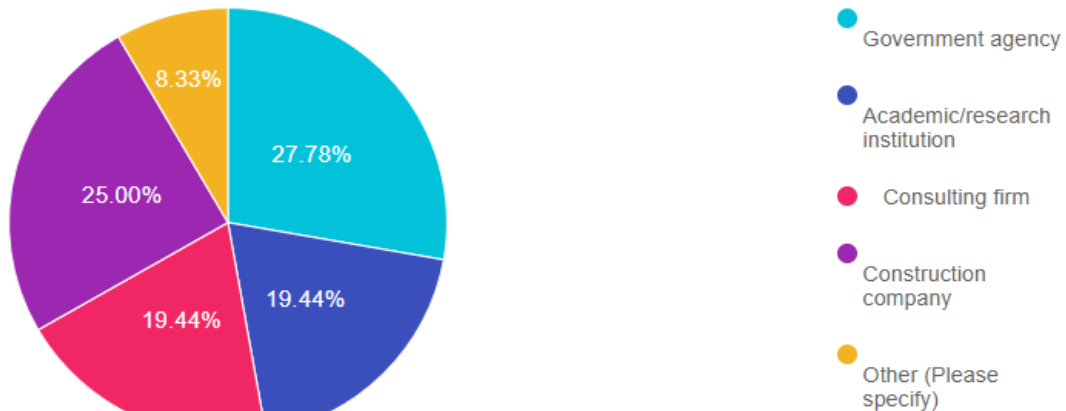
Figure 3.1: Survey Respondent Affiliations

A total of approximately 81% of the respondents had expertise in RI design, while 39% specialized in installation, 44% had expertise in QA/QC, and 47% focused on performance evaluation and monitoring. Only 11% were categorized as "Others", lacked expertise or had limited knowledge of this technology as shown in Figure 3.2. Since this question allowed multiple choices by an individual respondent, the total percentage was greater than 100%.

Figure 3.2: Expertise of Respondents in the RI Technology

Figure 3.3 shows that approximately 92% of respondents indicated the use of RIs for embankments, 67% for retaining or sound barrier walls, 44% for box culverts or drainage pipes, and 25% for bridge foundations. Furthermore, 42% selected the "Other" option, mentioning foundations for building structures, which are beyond the scope of this project as it focused on transportation applications.
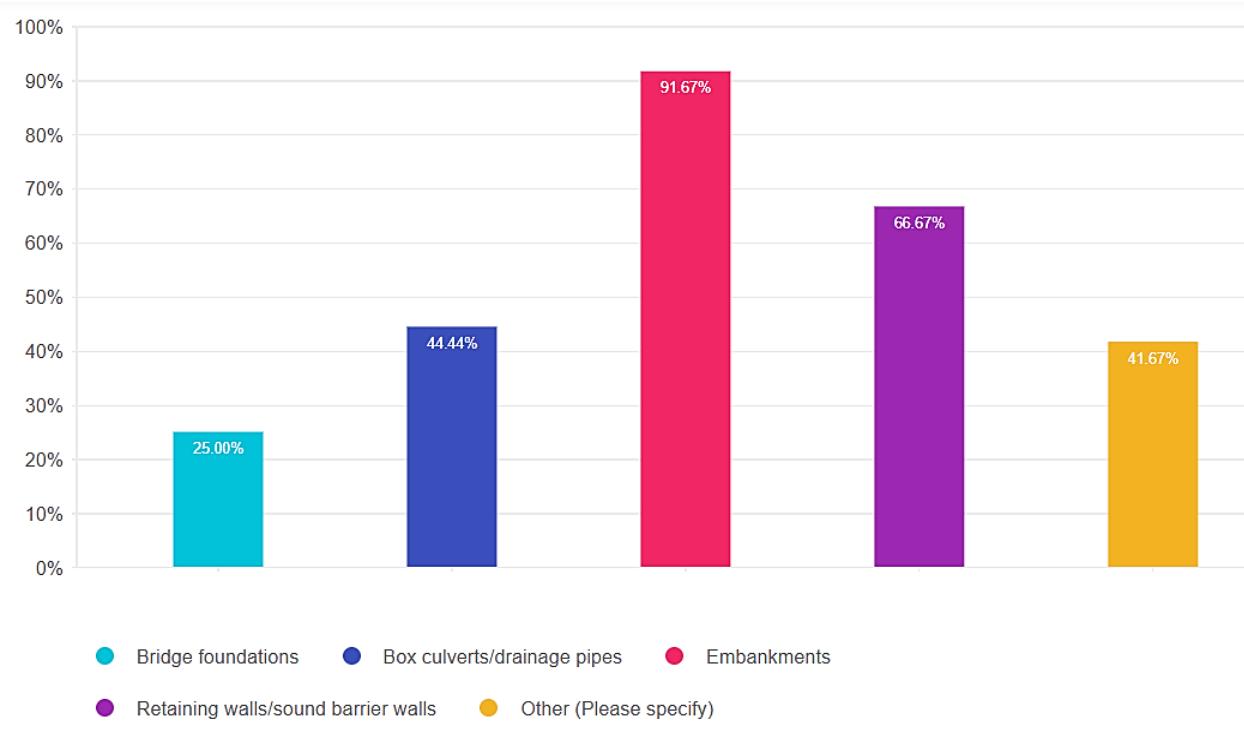
Figure 3.3: RI Applications in Transportation Projects

Regardless of RI types used in the practice, Figure 3.4 shows that approximately 69% of respondents selected DDCs, 56% selected ACIPs, 39% selected grouted gravel/stone columns and timber piles, 22% selected steel piles, 19% selected vibro-displacement columns, and 17% selected VCCs. Additionally, 19% of respondents selected the "Other" option, mentioning alternative types, such as pre-cast concrete piles (a type of displacement pile) and soil mix columns, which were not considered RIs in this study based on the defined scope.
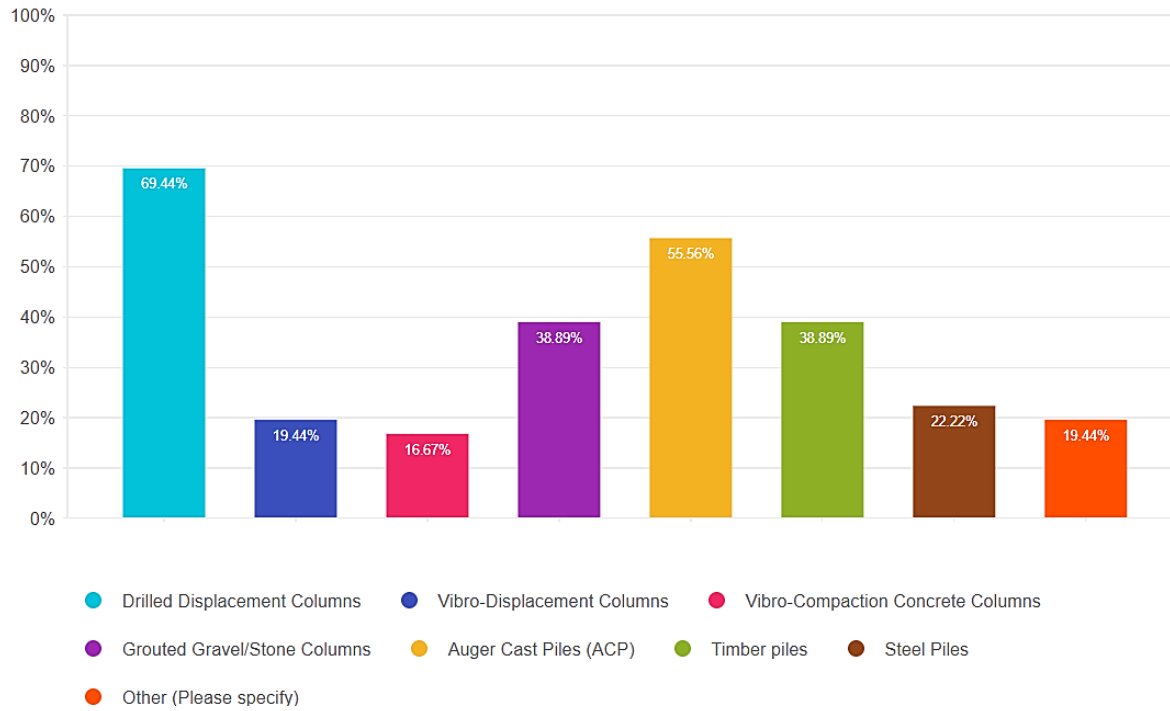
Figure 3.4: Types of RIs in Practice

Figure 3.5 shows that the following response percentages for RI objectives: approximately 94% for reducing settlement, 67% for improving bearing capacity, 31% for enhancing slope stability, and 22% for mitigating liquefaction.
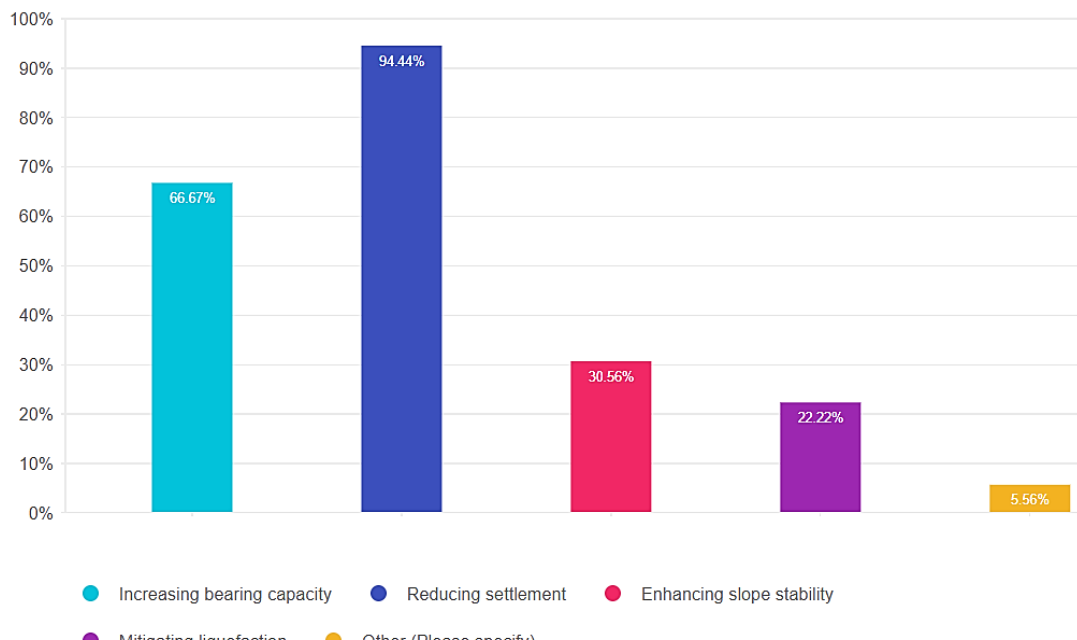
Figure 3.5: RI Objectives for Ground Improvement

In terms of soil type, Figure 3.6 shows that approximately 97% of respondents selected the use of RIs in clay, followed by 72% in organic soil, 58% in silt, 44% in peat, and 39% in loose sand or gravel. Furthermore, 6% chose the "Other" option by mentioning municipal solid waste and unsatisfactory fill as additional soil types.
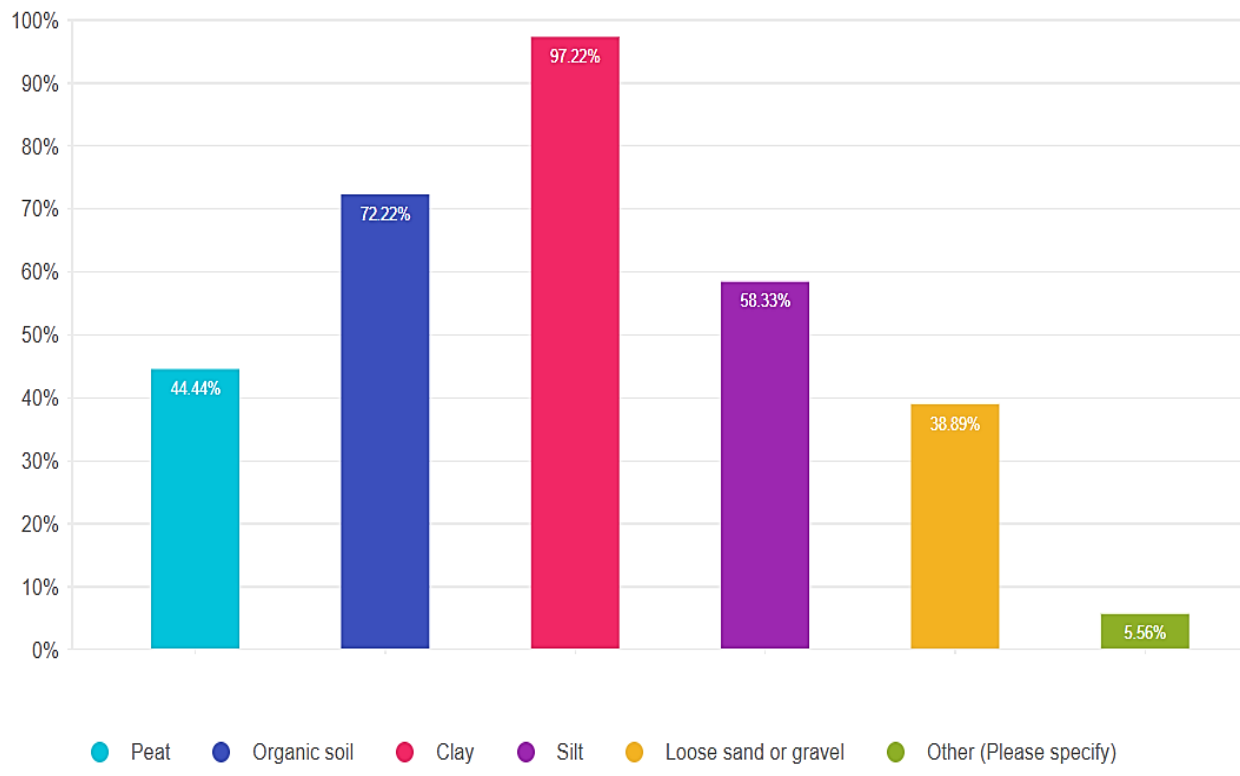
Figure 3.6: Types of Soils Improved by RIs

Figures 3.7 and 3.8 show survey results for RIS design and analytical methods, respectively. In terms of RIS design method, Figure 3.7 shows that over 86% of respondents selected analytical methods, approximately 78% selected numerical analysis, and 39% selected personal experience. Additionally, 8% selected "Other" and indicated load testing. For analytical methods, Figure 3.8 shows that approximately 56% of respondents selected the FHWA beam method, followed by 36% for the FHWA strain compatibility method, 28% for the BS 8006-1 method, 6% for the EBGEO method, 6% for the CUR226 method, and 3% for the Nordic method. Additionally, approximately 31% chose the "Other" option by listing GeogridBridge 3.0, Virginia Department of Transportation (VDOT), and CGPR (Centre for Geotechnical Practice and Research), which are other forms of FHWA strain compatibility. The sum of the "Other" option and the FHWA strain compatibility method was 67% of respondents for this method.
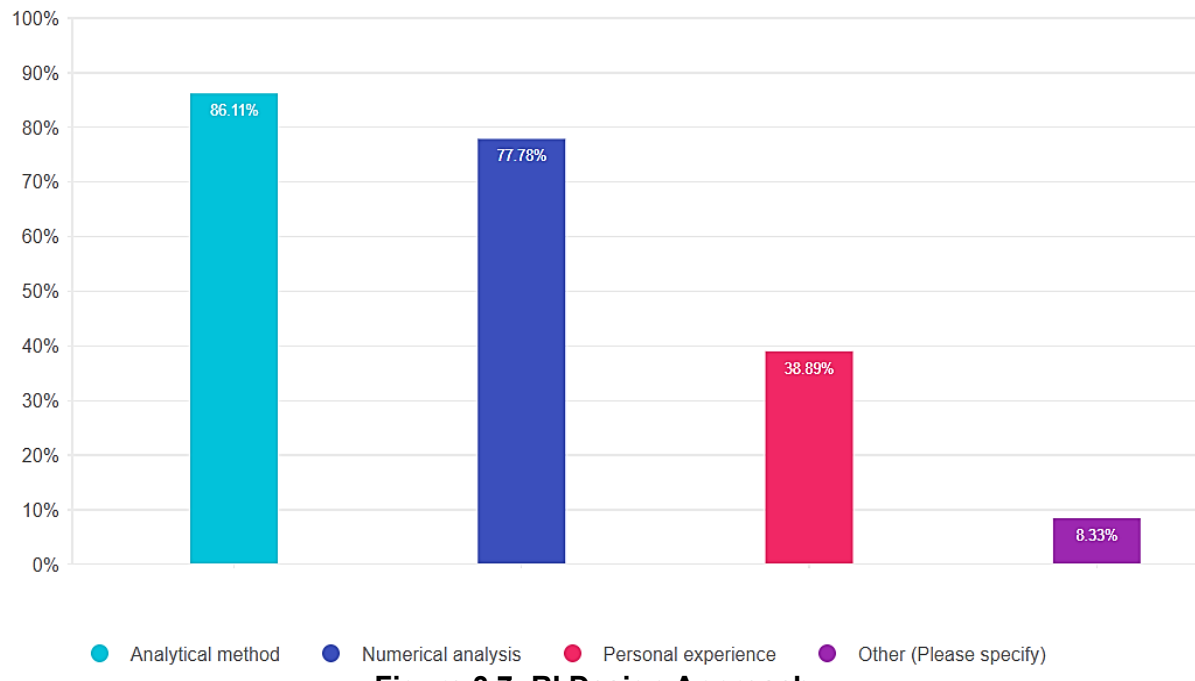
Figure 3.7: RI Design Approach
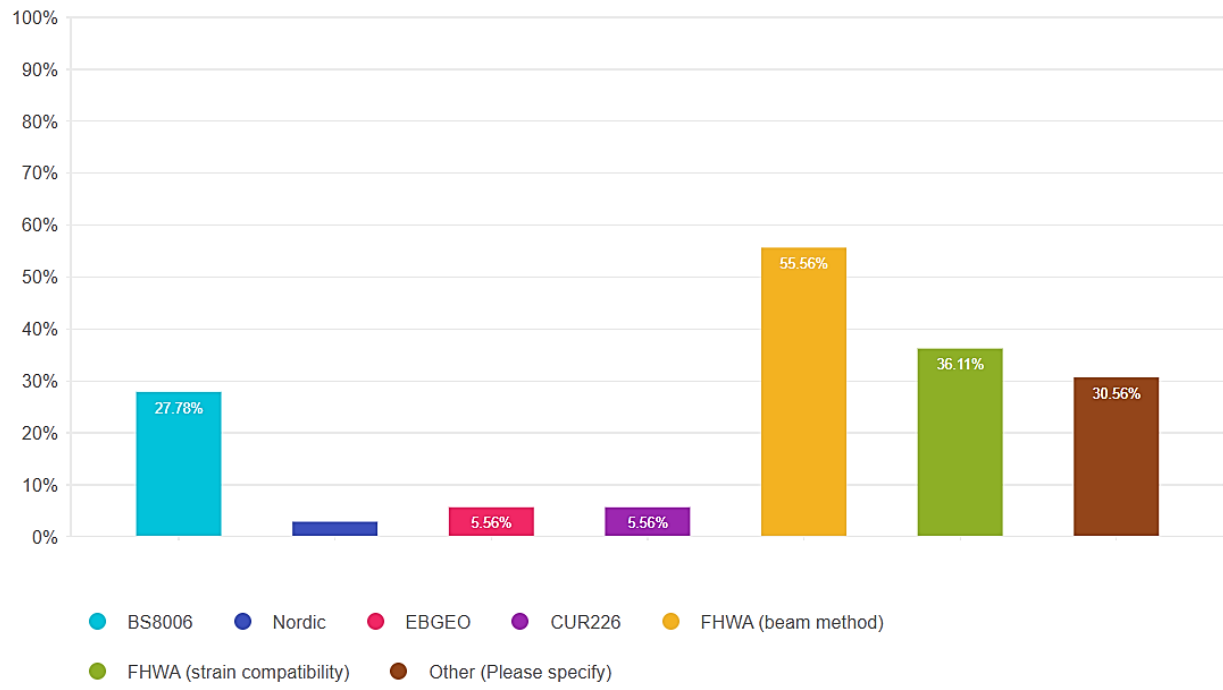
Figure 3.8: Common Analytical Methods for RI Design

According to Figure 3.9, a majority of respondents (over 77%) selected a diameter of 14 to 18 in. for RIs in transportation projects. However, over 55% of the respondents also selected the diameters of smaller than 14 inches. Figure 3.10 shows that over 91% of the respondents suggested

an RI spacing of 6 to 9 ft. However, approximately half of the respondents selected a spacing of less than 6 ft was also used.

Figure 3.9: Common RI Diameters

Figure 3.10: Commonly Adopted Spacing of RIs
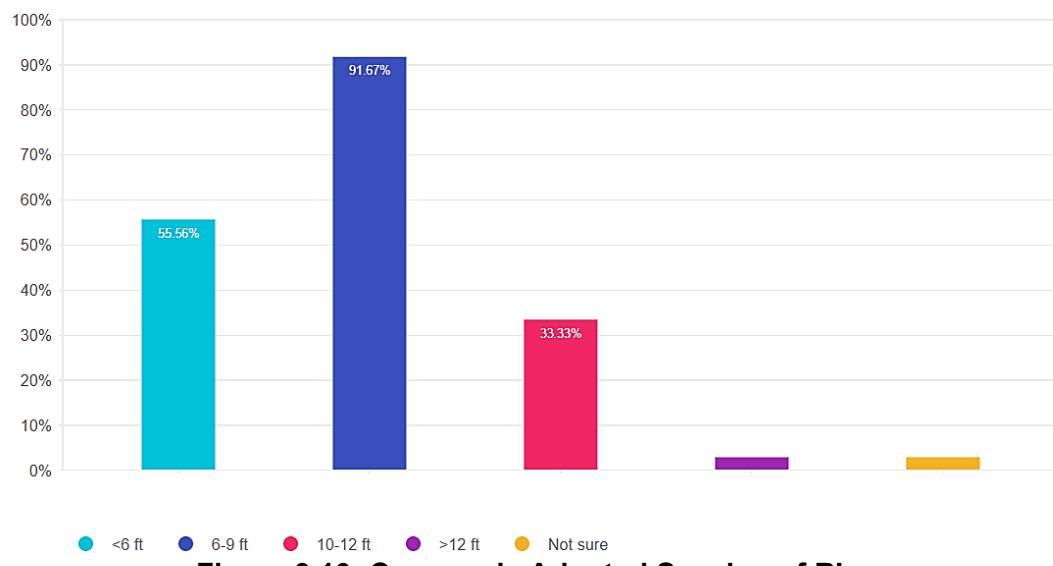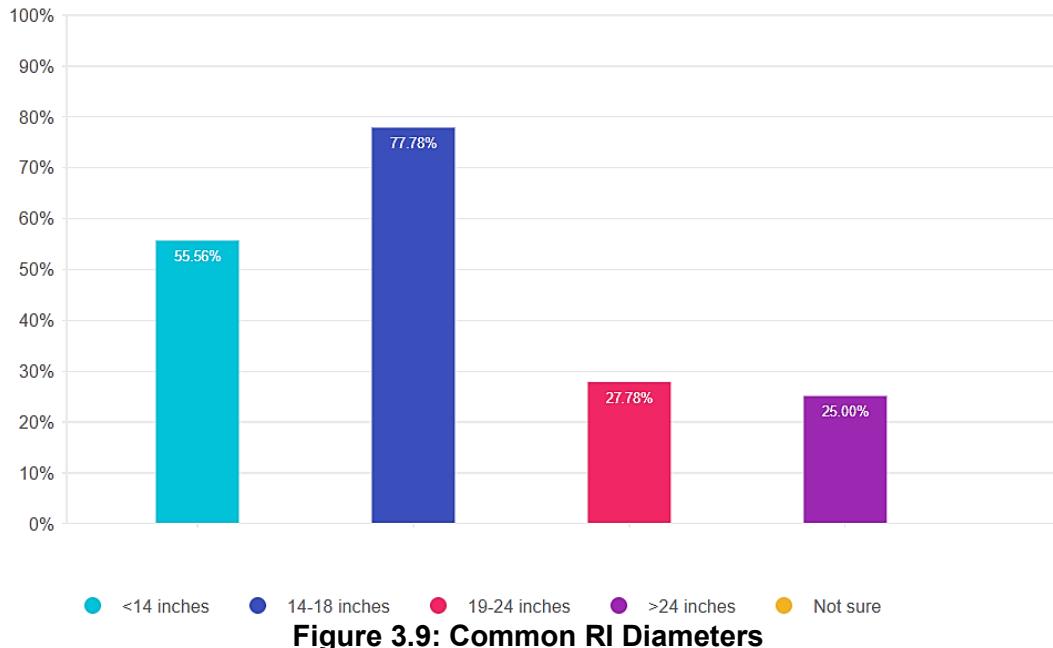
Figure 3.11 shows that over 55% of respondents indicated an area replacement ratio (i.e., the ratio of the cross-sectional area of RI head or cap to its influence area) of 2.5%–5.0%. However, approximately one-third of respondents indicated usage of a ratio less than 2.5% or 6%–10%.
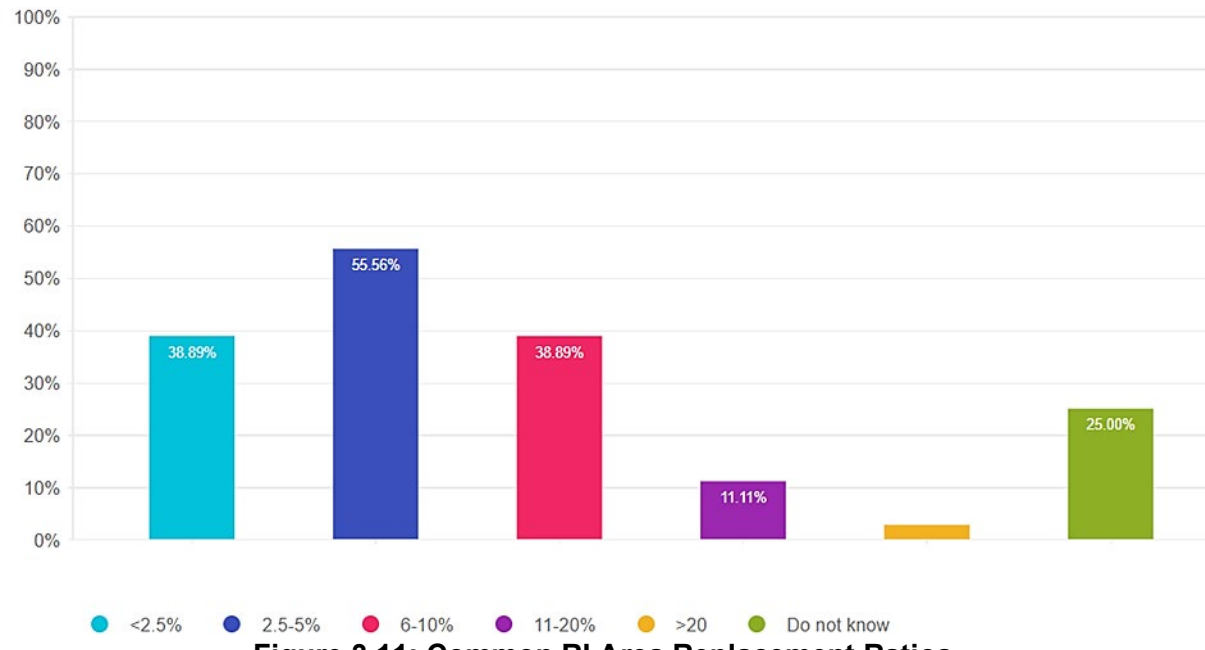
Figure 3.11: Common RI Area Replacement Ratios

Figure 3.12 shows that approximately 42% of respondents thought no caps were used on top of RIs in projects, while Figure 3.13 shows that more than 88% of respondents considered a length range of 30–60 ft as most common for RIs, followed by approximately 64% of respondents selecting a length less than 30 ft. Figure 3.14 shows that nearly half the respondents thought steel reinforcement had been rarely or never used in RIs for transportation projects.
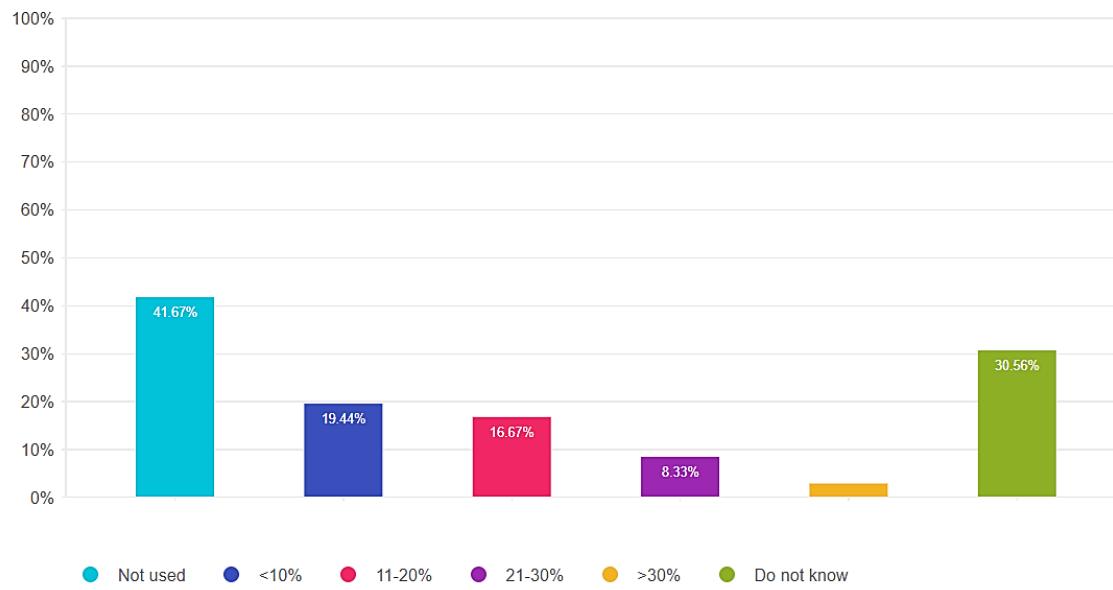
Figure 3.12: Common Percentage Coverage of Caps on Top of RIs
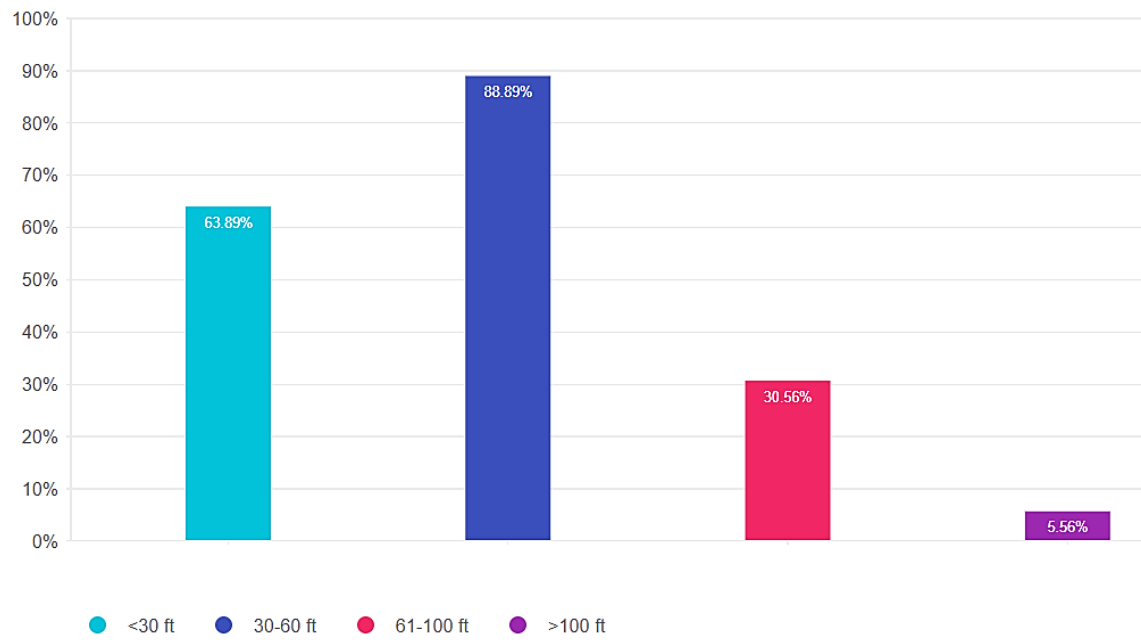
Figure 3.13: Installed Length of RIs
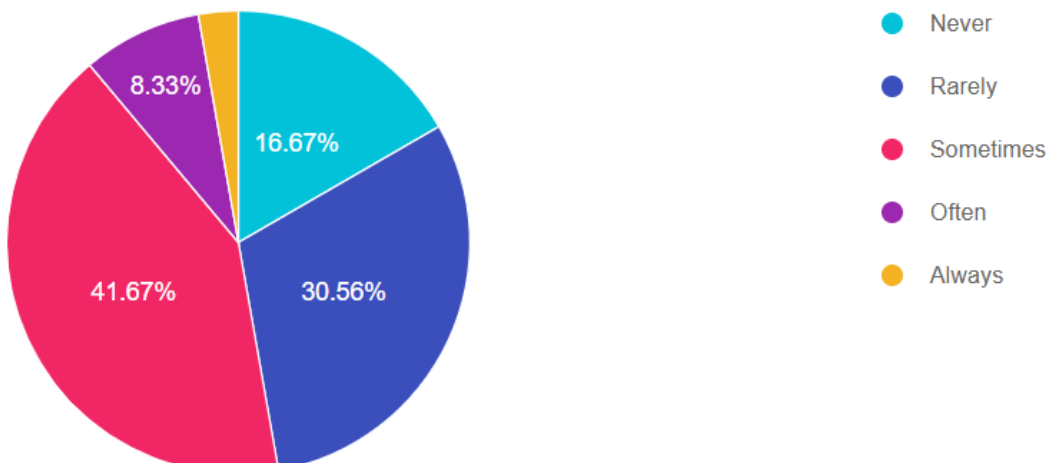
Figure 3.14: Use of Steel Reinforcement in RIs

Figure 3.15 shows that most respondents (56%–67%) indicated the use of steel reinforcement in RIs for conditions involving horizontal loads due to causes such as slope stability and seismic loading.
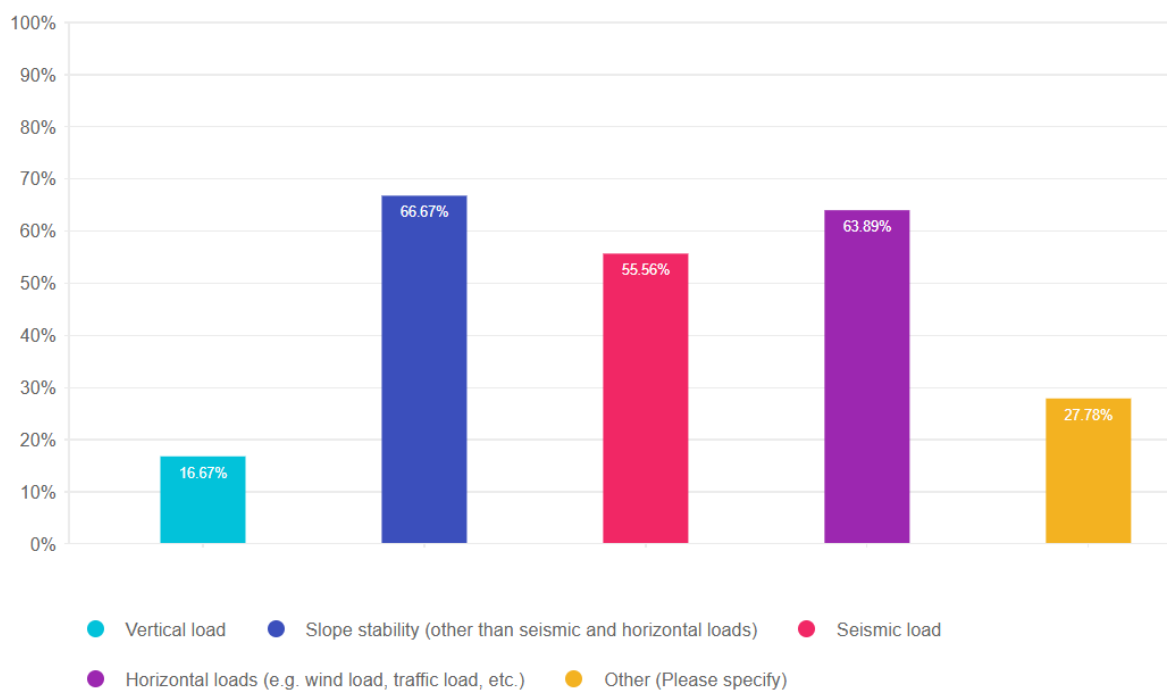
Figure 3.15: Usage Condition for Steel Reinforcement in RIs

According to Figure 3.16, most respondents identified the installation length of steel reinforcement as 50%–100%, while more than 36% of respondents did not know or were not aware of the use of steel reinforcement in RIs.
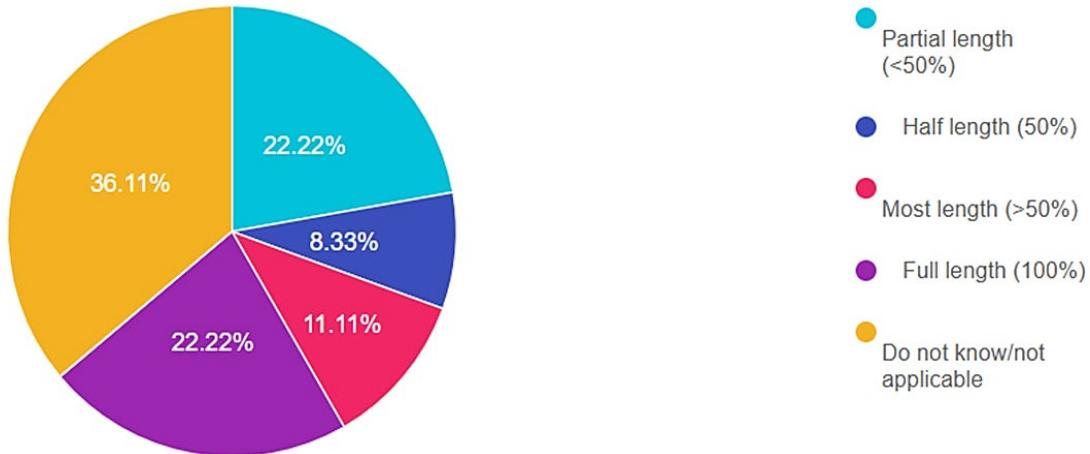
Figure 3.16: Percentage Length of Steel Reinforcement Common in RIs

As per the size of the embankment, Figure 3.17 shows that the majority of the respondents (over 50%) indicated the RIs were used to support embankments greater than 20 ft.
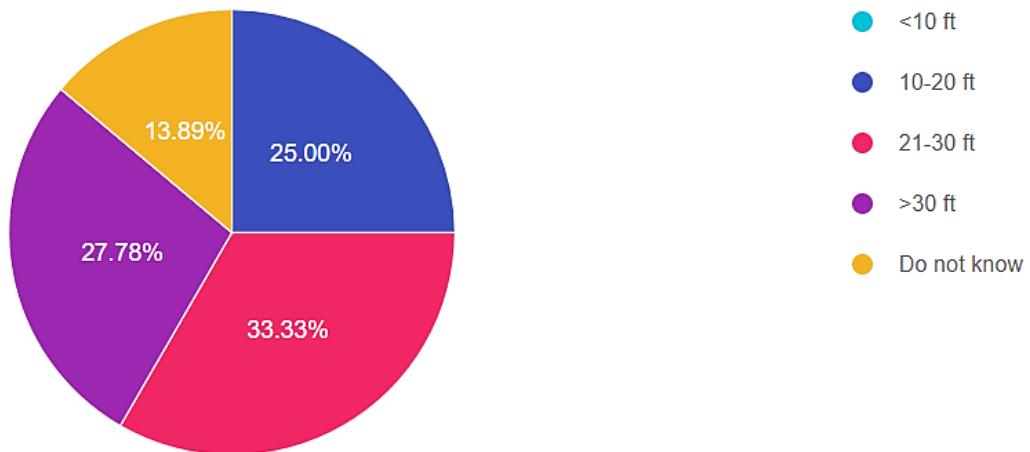
Figure 3.17: Common Embankment Heights on RI-Improved Ground

Figure 3.18 shows that more than 90% of respondents selected geogrids as the most common type of reinforcement in LTPs, while more than 30% of respondents mentioned the use of woven geotextile.
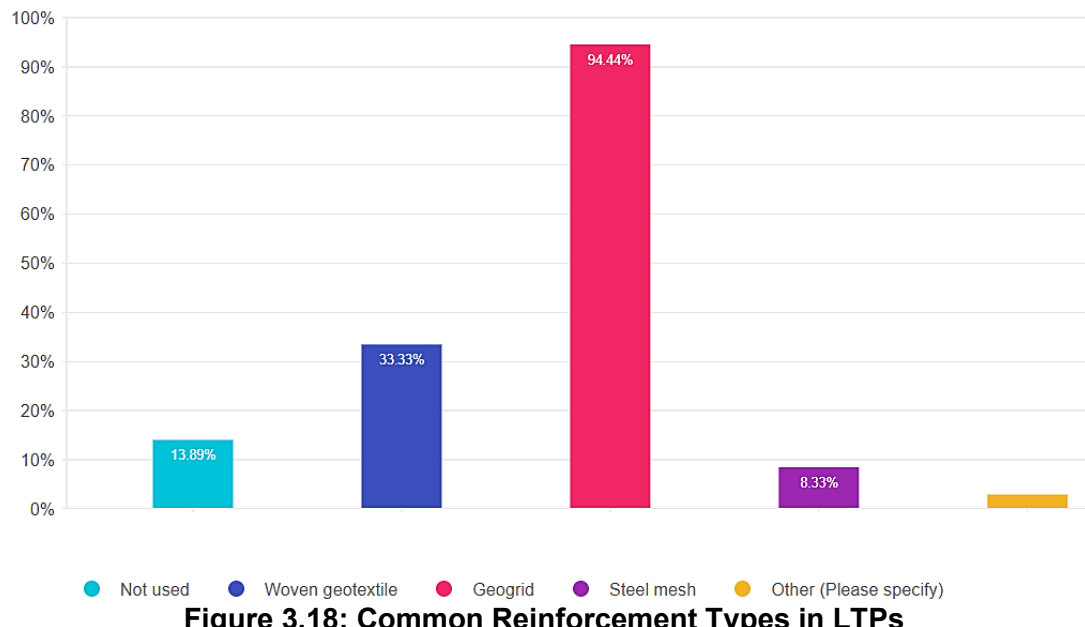
Figure 3.18: Common Reinforcement Types in LTPs

According to Figure 3.19, approximately 70% of respondents selected the gravel/graded aggregate base as the most preferred material for LTPs; sand was selected as a possible fill material by nearly 22% of the respondents. Figure 3.20 shows that more than 80% of respondents indicated use of static load tests on individual RIs to assess their quality and performance. However, 55.56% of respondents also mentioned pile integrity testing as another popular method to ensure the quality of RIs. Figure 3.21 shows that instrumentation and monitoring were not commonly used in RI projects, as only 13.69% of the respondents mentioned they always adopted them.
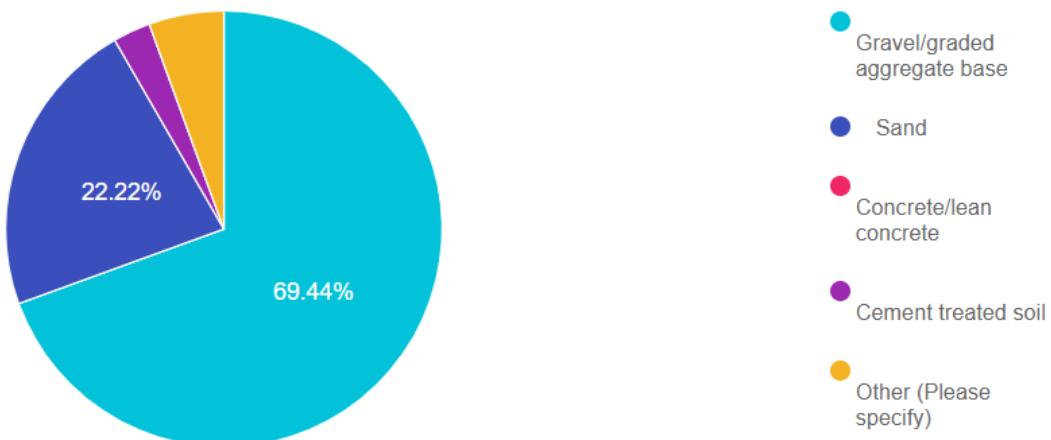
Figure 3.19: Commonly Used Fill Materials in LTPs
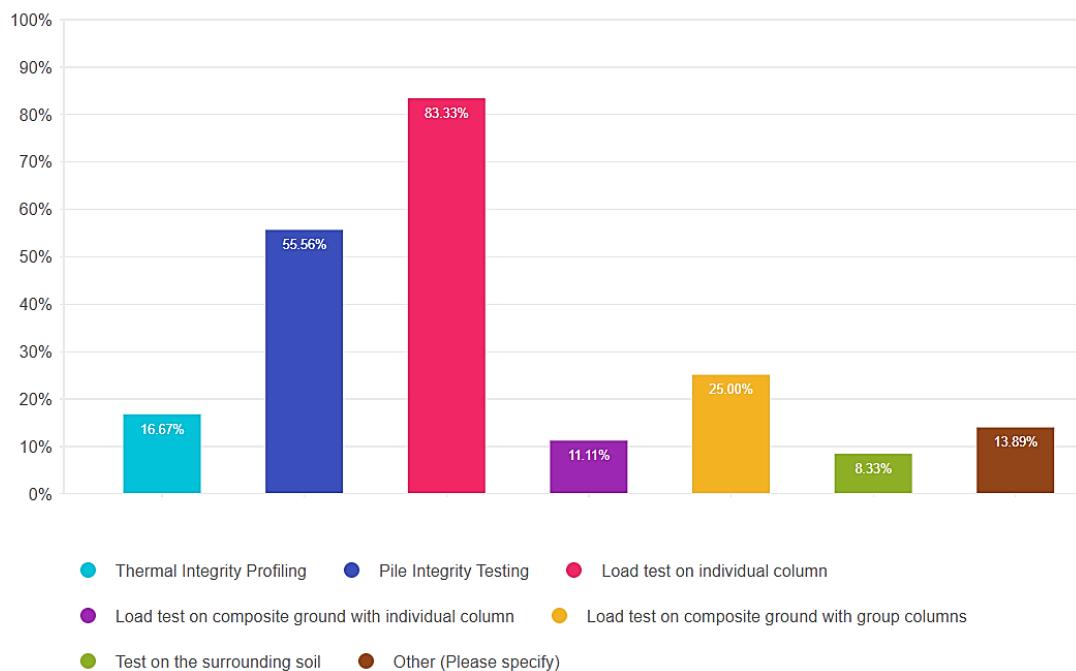
Figure 3.20: Common Methods to Assess Quality and Performance of RIs
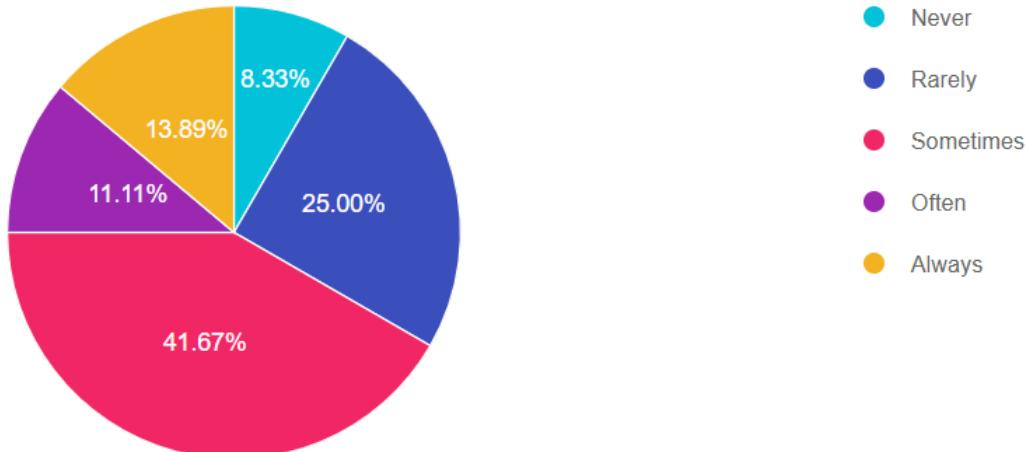
Figure 3.21: Frequency of Instrumentation and Monitoring of RI Projects

Approximately 45% of respondents considered downdrag forces in RI using the neutral plane method, while others considered them indirectly in the limit strength design or other approaches, such as numerical analysis, as shown in Figure 3.22.
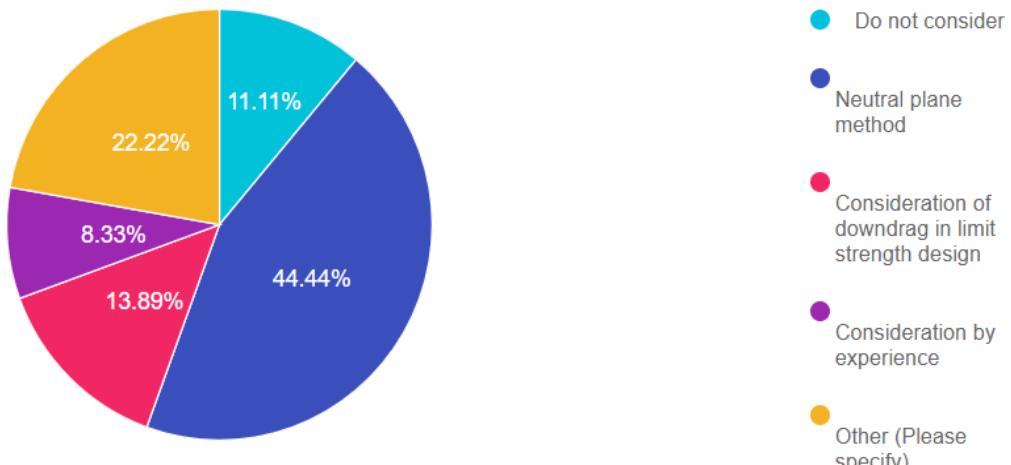
Figure 3.22: Consideration of Downdrag Forces along RIs

For contract methods, most respondents selected design-build (DB) and design-bid-build (DBB) methods, with more than 77% preferring the DB method, proving it is the most popular contracting method for implementing RI projects.
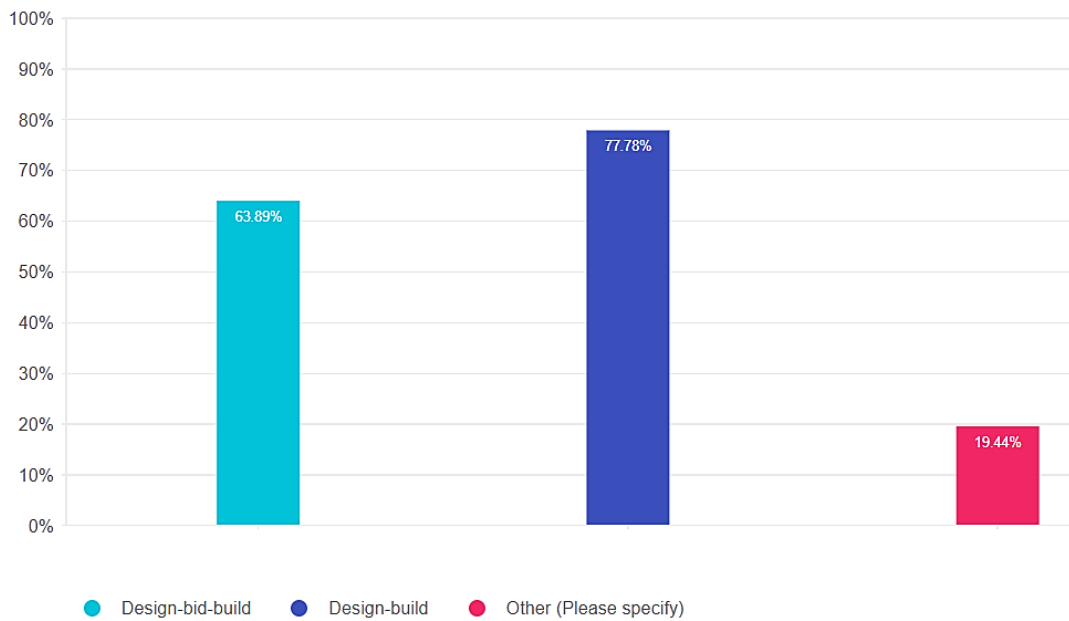
Figure 3.23: Common Contract Methods for RI Projects

Figure 3.24 shows that more than 57% of the respondents followed owner provisions for RI projects, while 20% of the respondents adhered to contractor specifications.
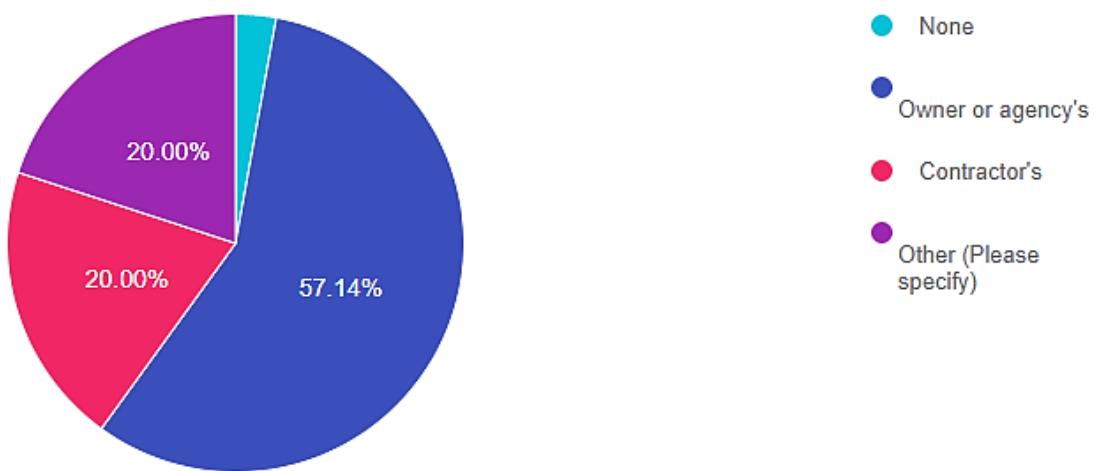
Figure 3.24: Common Specifications or Standards for RI Projects

3.4 Summary

An internet-distributed survey evaluated the state of practice for RI usage in transportation projects throughout the U.S. The survey included 25 multiple-choice questions, with 36 responses received from 67 invitations. Respondents represented a diverse range of sectors, including government agencies, construction companies, consulting firms, and academic institutions. The following key findings were compiled:

1. RIs are primarily used for embankments, followed by retaining walls. Other RI applications include bridge foundations, box culverts, and drainage pipes.

2. DDCs are the most widely used type of RIs, followed by ACIPs.

3. RIs are utilized in transportation projects primarily to reduce settlement, with additional objectives including increasing bearing capacity, improving global slope stability, and mitigating liquefaction.

4. Although RIs are suitable for installation in nearly all types of soil, the application of RI technology most commonly occurs in clay.

5. Analytical methods and numerical analyses are used most often for RI system design.

6. Analytical methods such as the FHWA strain compatibility method, BS 8006-1, EBGEO, and CUR226 are used to design LTPs in RI systems, with the FHWA method most widely utilized in the U.S.

7. The most common diameters of RIs are 14–18 in.; the most common spacing of RIs is 6–9 ft, although spacing less than 6 ft is used in many projects; and the common area replacement ratio of RIs is 2%–5%. RIs are typically installed without the use of caps, and typical depth range is 30–60 ft.

8. Steel reinforcement in RIs is primarily used to improve slope stability, account for seismic loads, and address other horizontal loads.

9. RIs are predominantly used to support embankments with heights of 20–30 ft.

10. Geogrid is the most widely used reinforcement type in LTPs, followed by woven geotextile.

11. Gravel or graded aggregate base is the primary backfill material in LTPs, followed by sand.

12. Instrumentation and monitoring are occasionally or rarely used in RI projects.

13. The neutral plane method is used to account for downdrag forces.

14. Load testing on individual RIs is the most widely used method to assess RI quality, followed by pile integrity testing.

15. Design-build and design-bid-build methods are preferred contract methods for RI projects; the design-build approach is most popular.

16. Most RIs are constructed following owner or agency provisions, while a smaller portion adhere to contractor standards or alternative specifications.

Chapter 4: Design Methods for Load Transfer Platforms

Based on the literature review and the survey, this study utilized the collected data (Chapter 2) and numerical analysis to evaluate four design methods (BS 8006-1, EBGEO, CUR226, and FHWA strain compatibility) commonly used for LTPs. Although the same output parameters were selected, each design method requires unique input parameters.

4.1 Design Parameters

This study evaluated input and output parameters of each design method. Some design methods require more input parameters than others, and the output parameters are often used to satisfy design criteria.

4.1.1 Input Parameters

The input parameters for all the design methods include the properties of fill material, subsoil, GR, and RIs, as listed in Table 4.1.

Table 4.1: Input Parameters for Design Methods

No.	Items	Input Parameters	Design Methods
1.	Embankment/Fill	Height (H)	BS 8006-1, EBGEO, CUR226, and FHWA
		Unit weight (γ)	
		Friction angle (ϕ)	
		Surcharge (q)	
		Elastic modulus of arching soil (E_a), Poisson's ratio (ν)	FHWA
2.	Geosynthetic reinforcement	Stiffness (J)	BS 8006-1, EBGEO, CUR226, and FHWA
3.	Rigid inclusion	Width of inclusion head/cap (a)	BS 8006-1, EBGEO, CUR226, and FHWA
		Spacing in both directly (S_x, S_y)	
		Young's modulus (E_c)	FHWA
		Length (L)	
4.	Soft soil	Subgrade modulus (K)	EBGEO and FHWA
		Thickness (d)	
		Elastic modulus of soft soil (E_s)	
		Compression index (C_c), recompression index (C_r), and overconsolidation ratio (OCR)	
		Coefficient of consolidation (C_v)	
		Time of consolidation (T)	

The properties of fill materials, GR, and RI configuration were taken from the literature while the subsoil properties were taken from the literature or back-calculated using available correlations. The subgrade soil moduli of subsoils for the case studies were taken from Pham and Dias (2021), and the thickness of the subsoil for analysis was estimated per Malikova (1972), using the following relationship:

$$d = \sqrt[4]{\frac{b}{a'}}$$

Equation 4.1

Where:

a' = 1.7×10⁻⁵/ft³ (6×10⁻⁴ /m³), and

$b = (s - a)$ = clear spacing between the heads of RIs (Pham & Dias, 2021).

The coefficient of volume compressibility (m_v) and elastic modulus (E_s) of the subsoil are related as follows:

$$E_s = \frac{\left(\frac{1}{m_v}\right)(1 + v)(1 - 2v)}{(1 - v)}$$

Equation 4.2

Where v is Poisson's ratio of the subsoil.

The compression index (C_c) and recompression index (C_r) are obtained as

$$C_c = 2.3 m_v \sigma_v'$$

Equation 4.3

Where σ_v' is the effective vertical stress.

$$C_r = \frac{C_c}{5}$$

Equation 4.4

Where C_r is typically (1/5 to 1/10) C_c.

The coefficient of consolidation (C_v) is a required input parameter for the FHWA method and was assumed to be 1.08×10⁻⁶ ft²/s (10×10⁻⁸ m²/s) (Sivakugan, 1990) for the cases of subsoil

(assumed as soft clay) that do not have this value. This assumption might induce some errors in the calculated results. However, since most of the embankment load is transferred to RIs, the rate of consolidation at the end of construction should have reached a high level; therefore, this error should not be significant. Nunez et al. (2013) reported the fast dissipation of excess pore water pressures after construction in their field project. A sensitivity analysis may be conducted in the future to verify the effect of this assumption.

4.1.2 Output Parameters

The output parameters calculated by all the design methods include load efficacy, differential settlement, and maximum tension in GR.

4.1.2.1 Load Efficacy

The load efficacy, which is defined as the proportion of the load exerted by an embankment and surcharge onto the top of RIs, can be categorized as arching efficacy or membrane efficacy. Arching efficacy (E_a) is associated with load transfer due to soil arching (Section 2.5.1) and can be obtained as:

$$E_a = \frac{P_c^a}{(\gamma H + q)S_x S_y} \cdot 100\%$$

Equation 4.5

Where P_c^a is the load transferred on RIs only due to arching.

In comparison, membrane efficacy (E_m) is related to additional load exerted on RIs due to the tension developed in the GR (Section 2.5.2). The EBGEO method works with a triangular load distribution, which gives a third-order polynomial function ($cx^3 + bdx^2$) while the CUR226 method works with an inverse-triangular load distribution for the cases with no or limited subsoil support, which gives a bx^3 function or with a uniform load distribution, which gives a parabolic shape. When the deflection of the GR is assumed to be in a parabolic shape, the membrane efficacy can be obtained as:

$$E_m = \frac{P_c^m}{(\gamma H + q)S_x S_y} \cdot 100\%$$

Equation 4.6

71

Where P_c^m is the load transferred on RIs only due to the membrane effect, which can be further estimated as:

$$P_c^m = 2a_x T_x sin\theta_x + 2a_y T_y sin\theta_y$$

Equation 4.7

Where:

T_x and T_y = the maximum tension generated in the GR in the x- and y-direction respectively, and

θ_x and θ_y = the inclination with the horizontal of the deflected GR at the edge of the pile or pile cap.

The load efficacy (E_t) can then be calculated as:

$$E_t = E_a + E_m$$

Equation 4.8

The BS 8006-1 method assumes that no load is transferred to the subsoil, meaning that it considers a void between RIs. Therefore, the total load efficacy is equal to 100%. The EBGEO and CUR226 methods provide the arching efficacy but require the determination of membrane efficacy to estimate the total load efficacy when GR is present. Using the GeogridBridge 3.0 worksheet, the FHWA method provides the stress reduction ratio (SRR_{fndn}) on the subsoil beneath the GR, which can be used to calculate the total load efficacy.

4.1.2.2 Differential Settlement

Differential settlement (S_d) is defined as the difference between the settlement at two locations. In this study, the differential settlement was the difference between the settlement at the center of the RI head or cap and the midpoint of the center-to-center spacing of the RIs.

4.1.2.3 Maximum Tension in Geosynthetic

The maximum tension (T) can be estimated using the difference in the vertical stresses above and below the GR between the heads of RIs. The formulas or procedures used to calculate the GR tension in various design methods are explained in Section 2.6 in this report.

4.2 Input Parameters from Case Studies

Table 4.2 provides the input parameters from case studies used to evaluate the design methods for load efficacy, differential settlement, and maximum tension.

Table 4.2: Input Parameters from Case Studies

No.	Case Studies	Type	Embankment and Surcharge						RI			Soil	GR
			H	γ	ϕ	c	ϕ_{eqv}	q	S_x	S_y	a	K_s	J
			ft	pcf	°	psf	°	psf	ft	ft	ft	pcf	kip/ft
1	Maddison and Jones (1996)*	Field	11.5	122.2	35.0	-	-	418	8.2	8.2	1.6	-	20
2	Vega-Meyer and Shao (2005)	Field	15.8	133.7	20.0	-	-	0	14.8	12.5	2.3	9549	254
3	Hoppe and Hite (2006)	Field	5.9	133.7	41.0	-	-	328	6.9	6.9	3.0	7639	123
4	Oh and Shin (2007)	Model	8.9	45.8	35.0	21	-	0	2.0	2.0	0.4	1502	16
5	Liu et al. (2007)	Field	18.4	117.8	30.0	209	34.0	0	9.8	9.8	3.3	3501	81
6	Almeida et al. (2007)	Field	4.1	114.6	-	-	68.0	0	8.2	8.2	2.6	-	82
7	Van Eekelen et al. (2010)*	Field	3.8	118.4	33.8	-	-	0	4.2	4.2	0.9	6366	273
8	Chen et al. (2010)	Field	13.1	133.7	32.0	209	35.0	0	6.6	6.6	3.3	3310	103
9	Duijnen et al. (2010)	Field	8.53	116.5	51.0	-	-	0	6.23	4.76	1.16	3056	359
10	Sloan (2011)	Field	7.5	137.0	45.0	-	-	0	6.0	6.0	1.8	-	34
11	Briançon and Simon (2012)	Field	16.4	117.8	20.0	-	-	0	6.6	6.6	1.1	2324	51
12	Van Eekelen et al. (2012)	Model	1.4	105.6	49.0	-	-	1942	1.8	1.8	0.3	-	155
13	Xing et al. (2014)	Field	13.1	114.6	33.0	-	-	1462	11.5	11.5	3.3	3756	38
14	Xu et al. (2016)	Model	1.3	113.9	38.0	313	71.0	418	1.6	1.6	1.0	2228	34
15	Zhang et al. (2016)	Field	16.4	120.9	24.6	351	32.5	0	11.5	11.5	3.3	6939	116
16	Chen et al. (2016)	Field	10.5	134.9	42.0	251	47.0	262	5.9	5.9	3.3	-	168
17	Fagundes et al. (2017)	Model	10.5	99.9	38.0	-	-	0	6.6	6.6	1.6	-	264
18	Briançon and Simon (2017)	Field	13.9	133.7	35.0	-	-	0	5.2	5.2	0.9	3310	909
19	Lee et al. (2020)	Model	8.4	128.6	33.0	-	-	0	3.9	3.9	1.3	1591	29
20	Zhao et al. (2019)	Field	7.9	120.9	22.0	349	31.0	0	14.8	8.2	3.3	5475	112
21	Chen et al. (2020)	Field	9.8	140.0	39.0	104	42.5	1044	9.8	9.8	5.9	2922	348
22	Van Eekelen et al. (2020)	Field	5.9	116.5	51.0	-	-	178	7.4	7.4	2.5	-	316
23	Lamb et al. (2022)*	Field	15.0	120.9	35.0	-	-	0	7.9	7.9	1.3	-	41

No.	Case Studies	Type	Embankment and Surcharge						RI			Soil	GR
			H	γ	ϕ	c	ϕ_{eqv}	q	S_x	S_y	a	K_s	J
			ft	pcf	°	psf	°	psf	ft	ft	ft	pcf	kip/ft
24	Gunnvard et al. (2022)*	Field	5.6	140.0	45.0	-	-	0	3.3	3.3	0.7	12095	78
25	Van Eekelen et al. (2023)*	Field	5.0	120.9	34.0	-	-	240	7.4	7.5	2.5	-	166
26	Izadifar et al. (2024)*	Field	23.0	124.8	45.0	-	-	0	3.5	3.5	0.9	5481	407

Source: Pham & Dias (2021)

Note: H - height of embankment/fill, γ - unit weight, ϕ - friction angle, ϕ_{eqv} - equivalent friction angle, c - cohesion, q - surcharge, S_x - RI spacing in the x-direction, S_y - RI spacing in the y-direction, a - equivalent width of square-shaped RI, K_s - modulus of subgrade reaction, J - geosynthetic stiffness (when this value is different in two directions for few cases, the lower value was used), * denotes additional case studies added to Pham and Dias (2021), and - denotes no available information.

4.3 Output Results

4.3.1 Load Efficacy

Table 4.3 presents the load efficacy values predicted by various methods versus the measured data from the case studies. Each calculated value was normalized by its corresponding measured value as a load efficacy ratio. Figure 4.1 compares these results, indicating that the EBGEO, CUR226, and FHWA methods provides more accurate predictions than the BS 8006-1 method, which overestimated the load efficacy. Other methods produced inconsistent results, including overestimation and underestimation. An overestimation of load efficacy is a prediction of more load to the RIs than measured, and an underestimation is less load to the RIs than measured. BS 8006-01 overpredicted RI loads because it is always 100%, which is unrealistic in many cases especially with more competent soils near ground surface.
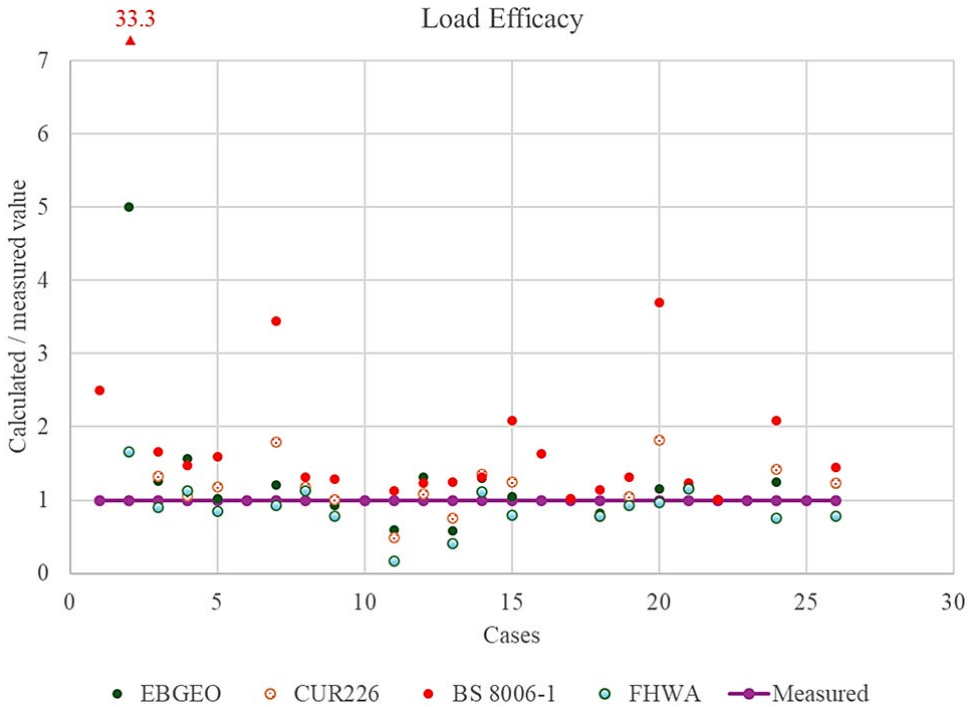
Figure 4.1: Comparison of Load Efficacy Ratios of Design Methods and Measured Data

Table 4.3: Load Efficacy Results from Design Methods and Measurements

No.	Case Studies	Arching Efficacy (E_a, %)			Membrane Efficacy (E_m, %)		Load Efficacy ($E_a + E_m$, %)				
		EBGEO	CUR226	BS8006	EBGEO	CUR226	EBGEO	CUR226	BS8006	FHWA	Measured
1	Maddison and Jones (1996)*	-	-	43	-	-	-	-	100	-	40
2	Vega-Meyer and Shao (2005)	15	20	10	0	6	15	26	100	5	3
3	Hoppe and Hite (2006)	76	76	56	0	3	76	80	100	54	60
4	Oh and Shin (2007)	51	39	46	56	25	107	72	100	77	68
5	Liu et al. (2007)	63	58	66	1	8	64	74	100	53	63
6	Almeida et al. (2007)	-	-	10	-	-	-	-	100	-	-
7	Van Eekelen et al. (2010)*	32	45	26	3	9	35	52	100	27	29
8	Chen et al. (2010)	85	81	83	2	6	87	90	100	86	76
9	Duijnen et al. (2010)	70	74	54	2	6	72	79	100	61	78
10	Sloan (2011)	-	-	58	-	-	-	-	100	-	-

No.	Case Studies	Arching Efficacy (E_a, %)			Membrane Efficacy (E_m, %)		Load Efficacy ($E_a + E_m$, %)				
		EBGEO	CUR226	BS8006	EBGEO	CUR226	EBGEO	CUR226	BS8006	FHWA	Measured
11	Briançon and Simon (2012)	51	16	51	2	25	53	43	100	15	89
12	Van Eekelen et al. (2012)	44	57	20	61	31	106	88	100	-	81
13	Xing et al. (2014)	47	53	45	0	7	47	60	100	33	80
14	Xu et al. (2016)	89	86	77	10	10	99	103	100	85	76
15	Zhang et al. (2016)	49	42	52	0	6	50	60	100	38	48
16	Chen et al. (2016)	-	-	87	-	-	-	-	100	-	61
17	Fagundes et al. (2017)	-	-	56	-	-	-	-	100	-	98
18	Briançon and Simon (2017)	39	43	32	33	29	72	69	100	69	88
19	Lee et al. (2020)	59	64	68	20	16	79	80	100	71	76
20	Zhao et al. (2019)	30	36	38	0	6	31	49	100	26	27
21	Chen et al. (2020)	95	88	79	1	5	95	95	100	94	81
22	Van Eekelen et al. (2020)	-	-	44	-	-	-	-	100	-	99
23	Lamb et al. (2022)*	-	-	32	-	-	-	-	100	-	-
24	Gunnvard et al. (2022)*	60	62	59	0	3	60	68	100	36	48
25	Van Eekelen et al. (2023)*	42	55	24	71	-	113	-	100	36	-
26	Izadifar et al. (2024)*	78	79	80	6	8	84	85	100	54	69

Note: * denotes additional case studies added to Pham and Dias (2021) and – denotes no available information.

4.3.2 Differential Settlement

Table 4.4 presents the calculated differential settlements for various methods compared to the case studies. Figure 4.2 shows a comparison of the differential settlement ratios, indicating that the EBGEO, CUR226, and FHWA methods provided more accurate predictions than the BS 8006-1 method, which overestimated the differential settlements. The main reason for the BS 8006-1 method overestimating these settlements is that no subsoil support is assumed under the LTPs.

Table 4.4: Differential Settlements from Design Methods and Measurements

No.	Case Studies	Differential Settlement (inches)				
		EBGEO	CUR226	BS 8006-1	FHWA	Measured
1	Maddison and Jones (1996)*	-	-	49.41	-	0.28
2	Vega-Meyer and Shao (2005)	2.90	2.17	55.75	1.73	4.06
3	Hoppe and Hite (2006)	0.91	0.51	6.33	1.61	0.59
4	Oh and Shin (2007)	2.78	1.79	4.76	2.36	2.40
5	Liu et al. (2007)	5.06	3.51	18.49	6.81	2.83
6	Almeida et al. (2007)	-	-	11.99	-	4.33
7	Van Eekelen et al. (2010)*	1.08	0.51	3.92	1.42	-
8	Chen et al. (2010)	1.70	1.61	4.33	3.70	1.57
9	Duijnen et al. (2010)	1.87	1.05	7.59	3.66	-
10	Sloan (2011)	-	-	11.89	-	10.67
11	Briançon and Simon (2012)	5.80	8.37	24.48	1.89	1.61
12	Van Eekelen et al. (2012)	2.25	1.57	3.05	-	2.13
13	Xing et al. (2014)	3.81	4.80	51.83	6.18	-
14	Xu et al. (2016)	0.37	0.24	0.54	0.28	0.09
15	Zhang et al. (2016)	3.81	2.19	25.52	4.33	2.83
16	Chen et al. (2016)	-	-	2.41	-	1.38
17	Fagundes et al. (2017)	-	-	7.32	-	10.44
18	Briançon and Simon (2017)	4.12	2.16	6.52	4.37	1.15
19	Lee et al. (2020)	3.95	2.91	5.79	4.41	-
20	Zhao et al. (2019)	3.27	1.45	37.27	3.90	1.34
21	Chen et al. (2020)	1.29	1.65	4.26	2.91	1.08
22	Van Eekelen et al. (2020)	-	-	6.47	-	3.94
23	Lamb et al. (2022)*	-	-	39.69	-	0.50
24	Gunnvard et al. (2022)*	0.75	0.31	4.56	0.83	1.18
25	Van Eekelen et al. (2023)*	7.65	5.08	9.20	5.63	4.33
26	Izadifar et al. (2024)*	1.62	1.27	2.89	0.31	0.28
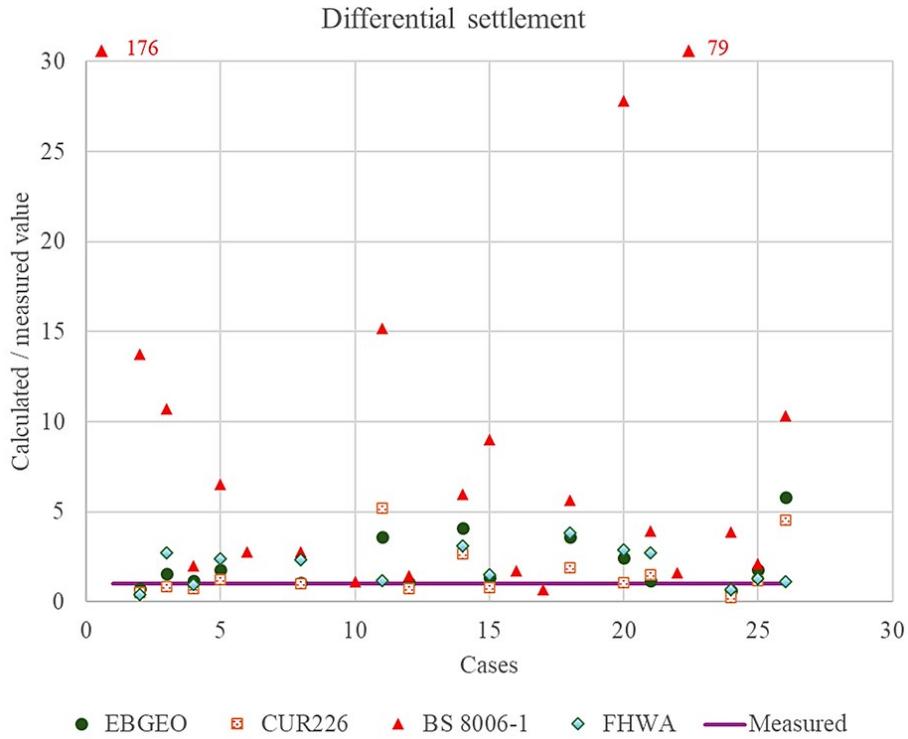
Figure 4.2: Comparison of Differential Settlement Ratios for Predicted and Measured Data

4.3.3 Geosynthetic Tension

Table 4.5 shows the calculated geosynthetic reinforcement tension for various methods compared to the case studies, and Figure 4.3 shows a comparison of the geosynthetic reinforcement tension ratios. Definite conclusions were difficult to draw due to limited available data, but the CUR226 and FHWA methods provided more accurate predictions than the BS 8006-1 and EBGEO methods, which overestimated geosynthetic reinforcement tension.

Table 4.5: Geosynthetic Tension from Design Methods and Measurements

No.	Case Studies	Geosynthetic Tension (lb/ft)				
		EBGEO	CUR226	BS 8006-1	FHWA	Measured
1	Maddison and Jones (1996)*	-	-	20752	-	-
2	Vega-Meyer and Shao (2005)	254	1998	94215	526	629
3	Hoppe and Hite (2006)	123	223	5902	372	-
4	Oh and Shin (2007)	966	504	1192	2354	404
5	Liu et al. (2007)	889	1460	11884	1597	1857
6	Almeida et al. (2007)	-	-	7034	-	939
7	Van Eekelen et al. (2010)*	547	469	7225	928	-
8	Chen et al. (2010)	514	791	3303	2453	-
9	Duijnen et al. (2010)	897	941	14787	4803	-
10	Sloan (2011)	-	-	4937	-	-
11	Briançon and Simon (2012)	1079	4951	19145	110	-
12	Van Eekelen et al. (2012)	6686	-	12308	-	-
13	Xing et al. (2014)	154	1478	28380	403	-
14	Xu et al. (2016)	206	164	425	117	-
15	Zhang et al. (2016)	466	1135	20885	593	-
16	Chen et al. (2016)	-	-	2636	-	959
17	Fagundes et al. (2017)	-	-	10867	-	27538
18	Briançon and Simon (2017)	15006	10690	37631	16774	9093
19	Lee et al. (2020)	1330	892	2602	1519	-
20	Zhao et al. (2019)	168	537	21787	508	-
21	Chen et al. (2020)	592	1582	7537	3515	-
22	Van Eekelen et al. (2020)	-	-	10112	-	2905
23	Lamb et al. (2022)*	-	-	27812	-	-
24	Gunnvard et al. (2022)*	117	159	4269	136	2330
25	Van Eekelen et al. (2023)*	7148	4625	10353	3964	3490
26	Izadifar et al. (2024)*	2850	2431	9137	57	1456
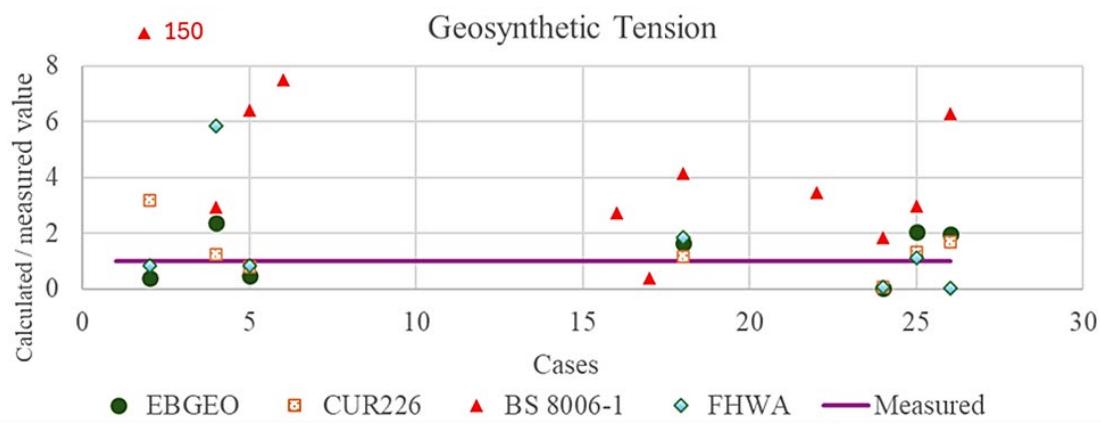
Figure 4.3: Comparison of Geosynthetic Tension Ratios for Predicted and Measured Data

4.4 Numerical Analysis

This study developed finite difference numerical models to simulate two case studies to evaluate the behavior and performance of the RIS embankment and the mechanically stabilized earth (MSE) wall and further assess the four design methods. Numerical simulation was carried out using FLAC3D V9.0, software developed by Itasca Consulting Group, Inc. The two cases considered for numerical analysis are discussed in detail in Sections 4.4.1 and 4.4.2.

4.4.1 ASIRI Project

The ASIRI project consisted of a full-scale experiment on four test sections at the Chelles test site located approximately 12 miles northeast of Paris, France, as described in Briançon and Simon (2012) and shown in Figure 4.4. Three test sections were analyzed in this study. Test section I consisted of a 16.4-ft (5-m) high embankment constructed on unsupported soil (Zone 1R), Test section II had an embankment supported by RIs with a diameter of 15 in. (380 mm) and a center-to-center spacing of 6.6 ft (2.0 m) without a LTP (Zone 2R), and Test section III had a two-layer geogrid-reinforced LTP supported by RIs in soft soil (Zone 4R), which was selected as a reinforced section instead of Zone 3R without any special reason. Figures 4.5 and 4.6 present the global and unit-cell numerical models, respectively. Table 4.6 provides the information required for the numerical models from the Chelles site.

a) Cross Section
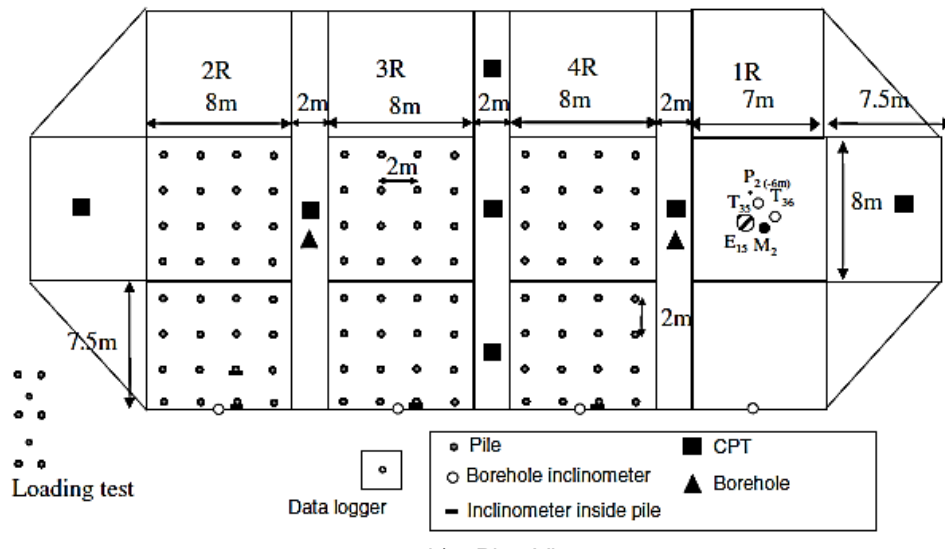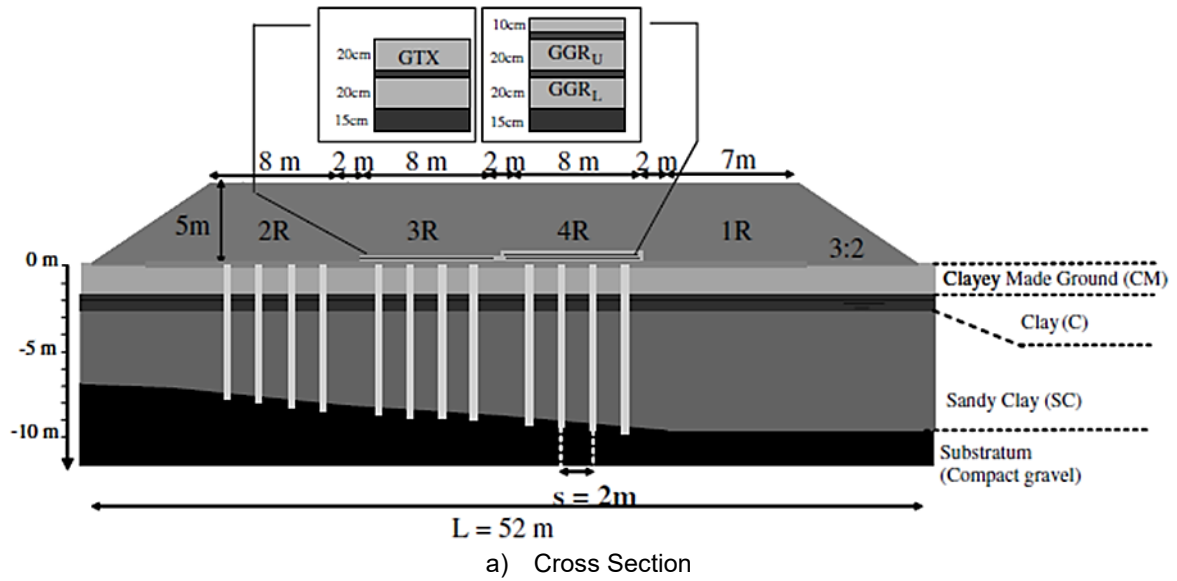
b) Plan View

Figure 4.4: Chelles Site Profile and Cross Section: (a) Cross Section and (b) Plan View
Source: Briançon and Simon (2012)
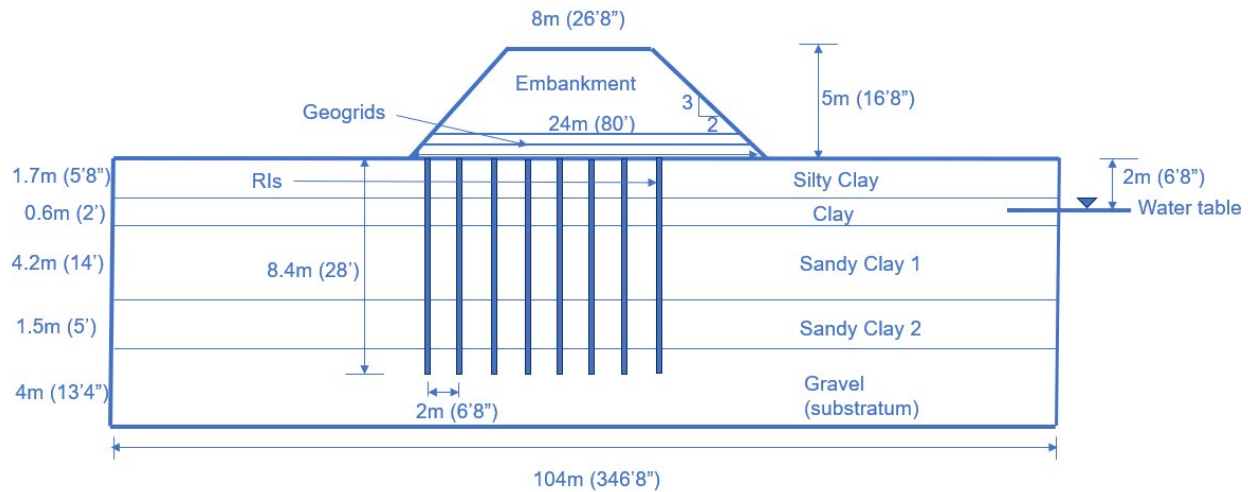
Figure 4.5: Simplified Global Numerical Model of Test Section Zone 4R
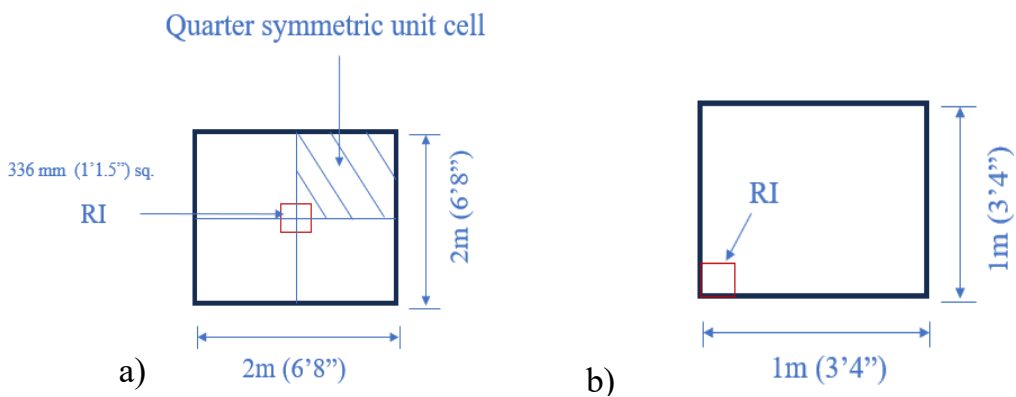
Figure 4.6: Plan View of the Unit Cell: (a) Full Model and (b) Quarter Model

Table 4.6: Input Parameters for Numerical Modeling of ASIRI Project

No.	Parameter	Units	Embankment	LTP	Silty Clay	Clay	Sandy Clay 1	Sandy Cay 2	Gravel
							Soil Layers		
1	Density, γ	pcf	122	134	127	95	127	127	127
2	Thickness	ft	16.4	1.6	5.6	2	13.8	4.9	13.1
3	Compressibility index, C_c	-	-	-	-	0.2	0.54	0.1	0.13
4	$\lambda = C_c/2.3$	-	-	-	-	0.087	0.235	0.044	0.056
5	Recompression index, C_r	-	-	-	-	0.03	0.05	0.01	0.01
6	$\kappa = C_r/2.3$	-	-	-	-	0.013	0.022	0.005	0.004
7	Void ratio, e_0	-	-	-	-	1	1.7	0.7	0.6
8	Specific volume reference, $v_\lambda = 1+e_0$	-	-	-	-9	2	2.7	1.7	1.6
9	Effective friction angle, ϕ'	°	36.6	36	26	26	26	26	33
10	Effective cohesion, c'	ksf	0.36	1.27	-	-	-	-	-
11	Dilatancy, Ψ'	°	6.6	3	-	-	-	-	-
12	Overconsolidation stress σ'_p	ksf	-	-	0.63	0.63 + σ'_v	0.63 + σ'_v	0.63 + σ'_v	-
13	Elastic modulus, E	ksf	1044	1462	-	-	-	-	-
14	Poisson ratio, ν	-	0.3	0.3	0.3	0.3	0.3	0.3	0.3
15	Reference pressure, p_1	ksf	-	-	0.02	0.02	0.02	0.02	-
16	Critical state ratio, $M = 6\sin\phi/(3-\sin\phi)$	-	-	-	-	1.026	1.026	1.026	1.026

The unit-cell model in Figure 4.7 covers one-quarter of the tributary area of an RI in the center for all three sections by advantageously utilizing its symmetry to simplify the analysis. Figure 4.8 presents the simplified global models for these three sections. The horizontal deformations were restrained by roller supports at the lateral boundaries, and fixed supports restrained all the deformations at the base of the model. The embankment fill or LTP material and the stiff bearing layer were simulated incorporating a Mohr-Coulomb constitutive model and the soft soil layers were simulated as Modified Cam Clays. Considering the square RI pattern and the square unit cell, the circular RIs were converted into square RIs with the same cross section area and modeled as a linearly elastic material. The geogrids were modeled as structural elements, and the interfaces between soil and RIs were modeled with the Mohr-Coulomb constitutive model.
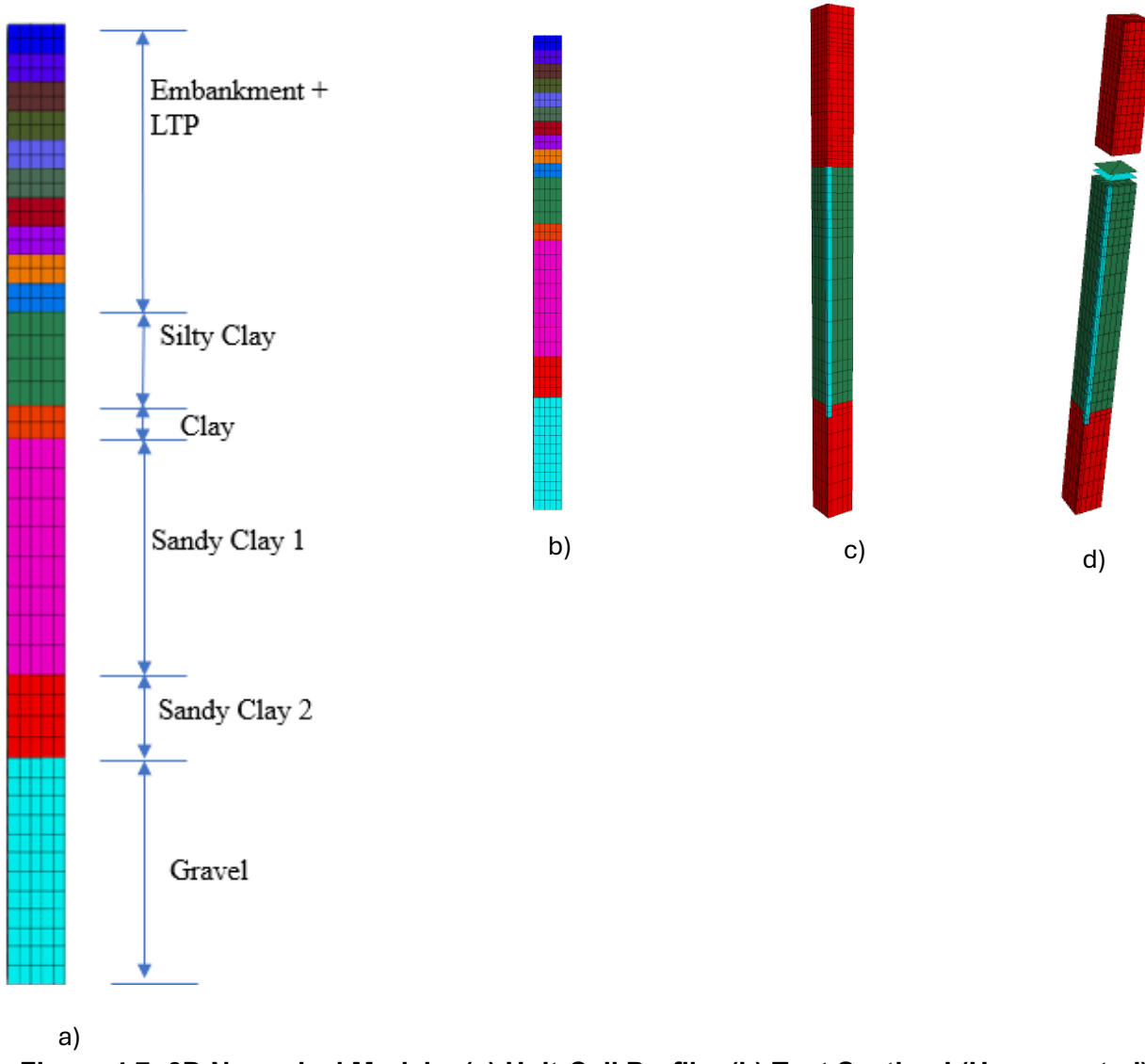
Figure 4.7: 3D Numerical Models: (a) Unit-Cell Profile; (b) Test Section I (Unsupported); (c) Test Section II (Supported with RI Only); and (d) Test Section III (Supported with RI and Two Layers of Geogrids)
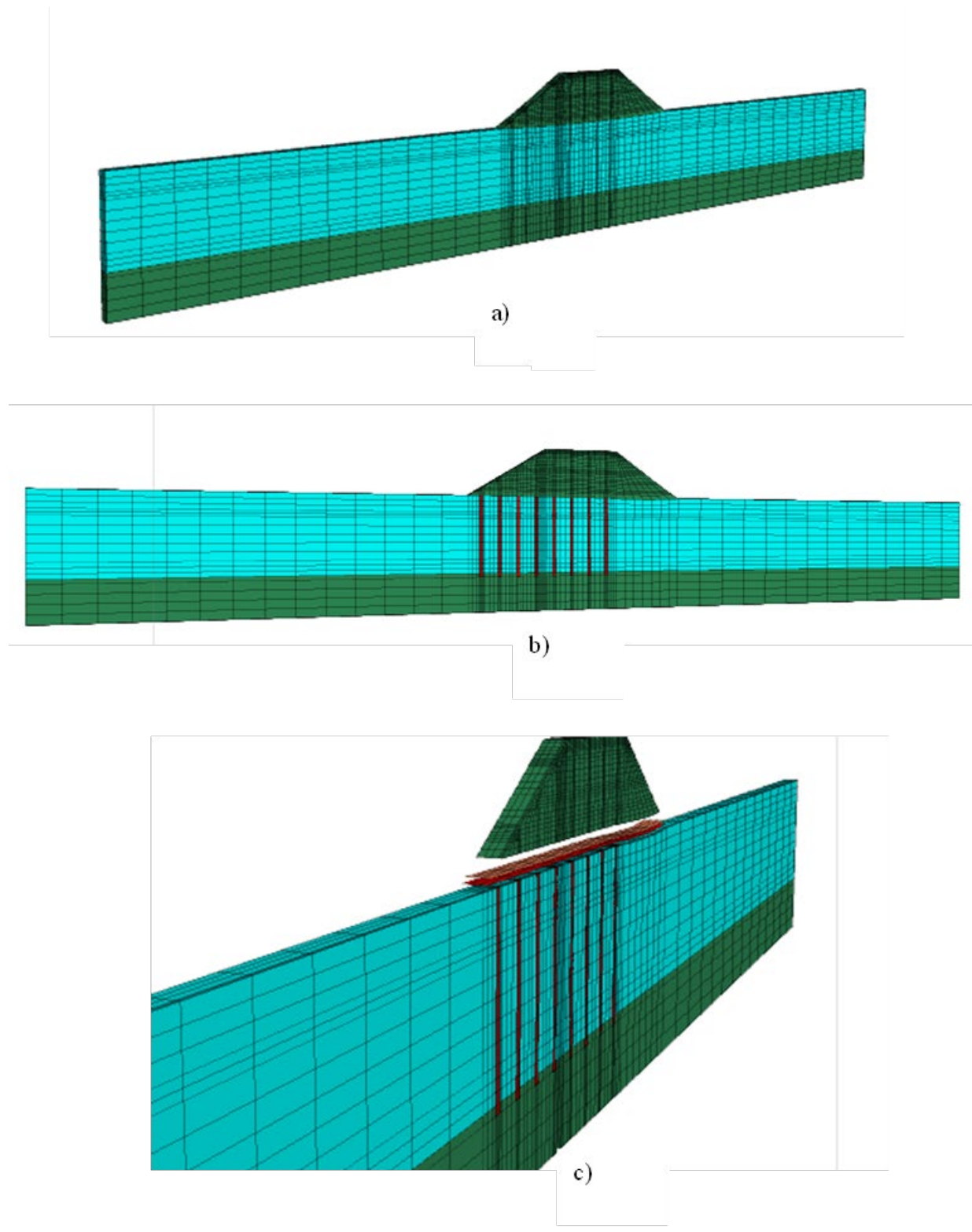
Figure 4.8: FLAC3D Models: (a) Test Section I (Unsupported); (b) Test Section II (Supported with RI Only); and (c) Test Section III (Supported with RI and Two Layers of Geogrids)

In the numerical analysis, the soft soil model was constructed and run to the equilibrium under gravity to create an initial ground. The RIs were installed by changing the properties of the respective volume elements at the RI locations and then the equilibrium was attained before the embankment fill or GR was placed at the actual elevations within the LTP. The simulation of staged construction of the embankment was carried out by placing the fill in 10 stages and the model was solved for the placement of each lift. This numerical analysis was performed in a large strain mode. Consolidation effect was not considered because the dissipation of excess pore water pressure was rapid (Nunez et al., 2013) and its effect was considered negligible. One of the reasons for the fast dissipation of excess pore water pressure is attributed to the load transfer from soil to RIs, which results in reduction of applied soil stresses (i.e., unloading) (Han, 2015).

After the numerical simulation, settlements of the subsoil in Section I were obtained at different depths and compared to settlements from the experiment (Briançon and Simon, 2012) as well as numerical results from Nunez et al. (2013) and Salah and Yassmina (2022), as shown in Figure 4.9 and Table 4.7, respectively. Tables 4.8 and 4.9 show the settlement efficacy and load efficacy calculated for different sections. The settlement efficacy, defined by Equation 4.9, is the percentage by which the settlement of the subsoil is reduced after installing RIs and GR.

$$Settlement\ Efficacy = \left[1 - \frac{Settlement\ with\ support (RI\ or\ RI + geogrid)}{Settlement\ without\ support} \right] \times 100\%$$

Equation 4.9

Greater settlement efficacy indicates less settlement of the subsoil after ground improvement with the use of RIs and GR. Numerical results from this study showed reasonable comparisons with the field data and other numerical results. A comparison of the load efficacy and differential settlement from this numerical analysis to calculations by the design methods and measurements showed that the numerical results for Sections I and III were close to the field data and previous numerical results by others. Even though the numerical results for Sections II from three numerical studies are close (especially between this study and Nunez et al., 2013), they are much different from the measured results. The reasons for these differences are unknown.

Table 4.7 also shows that the global model (GM) in Salah and Yassmina (2022) and this study calculated larger settlements than the unit cell model. This difference can be explained as

the global model allowed lateral deformations but the unit cell model restricted lateral deformations. It is not clear why the global model in Nunez et al. (2013) calculated smaller settlements in Section I but larger settlements in Sections II and III than the unit cell model.
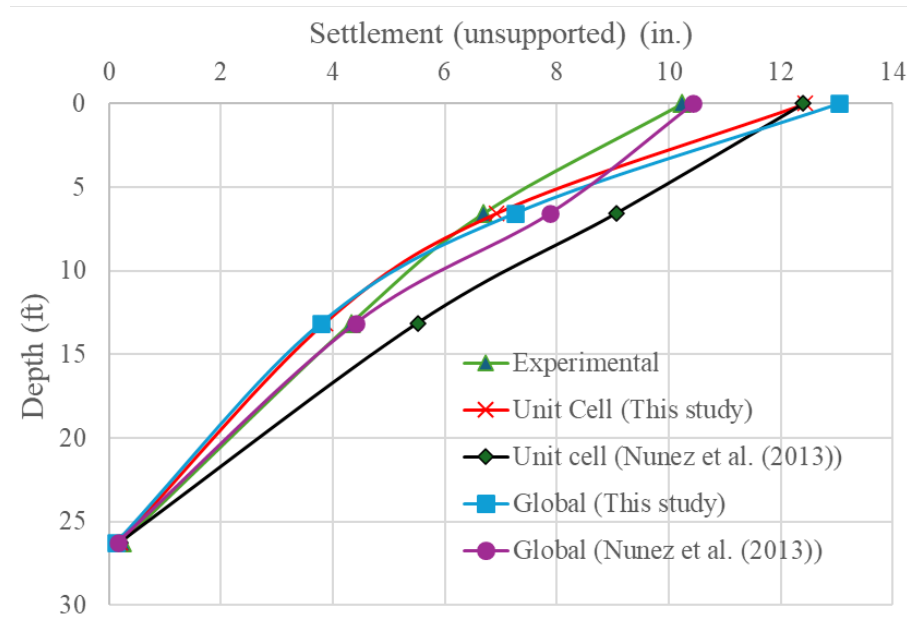
Figure 4.9: Comparison of Settlements from Numerical Analysis and Field Measurement for Section I

Table 4.7: Comparison of Settlements by Sections

Section	Depth (ft)	Soil Settlement (in.)								Difference from the Experiment (%)					
		Exp.	Nunez et al. (2013)		This study		Salah and Yassmina (2022)			Nunez et al. (2013)		This study		Salah and Yassmina (2022)	
			Unit Cell	GM	Unit Cell	GM	Unit Cell	GM		Unit Cell	GM	Unit Cell	GM	Unit Cell	GM
I (unsupported, Zone 1R)	0.0	10.2	12.4	10.4	12.4	13.0	12.0	13.8		21	2	22	27	18	35
	6.6	6.7	9.1	7.9	6.9	7.2	-	-		35	18	4	8	-	-
	13.1	4.3	5.5	4.4	3.9	3.8	-	-		27	2	-11	-13	-	-
	26.2	0.2	0.2	0.2	0.2	0.1	-	-		-17	-33	-17	-47	-	-
II (RI only, Zone 2R)	0.0	4.1	1.6	2.4	1.7	2.0	0.7	1.1		-62	-41	-60	-50	-83	-74
III (RI +geogrid, Zone 4R)	0.0	2.5	1.6	1.9	1.5	1.8	-	-		-38	-25	-42	-30	-	-

Note: GM = global model

Table 4.8: Comparison of Settlement Efficacies for Sections

Section	Settlement Efficacy (%)						
	Experiment	Nunez et al. (2013)		This Study		Salah and Yassmina (2022)	
		Unit Cell	Global	Unit Cell	Global	Unit Cell	Global
II (RI only, Zone 2R)	60	87	76	87	84	94	92
III (RI + geogrid, Zone 4R)	75	87	81	89	86	-	-

Table 4.9: Comparison of Load Efficacies for Sections

Section	Load Efficacy (%)				
	Experiment	Nunez et al. (2013)		This Study	
		Unit Cell	Global	Unit Cell	Unit Cell
II (RI only, Zone 2R)	18	46	50	70	85
III (RI + geogrid, Zone 4R)	74	53	66	77	90

Table 4.8 shows that this study obtained similar settlement efficacies as Nunez et al. (2013), but both overestimated the values as compared with the measured (experimental) data. The magnitude of this parameter depends not only on the settlement without RIs but also on the settlement with RIs. Large settlement without RIs and/or small settlement with RIs lead to small settlement efficacies.

Table 4.9 shows that the load efficacies for Section II calculated by Nunez et al. (2013) and this study were much greater than that measured. It seems that the measured load efficacy for Section II is unreasonably small. However, the load efficacies for Section III calculated in this study (especially the unit cell model) reasonably matched that measured.

Section III (Zone 4R) with RIs and GR was selected for the comparison of the measured data with those from the design methods in the following section.

Figures 4.10 and 4.11 compare the numerical results of load efficacy and differential settlement, respectively, to the design methods and the experiment results for Section III. The unit-cell model and the global model generated different results for load efficacy, and the numerical analysis using the unit-cell model provided more accurate load efficacy results than all the design methods. Results from the EBGEO and CUR226 methods were most similar to results from the

experimental data. The FHWA method underestimated the results, while the BS 8006-1 method overestimated the results since the BS 8006-1 method assumes all the load is transferred to the RIs via soil arching and tensioned membrane effect. In terms of the differential settlement, Figure 4.11 shows that the unit cell model and the global model generated the same results, while the FHWA method produced results that were most similar to the experimental values. All design methods overestimated the differential settlements, but the numerical analysis underestimated the results.
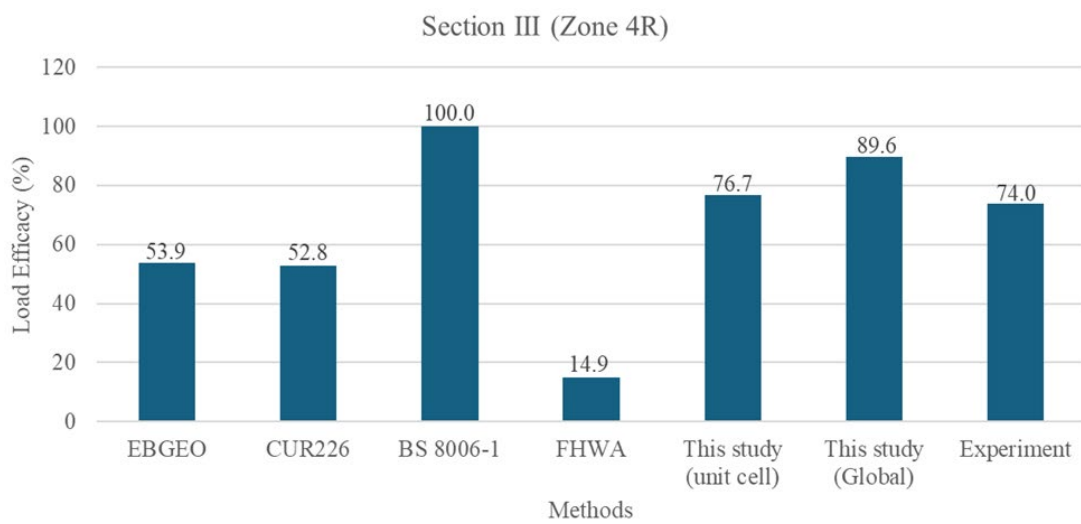
Figure 4.10: Comparison of Load Efficacy from Numerical Analysis, Design Methods, and Measurements
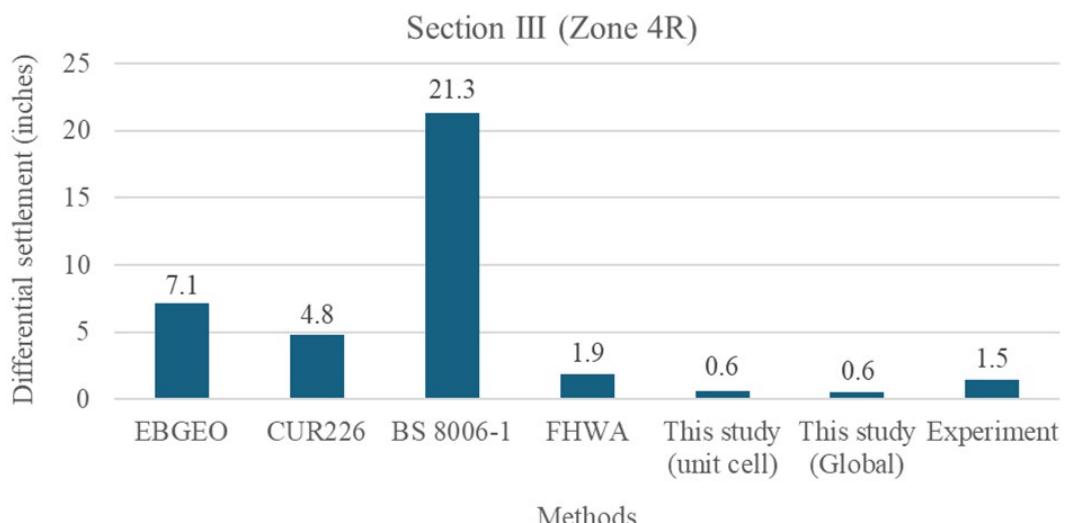
Figure 4.11: Comparison of Differential Settlements from Numerical Analysis, Design Methods, and Measurements

89

4.4.2 Louisiana Case Study

Izadifar et al. (2024) presented a case study of a geosynthetic-reinforced RIS MSE wall at the LA1 Intracoastal Bridge site in Port Allen, Louisiana. The MSE wall was 19.5 ft (5.93 m) high and supported by timber pile RIs with diameters of 1 ft (300 mm) and spacings of 3.5 ft (1.07 m). The geosynthetic-reinforced LTP on top of the RIs was 3.5 ft (1.07 m) thick. Figure 4.12 shows the soil profile of this site in which the geosynthetic reinforcement consisted of six geogrid layers (3 BXP30 and 3 UX1600) and two geotextile layers (Type D GTX) that were separated by fill every 0.5 ft (0.15 m).

For numerical analysis, the MSE wall material was modeled using a Mohr-Coulomb model, the LTP material was simulated with the plastic hardening model, the RIs were linear elastic material, and the GRs were modeled as structural elements. Table 4.10 provides the properties of these materials. The elastic modulus of timber piles was 1160 ksi (8 GPa). Horizontal deformations of the model were restrained by roller supports at the lateral boundaries, and all the deformations were restrained at the base of the model by fixed supports. Numerical modeling and simulation sequence were similar to those of the previous case study, although the consolidation of soft soils was simulated using the coupled fluid-mechanical approach. The semi-symmetric model (shaded region) shown in Figure 4.13 was developed using the symmetric condition to simplify and reduce computational effort.
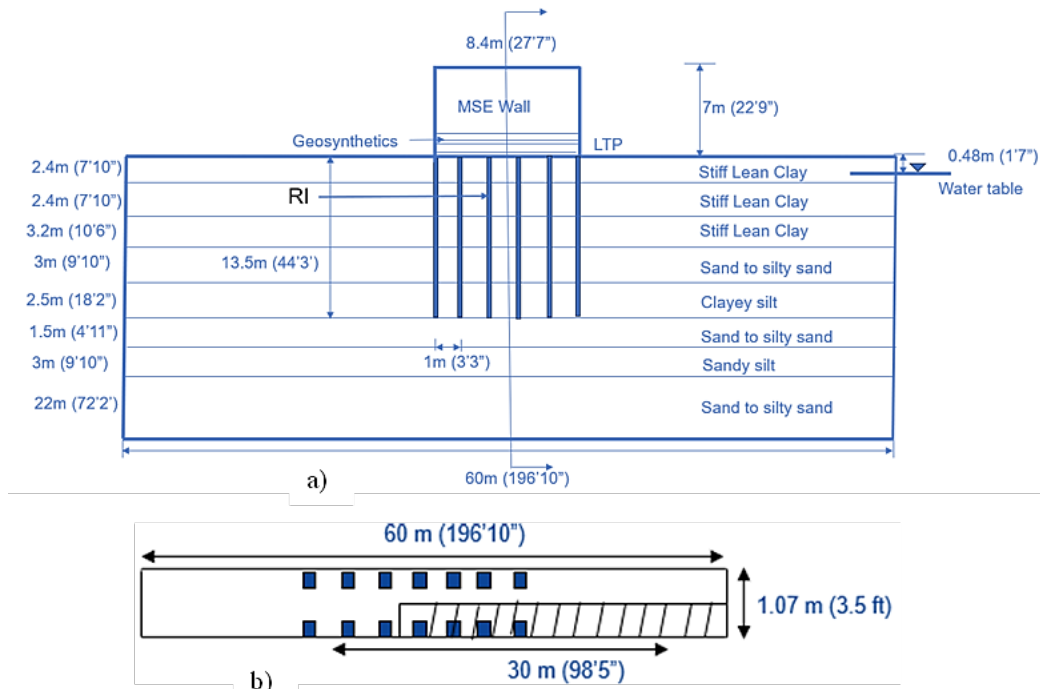
Figure 4.12: (a) Schematic Diagram of MSE Wall Supported by RIs (Not to Scale); (b) Plan View of Simplified Geometry
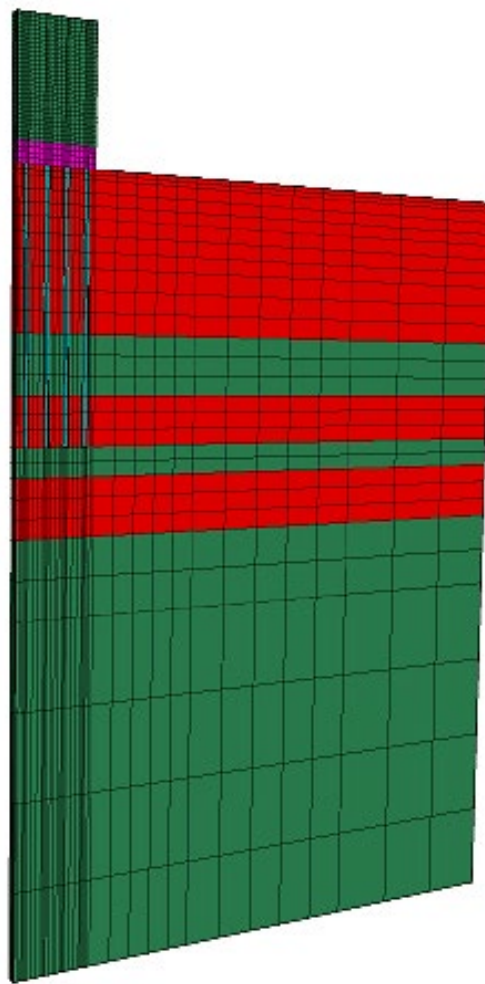
Figure 4.13: 3D Semi-Symmetric Numerical Model

Table 4.10: Input Parameters and Values in Numerical Modeling of the Louisiana Case Study

No	Parameter	Unit	Items									
			MSE wall	LTP	Stiff lean clay	MSE wall	Stiff lean clay	Sandy to silty sand	MSE wall	Sandy to silty sand	Sandy silt	MSE wall
1	Density (γ)	pcf	115	116	119	130	114	125	117	131	125	118
2	Thickness	ft	19.5	3.5	7.9	7.9	10.5	9.8	8.2	4.9	9.8	13.1
3	Cam-clay comp. index (λ)	-	-	-	0.071	0.085	0.052	-	0.045	-	0.059	-
4	Comp. index ($C_c = 2.3\lambda$)	-	-	-	0.142	0.17	0.104	-	0.1035	-	0.1357	-
5	Cam-clay recomp. index (κ)	-	-	-	0.016	0.032	0.0057	-	0.0343	-	0.0096	-
6	Recomp. index ($C_r = 2.3\kappa$)	-	-	-	0.037	0.074	0.0131	-	0.0789	-	0.0221	-
7	Void ratio (e_0)	-	0.42	-	1.03	0.97	0.94	0.71	0.84	0.64	0.837	0.53
8	Specific volume reference ($v_\lambda = 1+e_0$)	-	-	-	2.03	1.97	1.94	-	1.84	-	1.837	-
9	Effective friction angle (ϕ')	°	45	45	-	-	-	24	-	23.5	-	24
10	Effective cohesion (c')	ksf	1	418	-	-	-	2.5	-	2.5	-	-
11	Dilantacy (Ψ')	°	-	15	-	-	-	-	-	-	-	-
12	OC stress (σ'_p)	ksf	-	-	0.79	0.79 +σ'v	0.79 +σ'v	-	-	0.79 +σ'v	-	-
13	Coef. of earth pressure at rest (k_0)	-	0.1	-	0.91	0.91	0.76	0.59	0.61	0.6	0.53	0.59
14	Elastic modulus (E)	ksf	731	-	-	-	-	731	-	1358	-	1462
16	Poisson ratio (ν)	-	0.3	0.2	0.25	0.25	0.25	0.35	0.3	0.35	0.3	0.35

No	Parameter	Unit	Items									
			MSE wall	LTP	Stiff lean clay	MSE wall	Stiff lean clay	Sandy to silty sand	MSE wall	Sandy to silty sand	Sandy silt	MSE wall
17	Reference pressure (p_1)	ksf	-	-	0.02	0.02	0.02	-	-	0.02	-	-
18	Permeability ($k_v * 10^3$)	ft/day	283	-	0.88	0.69	0.95	283	3.83	283	2.69	2834
19	Critical state ratio ($M = 6\sin\phi/ (3-\sin\phi)$)	-	-	-	1.07	1.11	1.11	-	0.8	-	1.03	-
20	Elastic Modulus, MPa (kip/ft²) for LTP, E_{50}^{ref} = 35 (701), E_{oed}^{ref} = 26.4 (551), E_{ur}^{ref} = 103 (2155), Power (m) = 0.5											

Source: Izadifar et al. (2024)

This study computed settlements of the soil and the RIs using FLAC3D and then compared them to results from the field and the FEM (Izadifar et al., 2024). The numerical analysis in this study more accurately predicted the soil settlement at the mid-point between RIs, but slightly less accurately predicted the settlement of the RIs than those by Izadifar et al. (2024); thereby, increasing the differential settlement, as shown in Figure 4.14. These models provided generally closer predictions and also more conservative (higher) estimates of differential settlement than those in the previous case. One major difference between these two case studies is a wall without slopes versus an embankment with slopes. The effect of slopes on RI systems should be investigated in the future.
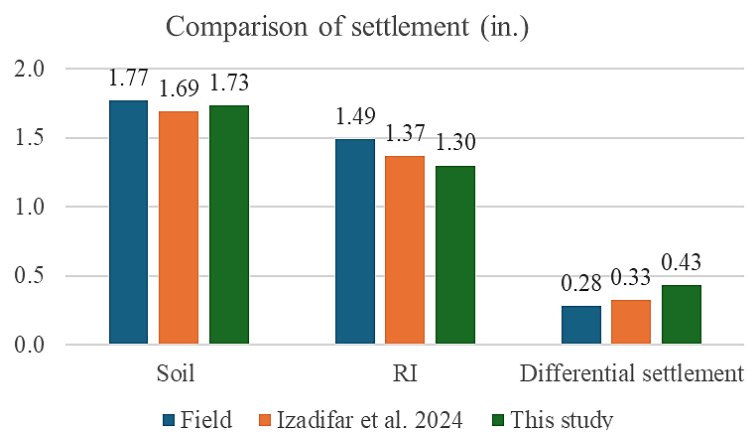

Figure 4.14: Comparison of Settlements Computed by Numerical Methods with Field Data

94

The load efficacy and differential settlement were calculated by the design methods and compared to the numerical results from this study and Izadifar et al. (2024). Izadifar et al. (2024) reported the stress concentration ratios (the ratio of the stress on the RI to stress on the soil) from the field and the FEM as 31 and 32, respectively, and their corresponding load efficacies as 37.7% and 42.4%, respectively. Unfortunately, these numbers do not satisfy the force equilibrium; in other words, the total applied load should be equal to the sum of the loads on the soil and the RI. Therefore, stress concentration ratio values provided by Izadifar et al. (2024) for both the field and the finite element method were used to recalculate the load efficacy (Equation 4.10), accurately representing loads on both the RI and the soil.

$$Load\ Efficacy\ (\%) = \frac{ha}{1 + a(\eta - 1)} \times 100\%$$

Equation 4.10

Where:

a = the area replacement ratio of RI, and

η = the stress concentration ratio.

As a result, the load efficacies for the stress concentration ratios of 31 and 32 were 67.9% and 68.6 % for an area replacement ratio of 6.4%, as shown in Figure 4.15. Results from Figures 4.15 and 4.16, which present the comparisons of load efficacy and differential settlement, respectively, show that the numerical methods provided more accurate results than the design methods because the numerical methods considered the three-dimensional effect and had better simulation of soil behavior. The FHWA method underestimated the load efficacy of the RIS system, while the BS 8006-1 method overestimated the results. Furthermore, results from the FHWA method were more similar to results from the numerical analysis and the field in terms of differential settlement than other design methods. However, the CUR226 and EBGEO methods slightly overestimated the results, while the BS 8006-1 method largely overestimated the results.

Louisiana case study
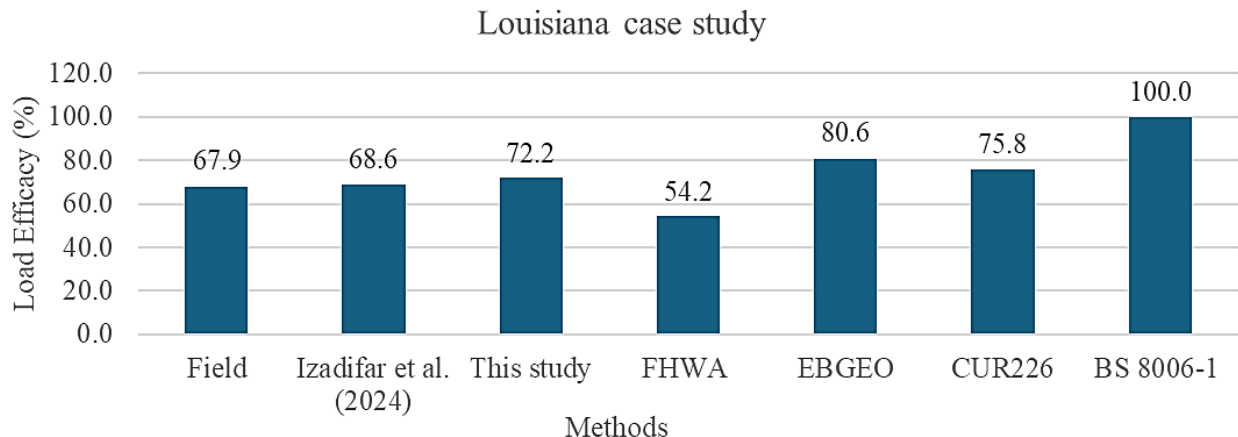
Figure 4.15: Comparison of Load Efficacy for Various Methods

Method	Load Efficacy (%)
Field	67.9
Izadifar et al. (2024)	68.6
This study	72.2
FHWA	54.2
EBGEO	80.6
CUR226	75.8
BS 8006-1	100.0

Louisiana case study
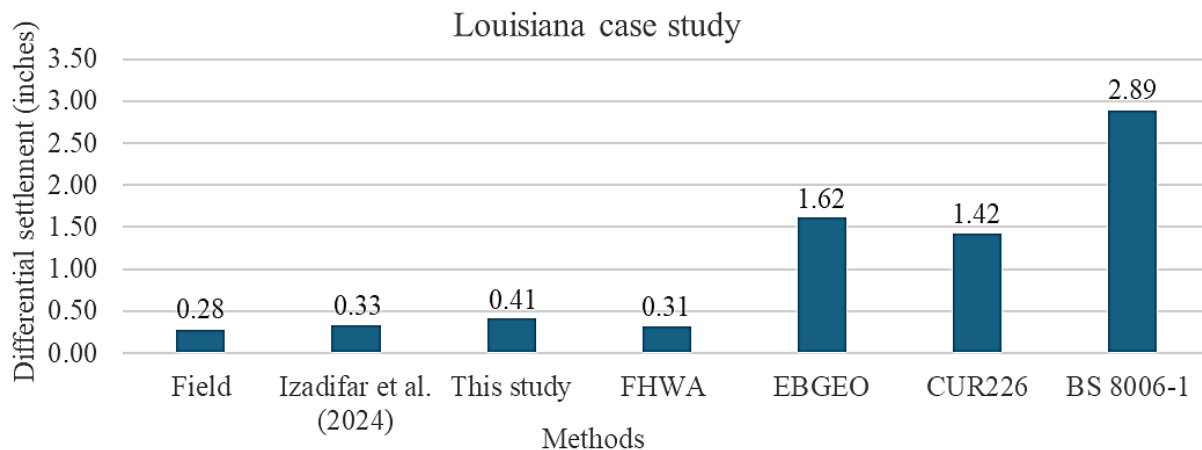
Figure 4.16: Comparison of Differential Settlement for Various Methods

Method	Differential settlement (inches)
Field	0.28
Izadifar et al. (2024)	0.33
This study	0.41
FHWA	0.31
EBGEO	1.62
CUR226	1.42
BS 8006-1	2.89

4.5 Summary

The evaluation of design methods using field data and numerical analysis can be summarized as follows:

1. The FHWA method gives comprehensive consideration of different influence factors, especially the support of subsoils but requires more input parameters than other methods.

2. The EBGEO and CUR226 method simplified the support of layered subsoils by a modulus of subgrade reaction.

3. The BS 8006-1 method did not consider subsoil support.

4. These design methods gave inconsistent results for load efficacy, differential settlement, and GR tension.

5. Compared to the other methods, the CUR226 and FHWA methods more accurately estimated GR tension.

6. For the ASIRI project, the numerical analysis more accurately computed the load efficacy compared to the field data than the calculations from the design methods because the numerical models considered slope effects, but the design methods did not. The FHWA method more accurately estimated the differential settlement than other design methods because it more accurately models subsoil behavior using soil compression indices than subgrade reaction moduli.

7. For the Louisiana project, numerical analysis, and the EBGEO and CUR226 methods more accurately calculated the load efficacy, while the numerical analysis and the FHWA method produced more accurate results for the differential settlement because of more accurately modeling subsoil behavior.

8. Unit-cell numerical and global models gave similar results for differential settlement and differing results for load efficacy.

Chapter 5: Stability Analysis Methods for RIS Embankments

This study evaluated the ESM, SRM, and PSM as compared to verified numerical models in terms of the calculated factor of safety (FS). The following sections describe the techniques used for numerical modeling, verify the numerical model, establish the models for the analysis methods, compare the calculated results, and discuss method limitations.

5.1 Numerical Modeling Techniques

In this study, FDM-based software FLAC2D was used for the slope stability analysis of RIS embankments on soft ground. This software adopts a strength reduction technique to obtain the factor of safety of an embankment slope. This study utilized the column-wall method (CWM) for 2D analysis and validated by the numerical results from the previous research by Zhang et al. (2014).

5.1.1 Strength Reduction Technique

Traditionally, the FS for a slope is the ratio of the mobilized soil shear strength to the applied shear stress to maintain slope equilibrium (Bishop, 1955). Duncan (1996) clarified that the FS could be the ratio of the actual soil shear strength to the soil shear stress that brings the slope to the verge of failure. Compared to the method of slices that identifies a critical slip surface via trial and error, the software incorporating a strength reduction technique can automatically determine a critical state by adjusting the shear strength of soil to reach the slope failure (Dawson et al., 1999).

To perform slope stability analysis with the shear strength reduction technique, the cohesion c and friction angle ϕ of the soil are adjusted by using a series of trial factors of safety, FS^{trial}:

$$c^{trial} = \frac{1}{FS^{trial}} c$$

Equation 5.1

$$\phi^{trial} = \arctan(\frac{1}{FS^{trial}} \tan \phi)$$

Equation 5.2

Many researchers have successfully used this method for stability analysis of slopes, embankments, and walls, including column-supported embankments and geosynthetic-reinforced walls (e.g., Han et al., 2004; Han et al., 2005; Han & Leshchinsky, 2010; Abusharar & Han, 2011; and Zhang et al., 2014).

5.1.2 Column-Wall Method

Individual columns (Figure 5.1[a]) can be converted into column walls (Figure 5.1[b]) for a 2D plane strain analysis by assuming the effective width of the column wall was the same as the diameter of individual columns (i.e., $b_w = d_c$, in which b_w is the width of the column wall and d_c is the diameter of individual columns). Equivalent properties of the column walls, such as equivalent elastic modulus, cohesion, and friction angle, were determined based on the area-weighted average of the column properties and the surrounding soft soils within each row of columns:

$$E_w = E_c a_{row} + E_s(1 - a_{row})$$

Equation 5.3

$$c_w = c_c a_{row} + c_s(1 - a_{row})$$

Equation 5.4

$$\phi_w = arc\tan(a_{row}\tan\phi_c + (1 - a_{row})\tan\phi_s)$$

Equation 5.5

Where:

E_w, E_c, and E_s = elastic moduli of column walls, individual columns, and soft soils, respectively;

c_w, c_c, and c_s = cohesion of column walls, individual columns and soft soils, respectively;

ϕ_w, ϕ_c and ϕ_s = friction angles of column walls, individual columns, and soft soils, respectively; and

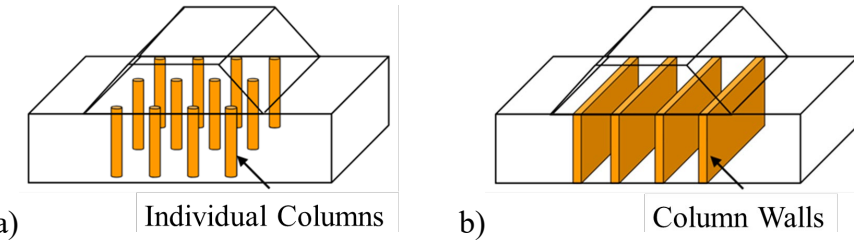a_{row} = area replacement ratio by columns within a row of columns.

Figure 5.1: CWM Models: (a) Individual Columns; (b) Column Walls
Source: Zhang et al. (2014)

To validate the CWM, the FDM program FLAC2D 8.1 was used to calculate the FS of the column-supported embankment over soft soil based on the CWM. It is preferred that a well-instrumented field case or well-analyzed numerical case for the stability of RI-supported embankments is used for this model validation. Unfortunately, no such case was identified at the time of research. Zhang et al. (2014) published a numerical analysis of the stability of embankments on stone column-supported embankments; therefore, this case was used for the model validation purpose. Due to the symmetry of the cross section, half of the embankment was simulated, as shown in Figure 5.2. The subsoil was 39.4 ft deep and 131.2 ft wide, consisting of a 32.8-ft thick soft clay overlying a 6.6-ft thick sand. The 16.4-ft high embankment had a crest that was 65.6 ft wide with a slope of 2H: 1V. No LTP was used in this analysis. A 1.5 ft thick surficial layer was assigned to the slope to prevent surficial failure of the embankment. The stone columns (diameter of 19.7 in. and a length of 32.8 ft) were installed in a square pattern at spacing of 2.6, 3.3, and 4.6 ft, which had corresponding overall area replacement ratios of 10%, 20%, and 30%, respectively. It should be noted that RIs have been designed with a much smaller area replacement ratio (typically 2% to 10%) as discussed earlier due to their rigidity and high load capacity. The effect of groundwater on the stability was not considered in this validation model. The sand layer was underlain by a firm deposit layer, such as bedrock so that the bottom boundary was fixed in both the horizontal and vertical directions. The two side boundaries were fixed in the horizontal direction but allowed to move freely in the vertical direction. Table 5.1 lists the material properties under undrained conditions. The Mohr-Coulomb model was used in simulations.
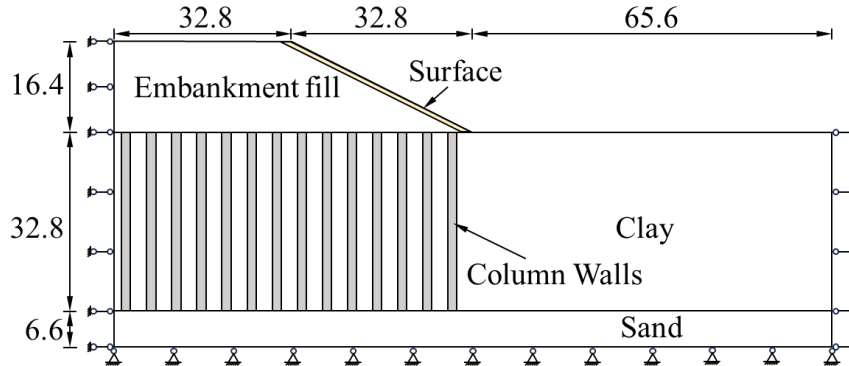
Figure 5.2: Cross Section of the Embankment Model Based on the CWM (ft)

Table 5.1: Material Properties for the Validation Model

Material	d (in.)	γ (lb/ft^3)	E (ksi)	ν	c (psi)	ϕ (°)	a_s	s (ft.)	a_{row}
Embankment	N/A	114.6	4.4	0.3	1.45	32	N/A	N/A	N/A
Surface	N/A	114.6	4.4	0.3	2.18	32	N/A	N/A	N/A
Clay	N/A	101.9	0.6	0.45	2.90	0	N/A	N/A	N/A
Sand	N/A	101.9	14.5	0.3	0	30	N/A	N/A	N/A
Stone Column	19.7	108.2	5.8	0.3	0	38	N/A	N/A	N/A
Column Wall	19.7	103.8	2.0	0.41	2.09	12.4	10%	4.6	28%
	19.7	104.4	2.7	0.39	1.75	17.2	20%	3.3	40%
	19.7	105.0	3.1	0.38	1.49	20.8	30%	2.6	49%

As shown in Figure 5.3, the FS of the 2D column-supported embankment computed using the CWM matched well with the FS calculated using the same method in the previous research (Zhang et al., 2014); thereby, validating the accuracy of the numerical model with stone columns in this study. It is preferred that a similar validation could be carried out with RIS embankments; unfortunately, this was not possible at the time of research. Therefore, the CWM validated by the stone column-supported embankment model was used for 2D stability analysis of RIS embankments considering typical geometry and properties of RIs in this study. It should be noted that the conversion of a three-dimensional problem to a two-dimensional problem may affect soil arching between RIs. Further research is required to assess this possible effect.
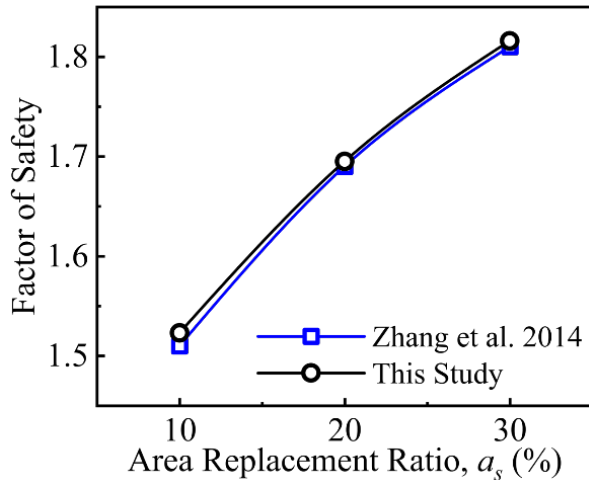
Figure 5.3: Computed FS to Validate the CWM

5.2 Models for Stability Analysis Methods

5.2.1 Finite Difference Method

For the numerical analysis, the FDM program FLAC2D 8.1 was used to calculate the FS of RIS embankments over soft soil. Due to the symmetry of the cross section, half of the embankment was simulated as shown in Figure 5.4. The subsoil was 49.2 ft deep and 164 ft wide, consisting of a 32.8-ft thick, soft clay overlying 16.4-ft thick sand. The 16.4-ft high embankment had a crest measuring 131.2 ft wide with a slope of 2H: 1V. A 1.5-ft thick surficial layer was assigned to the slope to prevent surficial failure of the embankment. RIs with diameters of 9.8 in. and lengths of 42.7 ft were installed in a square pattern at spacings of 2.6, 3.3, and 4.6 ft, which corresponded to overall area replacement ratios of 2.5%, 4.9%, and 7.7%, respectively. If RIs with a larger diameter (e.g., 12 to 16 in.) had been selected, large RI spacing (e.g., 6 to 9 ft) would be used to achieve similar area replacement ratios. The embedment depth of the RIs in the sand layer was 9.8 feet. The groundwater table was simulated at the ground surface in this analysis. The sand layer was underlain by a firm deposit layer, such as bedrock, so the bottom boundary was fixed in both horizontal and vertical directions. The two side boundaries were fixed in the horizontal direction but allowed to move freely in the vertical direction. Table 5.2 lists the material properties based on Mohr-Coulomb soil models. Undrained cohesion was used for clay, RI, and column walls.
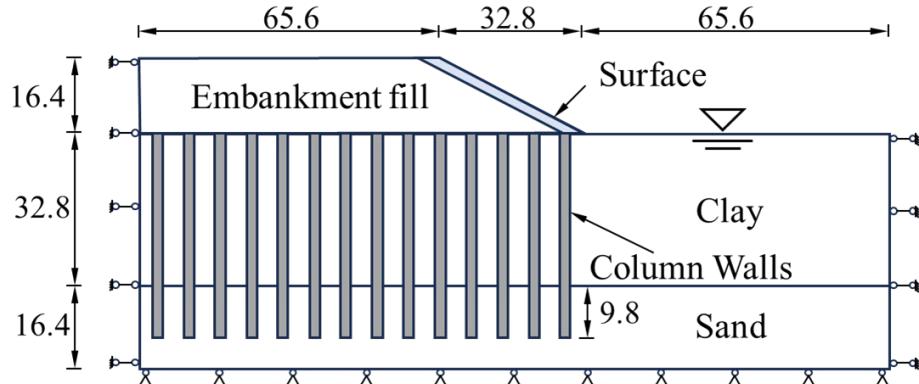
102

Figure 5.4: CWM Model for Stability Analysis and Comparison to Other Methods (ft)

Table 5.2: Material Properties for RIS Embankments

Material	d (in.)	γ (lb/ft³)	E (ksi)	ν	c (psi)	ϕ (°)	σ_t (psi)	a_{ri}	s (ft.)	a_{row}
Embankment	N/A	114.6	4.4	0.3	0	38	N/A	N/A	N/A	N/A
Surface	N/A	114.6	4.4	0.3	2.18	38	N/A	N/A	N/A	N/A
Clay	N/A	101.9	0.6	0.45	1.45	0	N/A	N/A	N/A	N/A
Sand	N/A	101.9	14.5	0.3	0	30	N/A	N/A	N/A	N/A
RI	9.84	152.8	203.1	0.2	1015	0	50.8	N/A	N/A	N/A
Column Wall	9.84	114.6	28.7	0.42	143	0	7.1	2.5%	4.6	14.0%
	9.84	117.1	40.0	0.40	200	0	9.9	4.9%	3.3	19.6%
	9.84	119.0	50.0	0.39	250	0	12.4	7.7%	2.6	24.5%

5.2.2 Models for Equivalent Strength Method

Table 5.3 and Figure 5.5 show the material properties and geometry, respectively, for the ESM models. Considering the benefit of RI strength, the improved zone in the subsoil was treated as an equivalent area with improved properties. Properties of the embankment, surface, clay layer, and sand layer were the same as properties in the CWM model.

Table 5.3: Material Properties for ESM Models

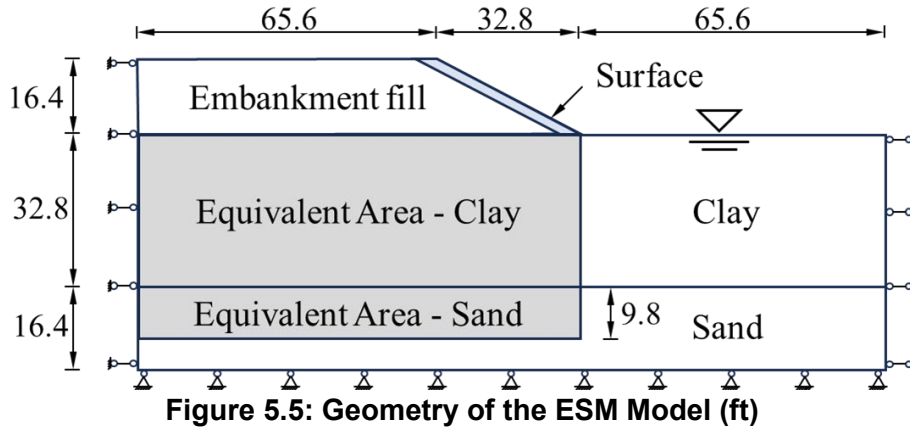|	Material (Equivalent Area)	γ (lb/ft3)	E (ksi)	ν	c (psi)	ϕ (°)	a_{ri}
Model 1	Clay	109.4	5.4	0.444	26.8	0	2.5%
	Sand	115.5	19.2	0.298	25.4	29.3	2.5%
Model 2	Clay	110.34	10.2	0.438	51.1	0	4.9%
	Sand	116.4	23.7	0.295	49.7	28.5	4.9%
Model 3	Clay	111.7	15.9	0.431	79.5	0	7.7%
	Sand	117.5	29.0	0.292	78.2	27.7	7.7%

Figure 5.5: Geometry of the ESM Model (ft)

5.2.3 Models for Stress Reduction Method

Because reduced stresses on the subsoil must be determined in the SRM, this study used the CWM models to determine these stresses on the subsoil (Figure 5.6), including cases with RI replacement areas of 2.5%, 4.9%, and 7.7%. Average stresses on the subsoil under the embankment crest were 5.67, 3.96, and 3.18 psi, respectively. Either the reduced stress distribution was applied on the subsoil (SRM 1), as shown in Figure 5.7(a) or a reduced unit weight of the embankment fill (SRM 2) was used, as shown in Figure 5.7(b). For the SRM 2, the reduced unit weights of the embankment in this study were 49.8, 34.8, and 27.9 lb/ft³, respectively. RIs were not included in either case because their benefit had been considered in the reduced vertical stresses. It should be noted that the reduced stresses on the subsoil may be determined using a soil arching model. Further research is required to assess possible differences in the calculated FS using these two models (numerical and soil arching models) for the stress reduction method.
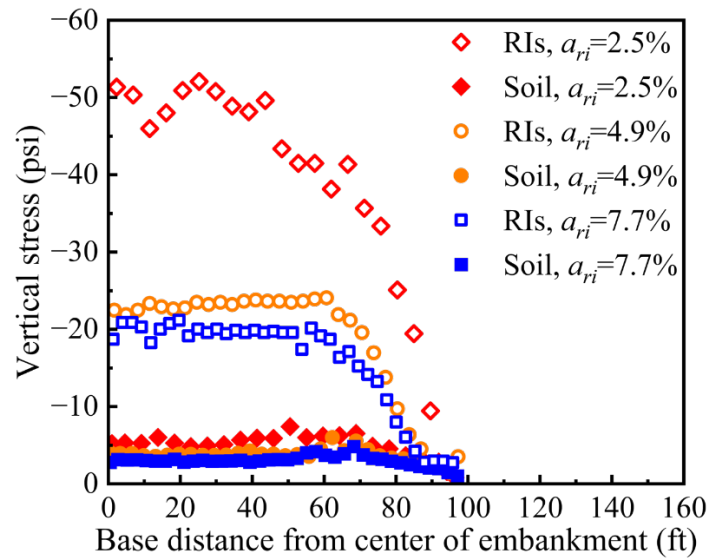
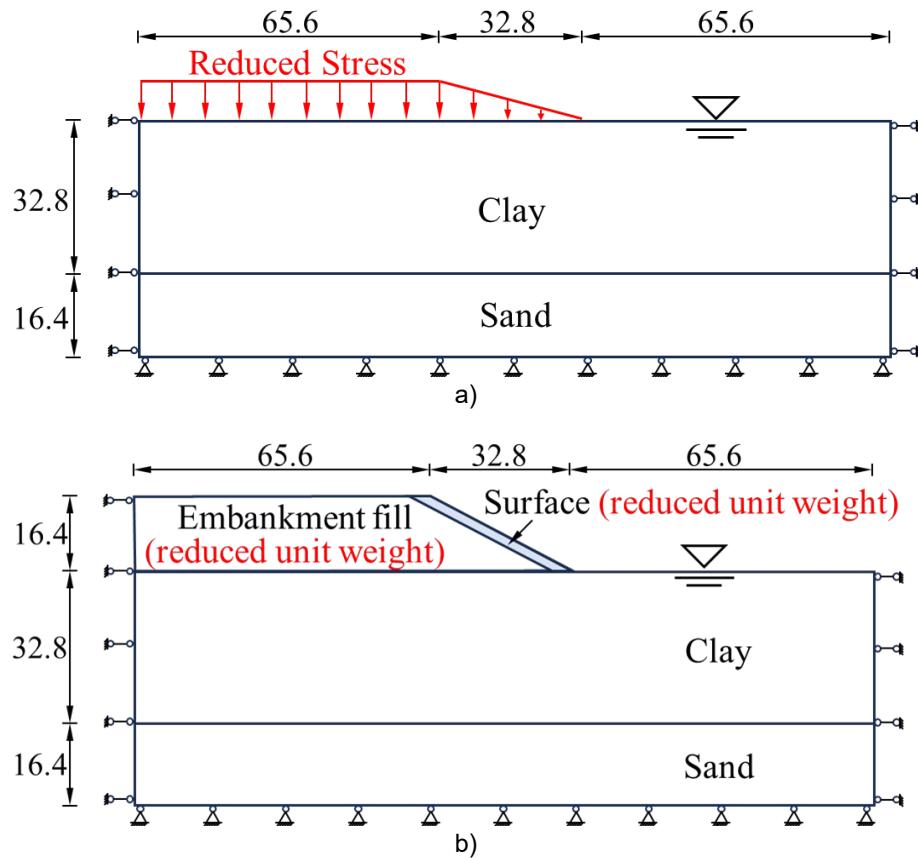**Figure 5.6: Vertical Stresses on RIs and Subsoil**

Figure 5.7: SRM Models: (a) Reduced Vertical Stresses; (b) Reduced Unit Weight

5.2.4 Pile Support Method

Guidelines in the BS 8006-1 method suggest using the PSM, which requires determination of a critical slip surface. In this study, the critical slip surface was obtained from the strain rate results of the numerical analysis of the CWM models, as shown in Figure 5.8, and then the subsoil and the embankment above the critical slip surface were divided into slices, as shown in Figure 5.9. The FS for the embankment slope was calculated as the ratio of the total resistance moment of the embankment, soil, and RIs to the driving moment.

a) a_{ri} = 2.5%, spacing = 4.6 ft

b) a_{ri} = 4.9%, spacing = 3.3 ft
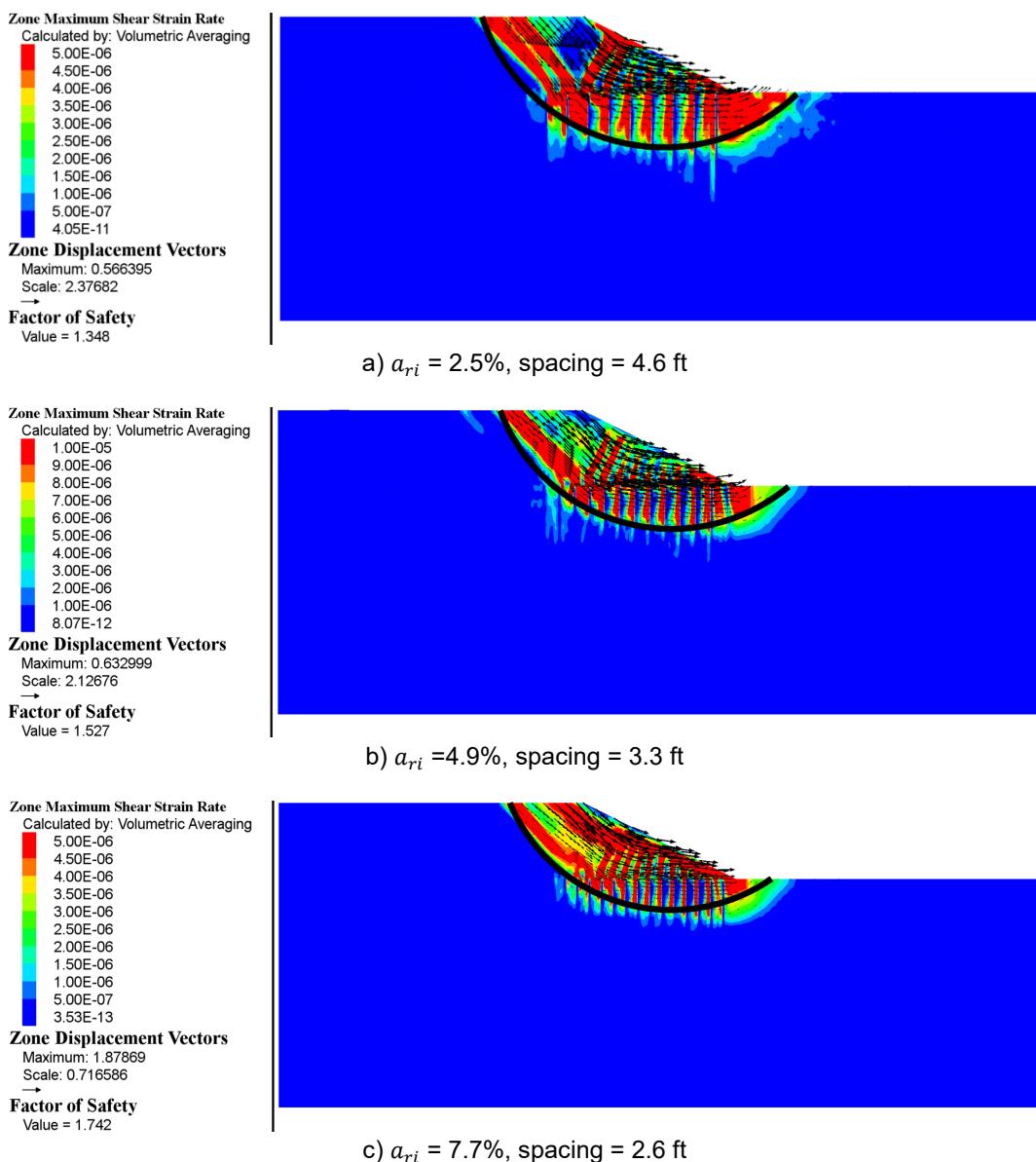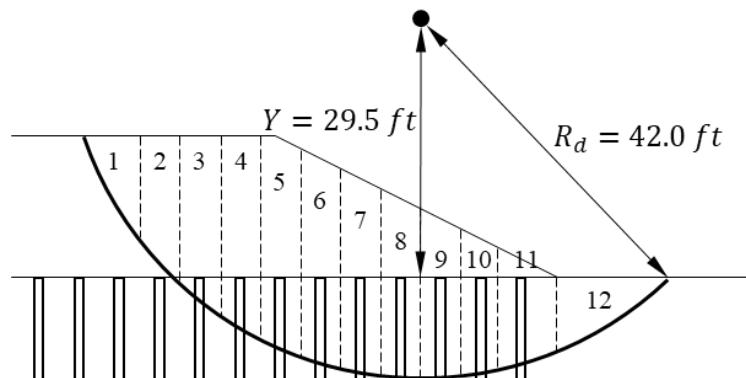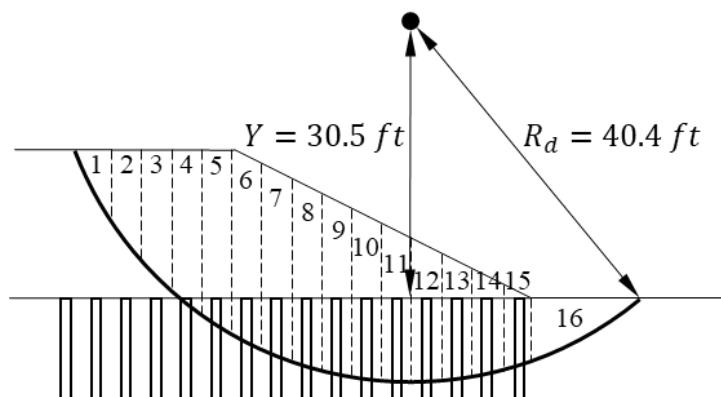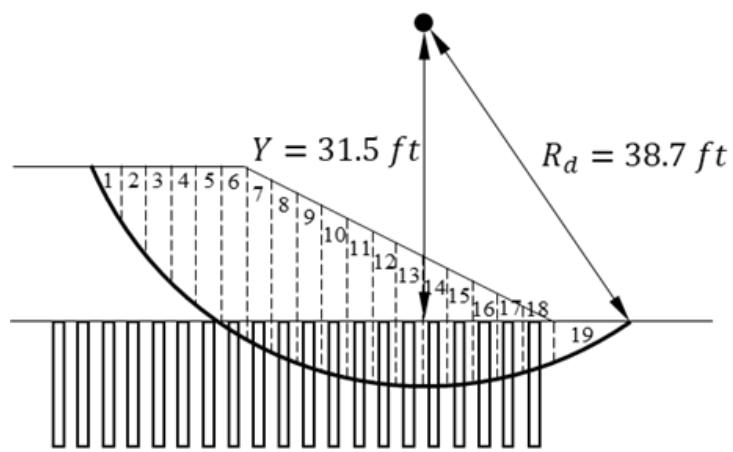

c) a_{ri} = 7.7%, spacing = 2.6 ft

Figure 5.8: Contours of the Shear Strain Rate of the Numerical CWM Models

a) a_{ri} = 2.5%, spacing = 4.6 ft

b) a_{ri} =4.9%, spacing = 3.3 ft

c) a_{ri} = 7.7%, spacing = 2.6 ft

Figure 5.9: PSM Models

5.3 Results and Discussion

5.3.1 CWM Model

Figure 5.8 shows the shear strain rate contours of the embankment on the RI-improved subsoil, which did not have continuous critical slip surfaces. However, approximate slip surfaces could be traced as shown, which are close to circular surfaces.

5.3.2 PSM Model

The PSM used the approximate slip surfaces estimated in Figure 5.8. Following the procedure suggested by the BS 8006-1, the factors of safety of RIS embankments over soft soil were calculated and will be presented and discussed later.

5.3.3 ESM Model

The ESM estimated much higher elastic modulus and cohesion of the equivalent area than the soft subsoil without RIs. As a result, the strength of the equivalent area could be higher than that of the embankment, as shown in Tables 5.2 and 5.3. This condition forced failure to happen within the embankment rather than a deep-seated failure in the soft subsoil as shown in Figure 5.10.

5.3.4 SRM Model

Analysis of the SRM showed that the model maintained the same properties of the subsoil by reducing the vertical stresses (Method 1) and the unit weight of the embankment fill (Method 2). The reduced vertical stresses were determined based on the numerical CWMs and the equivalent reduced unit weights were calculated based on the reduced vertical stresses by the numerical analysis. It should be noted that the reduced vertical stresses could also be estimated based on a soil arching model but this procedure was not adopted in the current study. Figures 5.11 and 5.12 show clear deep-seated circular slip surfaces, which were limited by the firm layer at the bottom. However, the locations of the slip surfaces were different from these two SRM methods. In addition, their slip surfaces were different from those in the CWMs. Models with Method 2

showed that the embankment more likely failed above the subsoil with the increased area replacement ratio of the RIs, as shown in Figure 5.12.

a) a_{ri} = 2.5%, spacing = 4.6 ft

b) a_{ri} =4.9%, spacing = 3.3 ft

c) a_{ri} = 7.7%, spacing = 2.6 ft

Figure 5.10: Contours of the Shear Strain Rate of ESM Models

Zone Maximum Shear Strain Rate
Calculated by: Volumetric Averaging
2.00E-04
1.60E-04
1.20E-04
8.00E-05
4.00E-05
0.00E+00
Factor of Safety
Value = 1.55
Zone Displacement Vectors
Maximum: 1.44564
Scale: 0.902836
→

a) a_{ri} = 2.5%, spacing = 4.6 ft

Zone Maximum Shear Strain Rate
Calculated by: Volumetric Averaging
2.00E-04
1.60E-04
1.20E-04
8.00E-05
4.00E-05
0.00E+00
Factor of Safety
Value = 2.3
Zone Displacement Vectors
Maximum: 0.938879
Scale: 1.3901
→

b) a_{ri} =4.9%, spacing = 3.3 ft

Zone Maximum Shear Strain Rate
Calculated by: Volumetric Averaging
2.00E-04
1.60E-04
1.20E-04
8.00E-05
4.00E-05
0.00E+00
Factor of Safety
Value = 2.836
Zone Displacement Vectors
Maximum: 0.878402
Scale: 1.48578
→

c) a_{ri} = 7.7%, spacing = 2.6 ft

Figure 5.11: Contours of the Shear Strain Rate from SRM Models (Method 1)

a) a_{ri} = 2.5%, spacing = 4.6 ft

b) a_{ri} =4.9%, spacing = 3.3 ft

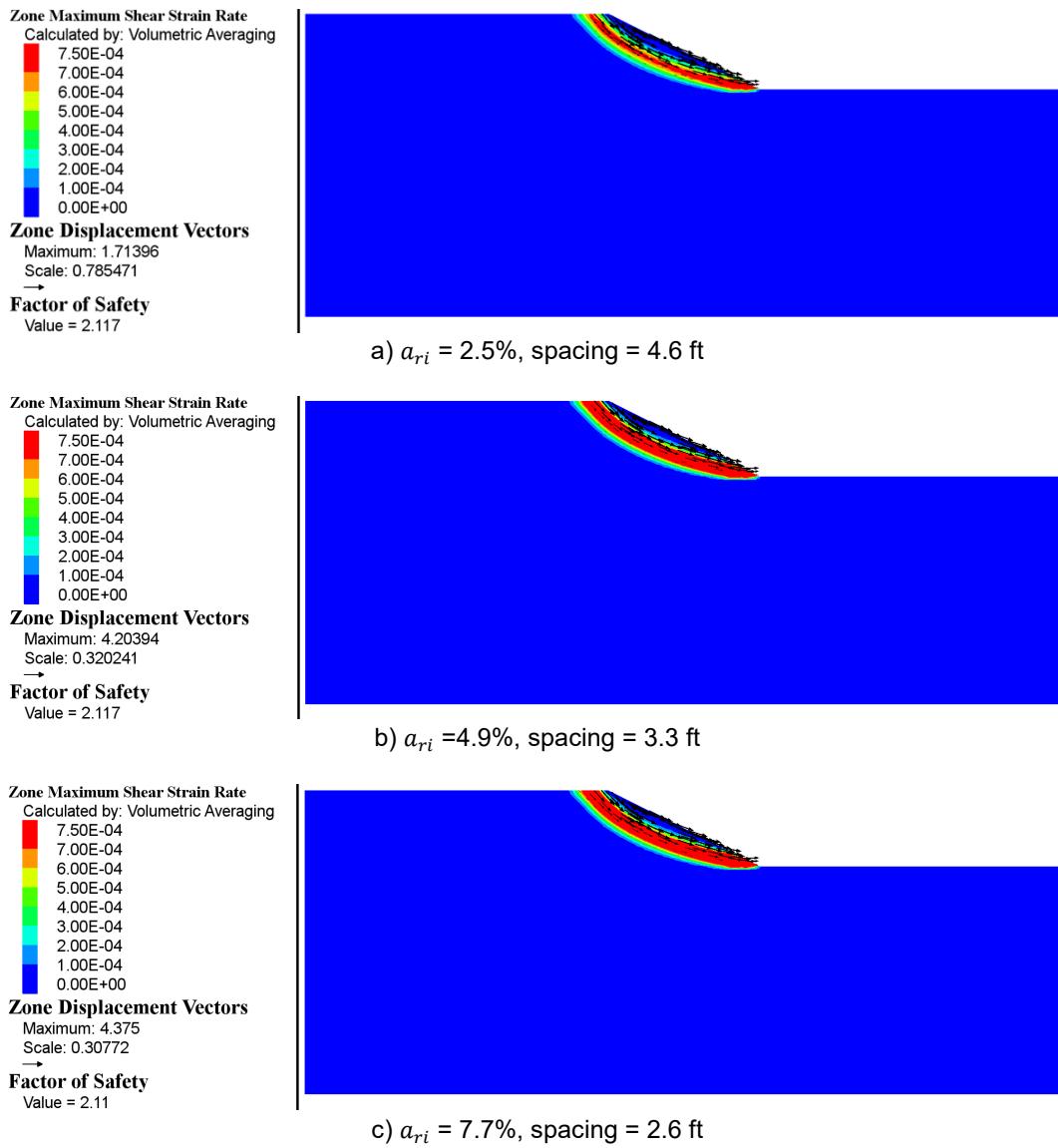c) a_{ri} = 7.7%, spacing = 2.6 ft

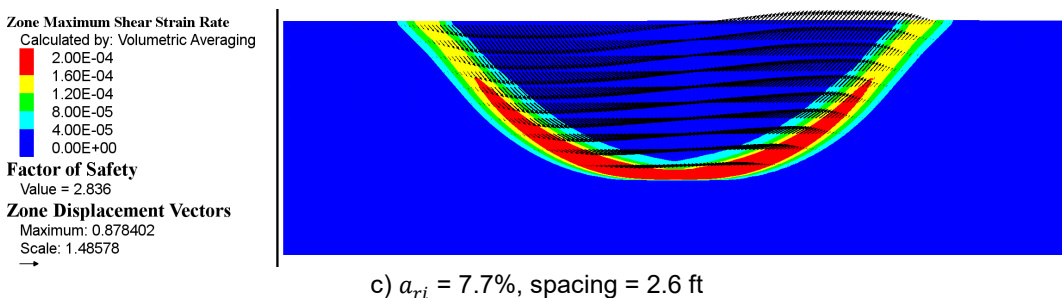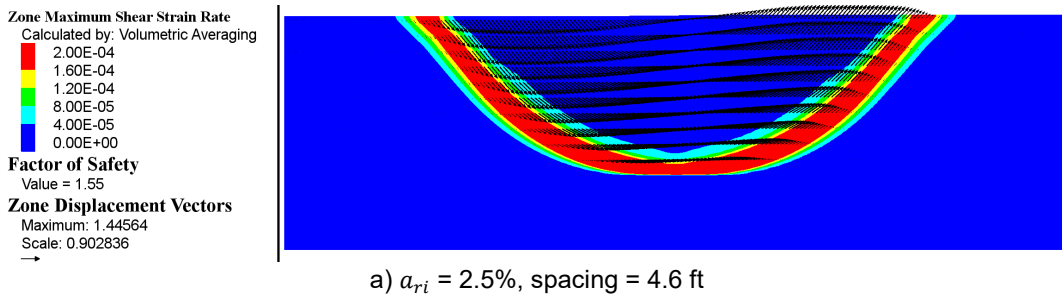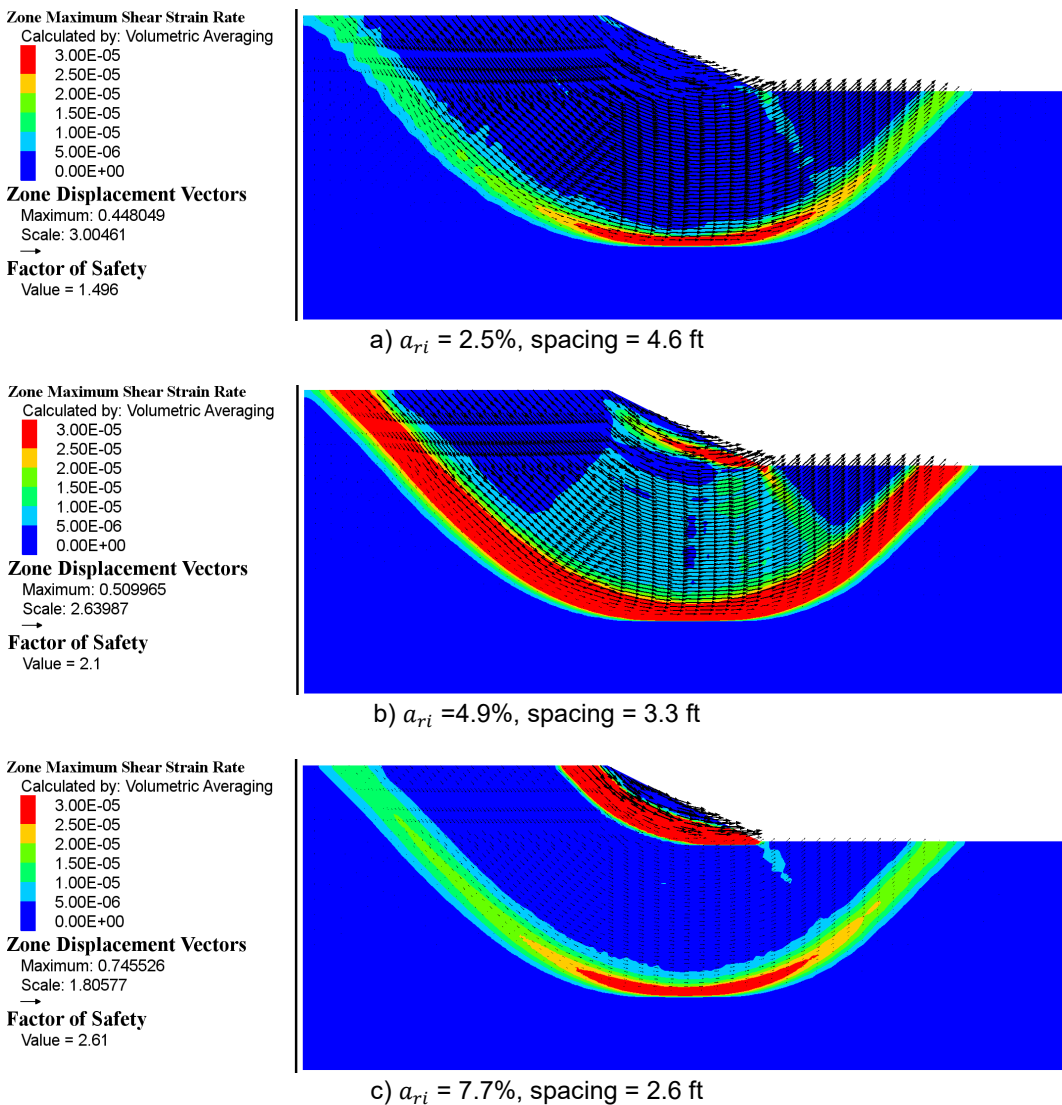**Figure 5.12: Contours of the Shear Strain Rate from SRM Models (Method 2)**

5.3.5 Factors of Safety from Different Analysis Methods

Figure 5.13 shows the comparison of the FS values obtained from different analysis methods. The CWM is considered the reference solution of these cases at different RI replacement ratio. This figure clearly shows that all other methods overestimated the FS as compared with the CWM. The ESM predicted constant FS because the RIs improved the subsoil with significantly high equivalent strength so that the failure occurred only above the subsoil. The two SRMs computed similar FS, but both SRMs overestimated the FS by an increased amount as the RI replacement ratio increased. It should be noted that if the reduced vertical stresses were estimated

111

by a soil arching model (e.g., the FHWA method), the calculated factors of safety may be different, which deserves further investigation. The PSM overestimated the FS more than any other method.
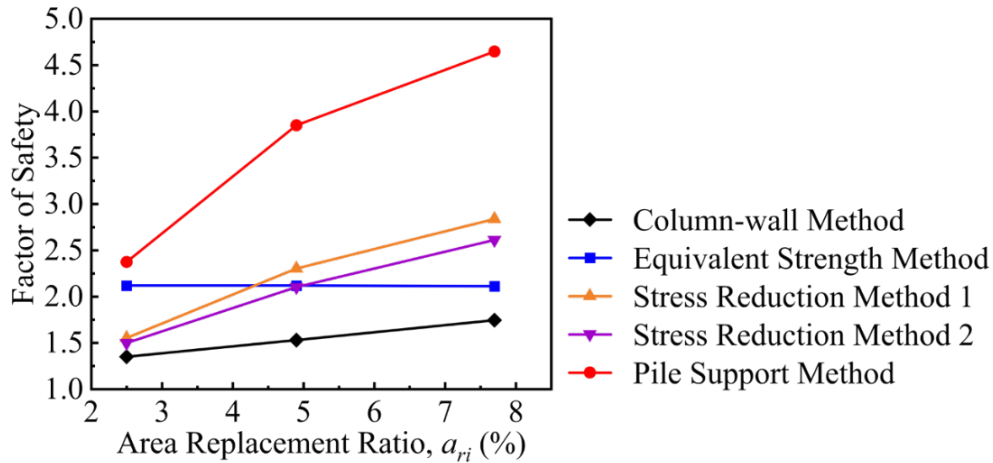

Figure 5.13: Factors of Safety Computed by Various Analysis Methods

5.4 Limitations of Stability Analysis Methods

The following limitations relate to existing stability analysis methods for RIS embankments over soft subsoils:

1. The ESM is based on shear strengths of both RIs and subsoil. Since RIs fail under bending or rotation instead of shear, this method significantly overestimates the shear strength of the equivalent area and therefore should not be used in practice.

2. The SRMs (Methods 1 and 2), which require reduced vertical stresses on the subsoils based on the CWM for analysis, overestimate the FS, especially at a great RI replacement ratio. This finding may be different if the reduced vertical stresses are estimated by a soil arching model (e.g., the FHWA method). Further investigation is required to verify this finding.

3. The PSM is limited by the method of slides: the location of the critical slip surface must be found by trial and error, and the assumed circular slip surface differs from the actual failure mode of the RIS embankment. This method significantly overestimated the FS and should not be used in practice.

Chapter 6: Knowledge Gaps and Plan for Phase II Study

6.1 Knowledge Gaps

The comprehensive literature review and evaluation of existing design methods have revealed several knowledge gaps and limitations in current practices. These gaps include missing data, inadequate procedures, and insufficient consideration of key factors as summarized below:

1. The common analytical methods in codes or reference manuals are not accurate or reliable enough to predict the performance of RIS embankments/structures over soft subsoils for transportation projects.

2. Limited analysis methods are available in codes or reference manuals to evaluate the stability of RIS embankments over soft subsoils. Except for the numerical method with actual RI layout and properties, all current methods overestimated the factor of safety. No field data is available to verify the accuracy of analysis methods for RIS embankment stability.

3. Limited field data shows RI installation effects on surrounding soils, RIs, and structures.

4. No field data is available to evaluate lateral capacities of RIs, and no detailed guidance is available for steel rebars in RIs.

5. No field data is available to compare the behavior of RIs under walls versus embankments.

6. No field data is available to evaluate the relevance of a single RI load test with group RIs under embankments.

7. No consistent specification is available for installing RIs, QC/QA, and instrumentation/monitoring during construction and for long-term performance.

6.2 Preliminary Plan for Phase II of the Study

The main objective of the Phase I study was to assess the state of the practice of RIs for transportation projects, evaluate the existing design methods, review the construction specifications, and identify the knowledge gaps and missing data/procedures to be addressed

through a full-scale field study in Phase II. A preliminary plan for the Phase II study is presented in the following sections.

6.2.1 Phase II Study Objectives

To address the knowledge gaps identified in the Phase I study, the following objectives are proposed for the Phase II study:

1. Gather full-scale test data for RI serviceability and failure limits (as practical as possible)
2. Improve analytical methods for load and deformation calculations
3. Evaluate installation-induced soil displacements and potential damage to adjacent RIs and structures as well as soil property changes
4. Evaluate load-displacement behavior of single RI versus group RIs under wall/embankment
5. Understand RI behavior under walls versus slopes
6. Evaluate lateral load capacities of RIs with and without steel rebars
7. Improve/develop an analytical method for slope stability with RIs
8. Develop guidelines for construction specifications and instrumentation.

To achieve these objectives, the research team proposed construction of test embankments with slopes and walls instrumented with sensors, as well as data reduction, analysis, and development.

6.2.2 Tentative Test Embankment

The researchers and KDOT tentatively selected a test site near Lawrence, Kansas, that contains soft soils (mostly clays) 53 ft deep with bedrock at a depth of 56 ft (Figure 6.1). The clays have unconfined compressive strengths of 0.70–0.87 tsf.

a) Soil Profile

Figure 6.1: Soil Profile of the Tentative Test Site

Bit Type	GEOLOGIC NAME	STRATIGRAPHIC COLUMN	DEPTH	ELEVATION	CLASSIFICATION OF MATERIALS DESCRIPTION AND REMARKS	UNCONFINED COMPRESSION (TSF)	ELASTIC MODULUS (PSF)	N60 COUNT (SPT)	ELEVATION
				785	Lean Clay, blue gray wet	0.7	26500		784.48
8" Hollow Augers	Alluvium		38.8	776.5	Clay, gray with fine sand	0.73	23600		774.48
			48.0	767.3	Sandy clay, dark gray stiff				
			53.0	762.3	Gravel, gray				
			56.0	759.3	Weathered Sandstone, gray				
	noxie Sandstone		57.5	757.8	Sandstone, dark gray, finely laminated fine grained sand. Very thin alternating layers of gray and dark gray sand. Coarser in the lower half with minor fine scaled cross bedding. Lacks calcite cementation. Poor RQD with very thin (0.01 ft) discontinuites due to poor cementation spaced 0.2 to 1.2 ft apart.	47.8	4050000		756.48

b) Soil Profile

Figure 6.1: Soil Profile of the Tentative Test Site (Continued)

The proposed test embankment will be 20 ft high and will consist of a vertical geosynthetic wrap-around temporary wall on one side and a 1:1 geosynthetic-reinforced slope on another side, as shown in Figure 6.2. RIs of 14 in. in diameter are planned for installation at a depth of 60 ft with a square pattern and spacings at 6 and 8 ft (i.e., area replacement ratios of 3.0% and 1.7%, respectively). The plan includes a 4:1 ramp on each end to allow construction equipment to travel.

117
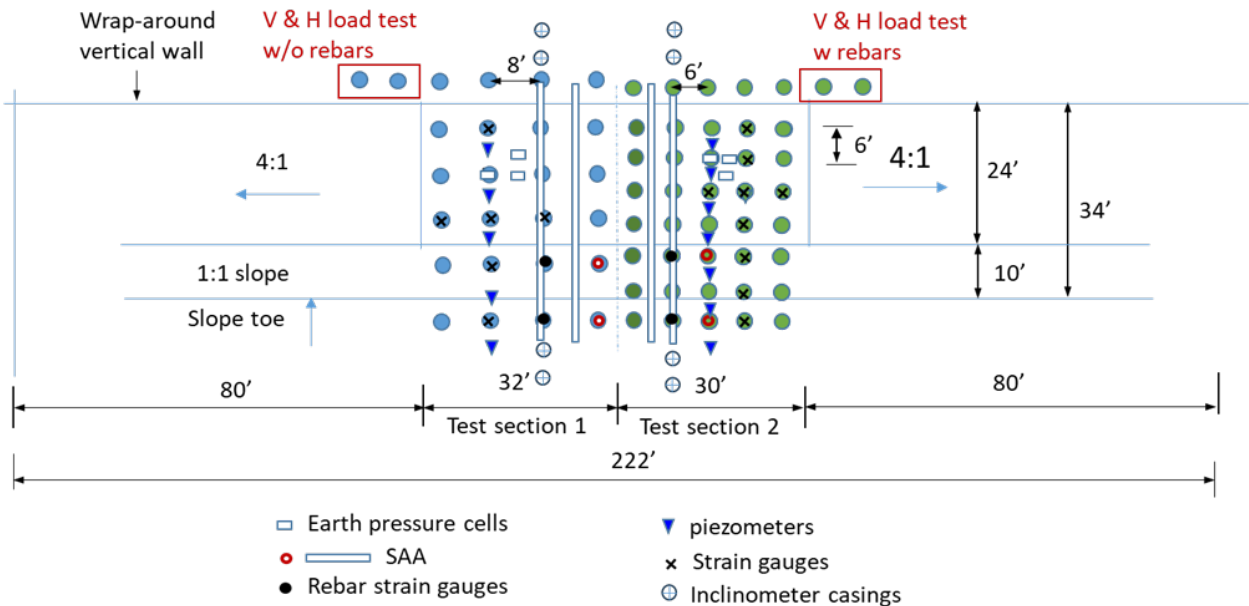
a) Plan View
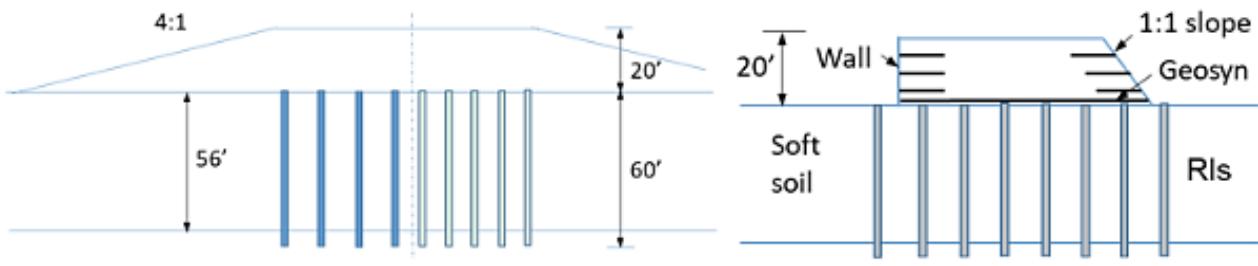
b) Cross-Sectional View

Figure 6.2: Plan and Cross-Sectional Views of Test Embankment

6.2.3 Instrumentation and Testing Plan

Proper instrumentation is planned to monitor RI installation effects and RIS embankment performance. Earth Pressure Cells (EPCs) will measure the load transfer between RIs and subsoil, and strain gauges in geosynthetics will measure the tension on the GR under embankment loads. Piezometers will measure variations of pore pressures in soils due to RI installation and embankment construction/loading. Inclinometer casings will be used to measure lateral displacements of soils during RI installation and embankment construction and post-construction. Shape acceleration arrays (SAAs) will measure horizontal and vertical deformations between RIs and subsoil during RI installation and embankment construction/loading. Rebar strain gauges will

118

be installed to measure the strains at various RI depths. In addition, vertical and horizontal load tests will be performed on RIs with and without steel rebars. At the end of field testing, subsoil in front of the slope and the wall will be excavated to induce deep-seated failures.

6.2.4 Data Analysis and Development

Test data will be reduced and analyzed including the installation effects of RIs, vertical and horizontal capacities of RIs, and RIS embankment performance. Design methods for the performance of RIS embankments with walls and slopes including load transfer, deformation, and stability will be examined and improved. This project will also develop construction specifications and instrumentation procedures.

6.2.5 Timeline and Budget

The Phase II project is estimated to be completed within three years. The project timeline and budget will depend on the schedule and effort for each of the following activities and subsequent challenges:

- Funding
- Project start date
- Site preparation
- Availability of a specialty contractor to install the RIs
- Mobilization of equipment and manpower
- Installation of RIs
- Instrumentation
- Loading tests on RIs
- Construction of embankment
- Monitoring and collection of data
- Analysis of data
- Preparation of final report

Chapter 7: Conclusions and Recommendations

The objective of this study was to assess the current state of the practice related to the use of RIs in transportation applications and identify knowledge gaps for future studies. This objective was achieved via literature review, online survey, evaluation of existing design methods, and numerical analysis. This chapter presents the conclusions and recommendations for future studies.

7.1 Conclusions

7.1.1 Current Practices

DDCs and ACIPs are commonly used as RIs under LTPs reinforced either geogrids or geotextiles to support 20-30 ft high embankments and retaining walls. RIs, which are used to improve all types of soils (e.g., clay, organic soils, and silts), are commonly installed by a design-build or design-bid-build contracting method. RIS embankments are typically designed by the FHWA design method in the U.S. Load tests and pile integrity testing of single RIs are often used to evaluate their quality and performance.

7.1.2 Design Methods

The EBGEO, CUR226, and FHWA methods were shown to more accurately estimate load efficacy and differential settlement than the BS 8006-1 method, and the CUR226 and FHWA methods more accurately estimated geosynthetic tension than the other methods. Numerical methods provided reasonable predictions of the field performance of RIS embankments over soft soils for estimated load efficacy and differential settlement.

7.1.3 Slope Stability Analysis

This study evaluated the calculated factor of safety for RIS embankment stability using the ESM, SRM, and PSM compared to the CWM. Analysis resulted in the following conclusions:

1. The deep-seated failure of embankments on RI-improved subsoil did not have continuous slip surfaces. RIs failed under bending or rotation.

2. The ESM estimated significantly high shear strength of the equivalent area that prevented deep-seated failure and forced the failure to happen above the subsoil (within the embankment).

3. Both SRMs overestimated the factor of safety of RIS embankments, and the degree of overestimation increased with an increased RI area replacement ratio.

4. The PSM significantly overestimated the factor of safety of RIS embankments.

7.1.4 Installation Effect

The installation of RIs with a displacement method caused lateral displacement, excess pore pressure of the surrounding soil, and possible deformation of adjacent structures. One case study showed that RI installation permanently deformed the adjacent structures located at 15 ft by 0.5 inches. The installation effects on the existing inclusions or adjacent structures could be more significant if the installation sequence is not properly considered.

7.2 Construction Specifications

Upon review of the special provisions for projects from various state DOTs, the following conclusions were made:

1. A wide range of RI types are allowed, including CMCs, continuous flight augers (CFAs), VCCs, DDCs, steel piles, ACPs, and prestressed piles. RI design should be carried out by a contractor based on FHWA-NHI-16-028 GEC 13 (Schaefer et al., 2017) to optimize RI spacing and diameter after static load testing per ASTM D1143. The RIs must penetrate at least twice their diameter into a dense bearing stratum.

2. Geogrid and geotextile can be used to reinforce the LTP.

3. For axial load tests, verification tests must be performed as per ASTM D1143 up to 200% design load and load tests for RI production up to 150% design load.

4. Pile integrity testing should be carried out on approximately 5% of production RIs as per ASTM D5882.

5. Instrumentation may include settlement plates, horizontal SAAs, strain gauges in test RIs, inclinometer tubes, and vibration monitoring.

6. Performance Criteria may include a global factor of safety for embankment stability greater than 1.5 and maximum allowable differential settlement of 0.25 to 0.75 in. (unit cell) or 0.5 in./100 ft to 1.5 in./1000 ft.

7.3 Recommendations for Future Studies

Based on knowledge gaps identified in Chapter 6, a comprehensive full-scale field test with instrumentation should examine possible differences in RI behavior under embankments with walls and slopes and evaluate RI behavior in load tests compared to RI behavior under embankments. Future studies should also improve existing design methods by considering installation effects, compressibility of layered soils, and allowable deformation and then develop an accurate analysis method for the stability of RIS embankments under undrained and drained conditions. Finally, future research should develop special provisions for RI projects and procedures for proper instrumentation and monitoring of RI installation and performance of RIS embankments.

References

Abusharar, S. W., Zheng, J. J., Chen, B. G., & Yin, J. H. (2009). A simplified method for analysis of a piled embankment reinforced with geosynthetics. *Geotextiles and Geomembranes*, *27*(1), 39–52. https://doi.org/10.1016/j.geotexmem.2008.05.002

Abusharar, S. W., & Han, J. (2011). Two-dimensional deep-seated slope stability analysis of embankments over stone column-improved soft clay. *Engineering Geology*, *120*(1–4), 103–110. https://doi.org/10.1016/j.enggeo.2011.04.002

Almeida, M. S. S., Ehrlich, M., Spotti, A. P., & Marques, M. E. S. (2007). Embankment supported on piles with biaxial geogrids. In *Proceedings of the Institution of Civil Engineers-Geotechnical Engineering*, *160*(4), 185–192. https://doi.org/10.1680/geng.2007.160.4.185

Basu, P., Prezzi, M., & Basu, D. (2010). Drilled displacement piles–Current practice and design. *DFI Journal-The Journal of the Deep Foundations Institute*, *4*(1), 3–20. https://doi.org/10.1179/dfi.2010.001

Bishop, R., Hill, R., & Mott, N. (1945). The theory of indentation and hardness tests. In *Proceedings of the Physical Society*, *57*(3), 147. https://doi.org/10.1088/0959-5309/57/3/301

Bishop, A. W. (1955). The use of the slip circle in the stability analysis of slopes. *Géotechnique*, *5*(1), 7–17. https://doi.org/10.1680/geot.1955.5.1.7

Briançon, L., Kastner, R., Simon, B., & Dias, D. (2004, January). Etat des connaissances-amélioration des sols par inclusions rigides. In *Proceedings of the International Symposium on Ground Improvement* (ASEP-GI 2004), 15–43. Paris, France.

Briançon, L., & Simon, B. (2012). Performance of pile-supported embankment over soft soil: Full-scale experiment. *Journal of Geotechnical and Geoenvironmental Engineering*, *138*(4), 551–561. https://doi.org/10.1061/(ASCE)GT.1943-5606.00005

Briançon, L., & Simon, B. (2017). Pile-supported embankment over soft soil for a high-speed line. *Geosynthetics International*, *24*(3), 293–305. https://doi.org/10.1680/jgein.17.00002

British Standards Institution (BSI). (2016). *Code of practice for strengthened/reinforced soils and other fills* (BS 8006-1:2010+A1:2016).

British Standards Institution (BSI). (2010). *Code of practice for strengthened/reinforced soils and other fills*. *Design of embankments with reinforced soil foundations on poor ground* (BS 8006-1).

Camp, W. M., & Siegel, T. C. (2007). Failure of a column-supported embankment over soft ground. In D. Chan, K. Tim Law (Eds.), *Proceedings of the Fourth International Conference on Soft Soil Engineering*, *Vancouver, Canada* (117-121).

Carlsson, B. (1987). Armerad jord beräkningsprinciper för vertikala väggar, branta slänter, bankar på lös undergrund, bankra på pålar. *Terrateam AB*, 4.

Chalajour, S., & Blatz, J. A. (2024). Interpretation considerations for field study of axial stresses/forces in driven H-piles due to construction activities for fill placement. *Canadian Geotechnical Journal*, *62*, 1–26. https://doi.org/10.1139/cgj-2024-0111

Chen, R. P., Chen, Y. M., Han, J., & Xu, Z. Z. (2008). A theoretical solution for pile-supported embankments on soft soils under one-dimensional compression. *Canadian Geotechnical Journal*, *45*(5), 611–623. https://doi.org/10.1139/T08-003

Chen, R. P., Liu, Q. W., Wang, H. L., Liu, Y., & Ma, Q. L. (2020). Performance of geosynthetic-reinforced pile-supported embankment on soft marine deposit. In *Proceedings of the Institution of Civil Engineers - Geotechnical Engineering*, *174*(6), 627–644. https://doi.org/10.1680/jgeen.19.00136

Chen, R. P., Wang, Y. W., Ye, X. W., Bian, X. C., & Dong, X. P. (2016). Tensile force of geogrids embedded in pile-supported reinforced embankment: A full-scale experimental study. *Geotextiles and Geomembranes*, *44*(2), 157–169. https://doi.org/10.1016/j.geotexmem.2015.08.001

Chen, R. P., Xu, Z. Z., Chen, Y. M., Ling, D. S., & Zhu, B. (2010). Field tests on pile-supported embankments over soft ground. *Journal of Geotechnical and Geoenvironmental Engineering*, *136*(6), 777–785. https://doi.org/10.1061/(ASCE)GT.1943-5606.0000295

Chevalier, B., Villard, P., & Combe, G. (2011). Investigation of load-transfer mechanisms in geotechnical earth structures with thin fill platforms reinforced by rigid inclusions. *International Journal of Geomechanics*, *11*(3), 239–250. https://doi.org/10.1061/(ASCE)GM.1943-5622.0000083

Chu, J., Varaksin, S., Klotz, U., & Menge, P. (2009). *State of the art report: Construction processes*. 17th International Conference on Soil Mechanics & Geotechnical Engineering, TC17 Meeting Ground Improvement.

Cirión, A., Paulín, J., Racinais, J., & Glandy, M. (2013). Displacement rigid inclusions. In *Proceedings of the 18th International Conference on Soil Mechanics & Geotechnical Engineering* (pp. 2453–2544), Paris, France.

Collin, J. G. (2004). Column supported embankment design considerations. In *Proceedings of the 52nd Annual Geotechnical Engineering Conference* (51–78), St. Paul, Minnesota.

CUR226. (2016). *Design guideline basal reinforced piled embankments.* CRC Press.

Dawson, E. M., Roth, W. H., & Drescher, A. (1999). Slope stability analysis by strength reduction. *Géotechnique*, *49*(6), 835–840. https://doi.org/10.1680/geot.1999.49.6.835

Duijnen, P. V., Eekelen, S. V., & Stoel, A. E. C. (2010). Monitoring of a railway piled embankment. In *Proceedings of the 9th International Conference on Geosynthetics* (pp. 1461–1464), Sao Jose, Brazil.

Duncan, J. M. (1996). State of the art: Limit equilibrium and finite-element analysis of slopes. *Journal of Geotechnical Engineering*, *122*(7), 577–596. https://doi.org/10.1061/(ASCE)0733-9410(1996)122:7(577)

EBGEO. (2011). *Recommendations for design and analysis of earth structures using geosynthetic reinforcements*. Ernst & Sohn.

Fagundes, D. F., Almeida, M. S., Thorel, L., & Blanc, M. (2017). Load transfer mechanism and deformation of reinforced piled embankments. *Geotextiles and Geomembranes*, *45*(2), 1–10. https://doi.org/10.1016/j.geotexmem.2016.11.002

Filz, G. M., & Smith, M. E. (2006). *Design of bridging layers in geosynthetic-reinforced, column-supported embankments*. Virginia Center for Transportation Innovation and Research.

Filz, G. M., Sloan, J. A., McGuire, M. P., Smith, M., & Collin, J. (2019). Settlement and vertical load transfer in column-supported embankments. *Journal of Geotechnical and Geoenvironmental Engineering*, *145*(10), 04019083. https://doi.org/10.1061/(ASCE)GT.1943-5606.0002130

Fredlund, D. G. (2021). *History of two-dimensional slope stability analyses*. Online Lecture. https://www.youtube.com/watch?v=wi2jiHdfI8Q

Gallant, A. P., Shatnawi, E., & Botero-Lopez, D. (2020). Field observations and analysis of the subgrade response beneath GRCS embankments at the council bluffs interchange system. *Journal of Geotechnical and Geoenvironmental Engineering*, *146*(5), 05020002. https://doi.org/10.1061/(ASCE)GT.1943-5606.0002220

Gallant, A. P., & Botero-Lopez, D. (2021). Lateral spreading and stability of embankments supported on fractured unreinforced high-modulus columns. *DFI Journal - The Journal of the Deep Foundations Institute*, *15*(2), 1–21. https://doi.org/10.37308/DFIJnl.20201015.226

Griffiths, D. V., & Lane, P. A. (1999). Slope stability analysis by finite elements. *Géotechnique*, *49*(3), 387–403. https://doi.org/10.1680/geot.1999.49.3.387

Guido, V. A., Knueppel, J. D., & Sweeny, M. A. (1987). Plate loading tests on geogrid-reinforced earth slab. In *Proceedings of the Geosynthetic'87 Conference* (pp. 216–225), New Orleans, Louisiana.

Gunnvard, P., Garcia, N., Mattsson, H., Laue, J., & Jia, Q. (2022). Monitoring of a timber pile-supported road embankment. In *Proceedings of the 11th International Conference on the Bearing Capacity of Roads, Railways and Airfields* (pp. 337–347), Trondheim, Norway.

Hamann, T., Qiu, G., & Grabe, J. (2015). Application of a coupled Eulerian–Lagrangian approach on pile installation problems under partially drained conditions. *Computers and Geotechnics*, *63*, 279–290. https://doi.org/10.1016/j.compgeo.2014.10.006

Han, J. (2015). *Principles and practice of ground improvement*. John Wiley & Sons.

Han, J. (2021a). *Geosynthetic-reinforced column supported embankments: Bridging theory and practice*. The Third Robert M. Koerner Lecture, 2021 Geosynthetics Virtual Conference, IFAI, Roseville, Minnesota.

Han, J. (2021b). Geosynthetic-reinforced column-supported embankments: Improving practice with better theory. *Geosynthetics*, August-September, 12–18.

Han, J., Chai, J., Leshchinsky, D., & Shen, S. (2004). Evaluation of deep-seated slope stability of embankments over deep mixed foundations. In *Proceedings of the GeoSupport Conference 2004* (pp. 945–954), Orlando, Florida. https://doi.org/10.1061/40713(2004)71

Han, J., & Gabr, M. A. (2002). Numerical analysis of geosynthetic-reinforced and pile-supported earth platforms over soft soil. *Journal of Geotechnical and Geoenvironmental Engineering*, *128*(1), 44–53. https://doi.org/10.1061/(ASCE)1090-0241(2002)128:1(44)

Han, J., & Leshchinsky, D. (2010). Analysis of back-to-back mechanically stabilized earth walls. *Geotextiles and Geomembranes*, *28*(3), 262–267. https://doi.org/10.1016/j.geotexmem.2009.09.012

Han, J., Oztoprak, S., Parsons, R. L., & Huang, J. (2007). Numerical analysis of foundation columns to support widening of embankments. *Computers and Geotechnics*, *34*(6), 435–448. https://doi.org/10.1016/j.compgeo.2007.01.006

Han, J., Parsons, R. L., Sheth, A. R., & Huang, J. (2005). Factors of safety against deep-seated failure of embankments over deep mixed columns. In *Proceedings of the International Conference on Deep Mixing Best Practice and Recent Advances* (pp. 231–236), Stockholm, Sweden.

Han, J., Wang, F., Al-Naddaf, M., & Xu, C. (2017). Progressive development of two-dimensional soil arching with displacement. *International Journal of Geomechanics*, *17*(12), 04017112. https://doi.org/10.1061/(ASCE)GM.1943-5622.0001025

Hewlett, W. J., & Randolph, M. F. (1988). Analysis of piled embankments. *Ground Improvement*, *21*(3), 12–18.

Hill, R. (1998). *The mathematical theory of plasticity*. Oxford University Press.

Holtz, R. D., & Massarsch, K. R. (1976). Improvement of the stability of an embankment by piling and reinforced earth. In *Proceedings of the 6th European Conference on Soil Mechanics and Foundation Engineering* (pp. 473–478), Vienna, Austria.

Hoppe, E. J., & Hite, S. L. (2006). *Performance of a pile-supported embankment* (No. FHWA/VTRC 06-R36). Virginia Transportation Research Council.

Huang, J., & Han, J. (2009). 3D coupled mechanical and hydraulic modeling of a geosynthetic-reinforced deep mixed column-supported embankment. *Geotextiles and Geomembranes*, *27*(4), 272–280. https://doi.org/10.1016/j.geotexmem.2009.01.001

IREX. (2012). *Recommendations for the design, construction and control of rigid inclusion ground improvements: ASIRI national project*. Presses des Ponts

Izadifar, M., Luo, N., Abu-Farsakh, M. Y., & Chen, S. (2023). Performance evaluation of design methods for geosynthetic-reinforced pile-supported embankments. *Transportation Research Record*, *2677*(11), 458–475. https://doi.org/10.1177/03611981231165994

Izadifar, M., Abu-Farsakh, M. Y., & Chen, S. (2024). Case study on instrumenting and monitoring geosynthetic-reinforced pile-supported mechanically stabilized earth wall built over soft soil. *Transportation Research Record*, *2678*(8), 1059–1076. https://doi.org/10.1177/03611981231224738

Jenck, O., Dias, D., & Kastner, R. (2005). Soft ground improvement by vertical rigid piles two-dimensional physical modeling and comparison with current design methods. *Soils and Foundations*, 45(6), 15–30. https://doi.org/10.3208/sandf.45.15

Kempfert, H. G., Gobel, C., Alexiew, D., & Heitz, C. (2004). German recommendations for soil reinforcement above pile-elements. In *Proceedings of the 3rd European Geosynthetics Conference* (pp. 279–283), Munich, Germany.

Kempfert, H. G., & Zaeske, D. (1999). Interactions in reinforced bearing layers over partial supported underground. In *Proceedings of the 12th European Conference on Soil Mechanics and Geotechnical Engineering* (pp, 1527–1532), Amsterdam, Netherlands.

Kempfert, H-. G., Zaeske, D. & Alexiew, D. (1999). Interactions in reinforced bearing layers over partial supported underground. In *Proceedings of the 12th European Conference on Soil Mechanics and Geotechnical Engineering, Amsterdam, Netherlands, 7–10 June 1999. Balkema, Rotterdam*, Volume 3, pp. 1527–1533.

King, D. J., Bouazza, A., Gniel, J. R., Rowe, R. K., & Bui, H. H. (2018). Geosynthetic reinforced column supported embankments and the role of ground improvement installation effects. *Canadian Geotechnical Journal*, *55*(6), 792–809. https://doi.org/10.1139/cgj-2017-0036

Lamb, R. A., Bentler, J. G., Theroux, B., Lucarelli, A., & Collin, J. (2022). *Duluth Twin Ports Interchange – Test Column Supported Embankment.* Personal Communication.

Larisch, M. D., Kelly, R., & Muttuvel, T. (2015). Improvement of soft soil formations by drilled displacement columns. In *Ground Improvement Case Histories - Embankments with Special Reference to Consolidation and Other Physical Methods* (pp. 573–622). Butterworth-Heinemann.

Le Hello, B. (2007). *Renforcement par géosynthétiques des remblais sur inclusions rigides, étude expérimentale en vraie grandeur et analyse mumérique* (Doctoral dissertation, Université Joseph-Fourier-Grenoble I).

Lee, T., Lee, S. H., Lee, I. W., & Jung, Y. H. (2020). Quantitative performance evaluation of GRPE: A full-scale modeling approach. *Geosynthetics International*, *27*(3), 342–347. https://doi.org/10.1680/jgein.19.00017

Lee, T., Van Eekelen, S. J., & Jung, Y. H. (2021). Numerical verification of the concentric arches model for geosynthetic-reinforced pile-supported embankments: Applicability and limitations. *Canadian Geotechnical Journal*, *58*(3), 441–454. https://doi.org/10.1139/cgj-2019-0625

Liu, H. L., Ng, C. W., & Fei, K. (2007). Performance of a geogrid-reinforced and pile-supported highway embankment over soft clay: Case study. *Journal of Geotechnical and Geoenvironmental Engineering*, *133*(12), 1483–1493. https://doi.org/10.1061/(ASCE)1090-0241(2007)133:12(1483)

Liyanapathirana, D. S. (2009). Arbitrary Lagrangian Eulerian based finite element analysis of cone penetration in soft clay. *Computers and Geotechnics*, *36*(5), 851–860. https://doi.org/10.1016/j.compgeo.2009.01.006

Lodder, H. J., Van Eekelen, S. J. M., & Bezuijen, A. (2012). The influence of subsoil reaction in a basal reinforced piled embankment. In *Proceedings of the 5th European Geosynthetics Congress* (pp. 390–394), Valencia, Spain.

Low, B. K., Tang, S. K., & Choa, V. (1994). Arching in piled embankments. *Journal of Geotechnical Engineering*, *120*(11), 1917–1938. https://doi.org/10.1061/(ASCE)0733-9410(1994)120:11(1917)

Maddison, J. D., & Jones, D. B. (1996). Design and performance of an embankment supported using low-strength geogrids and vibro concrete columns. In *Proceedings of the 1st European Geosynthetics Conference* (pp. 325–332), Maastricht, Netherlands.

Malikova, T. A. (1972). Analysis of natural settlements of slab and box foundations of multistory buildings. *Soil Mechanics and Foundation Engineering*, *9*(2), 99–104. https://doi.org/10.1007/BF01702896

Marston, A., & Anderson, A. O. (1913) *The theory of loads on pipes in ditches and tests of cement and clay drain tile and sewer pipes*. Bulletin 3I, Iowa Engineering Station, Iowa State College of Agriculture and Mechanic Arts.

Masse, F., Potter-Weight, A., Swift, S., & Buschmeier, B. (2020). Rigid inclusions: Current state of practice in North America. In *Proceedings of the Geo-Congress 2020* (pp. 431–448), Minneapolis, Minnesota. https://doi.org/10.1061/9780784482780.04

McGuire, M. P. (2011). *Critical height and surface deformation of column-supported embankments* (Doctoral dissertation, Virginia Polytechnic Institute and State University).

McGuire, M. P., & Filz, G. M. (2008). Quantitative comparison of theories for geosynthetic reinforcement of column-supported embankments. In *Proceedings of the 1st Pan American Geosynthetics Conference and Exhibition* (pp. 1–5), Cancun, Mexico.

McGuire, M. P., Hunstein, E. M., Hummel, E. G., & Sloan, J. A. (2022). *Theory manual for GeogridBridge 3.0*. GeoTechTools.org.

Neagoe, I. V. (2013). Soft soils reinforced by rigid vertical inclusions. *Constructii*, *14*(2), 48.

Nguyen, H. H., Khabbaz, H., & Fatahi, B. (2019). A numerical comparison of installation sequences of plain concrete rigid inclusions. *Computers and Geotechnics*, *105*, 1–26. https://doi.org/10.1016/j.compgeo.2018.09.001

Nobahar, M., Abu-Farsakh, M. Y., & Izadifar, M. (2024). Evaluating the mechanisms and performance of geosynthetic-reinforced load transfer platform of pile-supported embankments design methods. *Geotextiles and Geomembranes*, *52*(6), 1112–1133. https://doi.org/10.1016/j.geotexmem.2024.07.009

Nunez, M. A., Briancon, L., & Dias, D. (2013). Analyses of a pile-supported embankment over soft clay: Full-scale experiment, analytical and numerical approaches. *Engineering Geology*, *153*, 53–67. https://doi.org/10.1016/j.enggeo.2012.11.006

Oh, Y. I., & Shin, E. C. (2007). Reinforcement and arching effect of geogrid-reinforced and pile-supported embankment on marine soft ground. *Marine Georesources & Geotechnology*, *25*(2), 97–118. https://doi.org/10.1080/10641190701359591

Pham, T. A. (2020). Load-deformation of piled embankments considering geosynthetic membrane effect and interface friction. *Geosynthetics International*, *27*(3), 275–300. https://doi.org/10.1680/jgein.19.00030

Pham, T. A., & Dias, D. (2021). Comparison and evaluation of analytical models for the design of geosynthetic-reinforced and pile-supported embankments. *Geotextiles and Geomembranes*, *49*(3), 528–549. https://doi.org/10.1016/j.geotexmem.2020.11.001

Pucker, T., & Grabe, J. (2012). Numerical simulation of the installation process of full displacement piles. *Computers and Geotechnics*, *45*, 93–106. https://doi.org/10.1016/j.compgeo.2012.05.006

Rangel-Núñez, J. L., Gómez-Bernal, A., Aguirre-González, J., Sordo-Zabay, E., & Ibarra-Razo, E. (2008). Dynamic response of soft soil deposits improved with rigid inclusions. In *Proceedings of the 14th World Conference on Earthquake Engineering*, Beijing, China.

Rathmayer, H. (1975). Piled embankment supported by single pile caps. In *Proceedings of the Istanbul Conference on Soil Mechanics and Foundation Engineering*, Bayezit, Turkey.

Reid, W. M., & Buchanan, N. W. (1984). Bridge approach support piling. In *Piling and Ground Treatment* (pp. 267–274). Thomas Telford Publishing.

Russell, D., & Pierpoint, N. D. (1997). A numerical investigation of the behaviour of piled embankments. *Ground Engineering*.

Russell, D., Naughton, P. J., & Kempton, G. (2003). A new design procedure for piled embankments. In *Proceedings of the 56th Canadian Geotechnical Conference and 2003 NAGS Conference* (pp. 858–865), Two Rivers, Canada.

Samy, M., Abdelfattah, A., Fayed, A., Sorour, T., & Elshawaf, M. (2023). Prediction of the settlement associated with construction on soft clay improved using rigid inclusions considering the installation effect. *Engineering Research Express*, *5*(1), https://doi.org/015071. 10.1088/2631-8695/acc3de

Salah, M., & Yassmina, N. (2022). 3D numerical modeling of soft soil improved by rigid inclusions supported an embankment. *Engineering and Technology Journal*, *40*(5), 636–648. https://doi.org/10.30684/etj.2021.132023.1083

Schaefer, V. R., Abramson, L. W., Drumheller, J. C., & Sharp, K. D. (1997). *Ground improvement, ground reinforcement and ground treatment: Developments 1987-1997*. American Society of Civil Engineers.

Schaefer, V. R., Berg, R. R., Collin, J. G., Christopher, B. R., DiMaggio, J. A., Filz, G. M., & Ayala, D. (2017). *Ground modification methods-Reference manual (Volumes 1 and 2)* (Publication No. FHWA-NHI-16-027). National Highway Institute.

Simon, B. (2012). *General report S5: Rigid inclusions and stone columns*. ISSMGE-TC211.

Sivakugan, N. (1990). Discussion of "Constitutive parameters estimated by plasticity index" by Akio Nakase, Takeshi Kamei, and Osamu Kusakabe (July 1988, Vol. 114, No. 7). *Journal of Geotechnical Engineering*, *116*(10), 1594–1597. https://doi.org/10.1061/(ASCE)0733-9410(1990)116:10(1591.2)

Sloan, J. A. (2011). *Column-supported embankments: Full-scale tests and design recommendations* (Doctoral dissertation, Virginia Polytechnic Institute and State University).

Spencer, E. (1967), A method of analysis of the stability of embankments assuming parallel interslice forces. *Geotechnique*, *17*, 11-26. https://doi.org/10.1680/geot.1967.17.1.11

Suleiman, M. T., Ni, L., Davis, C., Lin, H., & Xiao, S. (2016). Installation effects of controlled modulus column ground improvement piles on surrounding soil. *Journal of Geotechnical and Geoenvironmental Engineering*, *142*(1), 04015059. https://doi.org/10.1061/(ASCE)GT.1943-5606.0001384

Swift, S. S., Pearlman, S., & Ramp, S. (2024). A compilation of transportation projects using rigid inclusions. *Geo-Structures 2024*, GSP 361, 280-293

Terzaghi, K. (1943). *Theoretical soil mechanics*. John Wiley & Sons.

Van Eekelen, S. J. M., Bezuijen, A., & Alexiew, D. (2010). The Kyoto Road piled embankment: 31/2 years of measurements. In *Proceedings of the 9th International Conference on Geosynthetics* (pp, 1941–1944), Guarujá, Brazil.

Van Eekelen, S. J. M., Bezuijen, A., Lodder, H. J., & van Tol, E. A. (2012). Model experiments on piled embankments. Part II. *Geotextiles and Geomembranes*, *32*, 82–94. https://doi.org/10.1016/j.geotexmem.2011.11.003

Van Eekelen, S. J. M., Bezuijen, A., & Van Tol, A. F. (2013). An analytical model for arching in piled embankments. *Geotextiles and Geomembranes*, *39*, 78–102. https://doi.org/10.1016/j.geotexmem.2013.07.005

Van Eekelen, S. J. M., & Han, J. (2020). Geosynthetic-reinforced pile-supported embankments: State of the art. *Geosynthetics International*, *27*(2), 112–141. https://doi.org/10.1680/jgein.20.00005

Van Eekelen, S. J. M., Venmans, A. A. M., Bezuijen, A., & Van Tol, A. F. (2020). Long-term measurements in the Woerden geosynthetic-reinforced pile-supported embankment. *Geosynthetics International*, *27*(2), 142–156. https://doi.org/10.1680/jgein.17.00022

Van Eekelen, S. J. M., Zwaan, R. A., Nancey, A., Hazenkamp, M., & Jung, Y. H. (2023). Four years field measurements in a partly submerged woven geotextile-reinforced pile-supported embankment. *Geosynthetics: Leading the Way to a Resilient Planet* (pp. 1072–1077), CRC Press.

Vega-Meyer, R., & Shao, Y. (2005). Geogrid-reinforced and pile-supported roadway embankment. In *Proceedings of the Geo-Frontiers 2005: Contemporary Issues in Foundation Engineering*, Austin, Texas. https://doi.org/10.1061/40777(156)9

Vesic, A. S. (1975). Bearing capacity of shallow foundations. *Foundation Engineering Handbook* (pp. 121–147). Van Nostrand Reinhold.

Vesic, A. S. (1977). *NCHRP synthesis of highway practice 42: Design of pile foundations*. Transportation Research Board.

Xing, H., Zhang, Z., Liu, H., & Wei, H. (2014). Large-scale tests of pile-supported earth platform with and without geogrid. *Geotextiles and Geomembranes*, *42*(6), 586–598. https://doi.org/10.1016/j.geotexmem.2014.10.005

Xu, C., Song, S., & Han, J. (2016). Scaled model tests on influence factors of full geosynthetic-reinforced pile-supported embankments. *Geosynthetics International*, *23*(2), 140–153. https://doi.org/10.1680/jgein.15.00038

Yu, H.-S. (2000). *Cavity expansion methods in geomechanics*. Springer Science+Business Media.

Yu, X., Zheng, G., Zhou, H., & Chai, J. (2021). Influence of geosynthetic reinforcement on the progressive failure of rigid columns under an embankment load. *Acta Geotechnica*, *16*, 3005–3012. https://doi.org/10.1007/s11440-021-01160-6

Zaeske, D. (2001). Zur Wirkungsweise von unbewehrten und bewehrten mineralischen Tragschichten über pfahlartigen Gründungselementen. *Schriftenreihe Geotechnik, Uni Kassel, Heft 10, February 2001* (in German).

Zhang, J., Zheng, J., Zhao, D., & Chen, S. (2016). Field study on performance of new technique of geosynthetic-reinforced and pile-supported embankment at bridge approach. *Science China Technological Sciences*, *59*, 162–174. https://doi.org/10.1007/s11431-015-5995-9

Zhang, Z., Han, J., & Ye., G. (2014). Numerical investigation on factors for deep-seated slope stability of stone column-supported embankments over soft clay. *Engineering Geology*, *168*, 104–113. https://doi.org/10.1016/j.enggeo.2013.11.004

Zhao, M., Liu, C., El-Korchi, T., Song, H., & Tao, M. (2019). Performance of geogrid-reinforced and PTC pile-supported embankment in a highway widening project over soft soils. *Journal of Geotechnical and Geoenvironmental Engineering*, *145*(11), 06019014. https://doi.org/10.1061/(ASCE)GT.1943-5606.0002157

AD ASTRA PER ASPERA

Kansas
Department of Transportation